Master Thesis

Evaluating nature-based solutions for flooding in the Geul catchment using openLISEM

Author: Julius Overhoff (2777088)

1st supervisor: Dr. Hans de Moel (VU Amsterdam)
2nd supervisor: Dr. Kymo Slager (Deltares)

A thesis submitted in fulfillment of the requirements for the Master of Science degree in Hydrology

July 27, 2024

Figure 1: Flooding in Valkenburg (NL - Geul catchment) in July 2021

Abstract

Flash floods and heavy rainfalls, like those in July 2021 in the Geul catchment, are projected to increase in severity and frequency. In addition to structurally engineered grey flood mitigation measures such as dikes and reservoirs, nature-based solutions, like afforestation and hedgerows, are also being considered. However, the effectiveness of these measures in mitigating floods during extreme rainfall events remains debated.

This study aims to evaluate the impact of afforestation and hedgerows on reducing flooding in the Geul catchment during the heavy rainfall of July 2021. The hydrological and hydrodynamic model openLISEM was used for this purpose. The event-based model setup was calibrated to water levels and discharges at Sippenaeken and Kelmis. The flood extent along the Geul covering the cities of Valkenburg, Schin op Geul, Partij, and Gulpen was simulated with a Critical Success Index (CSI) of approximately 84.

Results indicate that small-scale afforestation and hedgerows would not have significantly prevented flooding. However, full catchment afforestation, using mid-aged forest parameterization, reduces peak flow at Meerssen by about 35%. Young forest parameterization increases the peak discharge at Meerssen by 47%, whereas old forest parameterization decreases it by 74% compared to mid-aged forests. This suggests that the flood-mitigating effect of a forest is sensitive to its parameterization and increases with forest age and associated influence on soil properties.

Results show that seasonality and interception play minor roles, suggesting that infiltration primarily drives the flood-mitigating effect of forests during heavy rainfall events. The potential underestimation of stream flow for a 50% reduction of event rainfall highlights one of the uncertainties in the event-based model setup. Despite the low flood mitigation impact for heavy rainfall events, the implementation of small-scale afforestation and hedgerows should still be considered as they can provide various co-benefits, such as carbon sequestration, increased biodiversity, and improved soil quality. Future research should evaluate their impact on the other hydrologic extreme, drought, before they find practical application.

Preface

The devastating impacts of the flooding in the summer of 2021, which affected Belgium, Germany, Luxemburg, and the Netherlands, and the projected increase in frequency of events of the same magnitude resulted in the formation of cross-national research programs such as JCAR ATRACE with the ambition to find drought and flood risk management solutions for resilient watershed management under a changing climate. International collaboration is crucial for building resilience. For smaller and transboundary rivers, a common water management strategy often does not exist, resulting in higher vulnerability to flood impacts.

This thesis contributes to the efforts of JCAR ATRACE by evaluating the effect of two nature-based solutions, afforestation and hedgerows, in the transboundary Geul catchment, which spreads over Belgium, Germany, and the Netherlands, using the hydrologic and hydrodynamic model openLISEM.

It is important to acknowledge the MSc theses of Huub Koper, who investigated the impact of afforestation and hedgerows on flooding in the Geul catchment using the SFINCS (*Super-Fast INundation of CoastS*) model, and Romijn Servaas, who analyzed afforestation in the Meuse basin using the GEB (*Geographical Environmental Behavioural*) model. Using different hydrological and hydrodynamic models for the same purpose is relevant as each model offers unique strengths and limitations tailored to specific applications. The comparative analysis of these three theses can ultimately help determine which model best fits the intended purpose.

Acknowledgements

A great thank you goes to Hans de Moel for his supervision throughout my thesis on parts of the VU. His quick thinking, problem-solving attitude, and valuable feedback during our frequent meetings greatly supported me throughout the modeling and writing process.

I would also like to express my gratitude towards Kymo Slager for his guidance and encouragement in thinking critically and questioning the causes and implications of modeling results. Additionally, I am grateful for the opportunity he provided to contribute to the JCAR ATRACE program and to combine this thesis with an internship at Deltares. The discussions over coffee with colleagues from the flood risk management department, particularly with Angela Klein, Nathalie Asselmann, and Siep Bakker, about nature-based flood mitigation measures, the flooding of 2021, and the hydrological response of the Geul catchment were very valuable and insightful.

I would also like to thank Jeroen Aerts, who, alongside Jens de Bruijn, supervised the monthly GEB meetings at the VU, for his inspiring feedback. These meetings were an appreciated opportunity to reflect on and discuss my ongoing modeling study and also offered interesting insights into current modeling projects at the IVM, which overall contributed to a better understanding of hydrological and hydrodynamic modeling.

I sincerely enjoyed the frequent chats with my fellow students Huub Koper, Romijn Servaas, and Rafi Senden during lunch and coffee breaks. Sharing and discussing our experiences throughout the thesis process was very supportive and motivating.

Finally, I want to thank my family and friends for their endless support and encouragement.

Contents

List of Figures

List of Tables

Glossary

ADCP	Acoustic Doppler Current Profiler
BD	Bulk Density
CSI	Critical Success Index
DEM	Digital Elevation Model
ESA	European Space Agency
ET	Evapotranspiration
HRU	Hydrologic Response Unit
KNMI	Koninklijk Nederlands Meteorologisch Instituut
ksat	Saturated Hydraulic Conductivity
LAI	Leaf Area Index
LUCC	Land Use and Land Cover Change
LULC	Land Use and Land Cover
NBS	Nature-based Solutions
NDVI	Normalized Difference Vegetation Index
NIR	Near-Infrared Spectrum
NSE	Nash-Sutcliffe Efficiency Coefficient
OMC	Organic Matter Content
OSM	Open Street Map
PTFs	Pedotransfer Functions
RR	Random Roughness
SOC	Soil Organic Carbon

1

Introduction

Major **flash floods** in the summer of 2021 in west and central Europe caused high economic damages, destroyed infrastructure and caused over 200 casualties. Also, the transboundary Geul catchment, which spreads over Belgium, Germany, and the Netherlands and drains into the Meuse, was severely affected by flooding during the heavy rainfall in July 2021, with major damages occurring in the city of Valkenburg (ENW, 2021). Because of anthropogenic climate change, which increases the severity and frequency of hydrologic extremes, the probability of the recurrence of rainfall events in the same magnitude as in the summer of 2021 is projected to increase (Rodell and Li, 2023; IPCC, 2021; Tradowsky et al., 2023; Asselman and Van Heeringen, 2023). Combined with the historic straightening of river courses to improve navigation, which reduced the space for naturally occurring floods, and post-industrial urbanization in proximity to rivers, which amplified exposure, riverine flood risk has increased on a global scale. A recent study from Dottori et al. (2023) states that if no adaptation actions are taken for a 3 ℃ climate warming scenario, annual riverine flood damages within Europe could increase from 7.6 billion to 44 billion by the end of the century. This poses new challenges to current flood defense systems and creates an **urgent need for efficient and sustainable flood adaptation strategies**.

Structurally engineered flood defense structures, such as embankments, levees, and reservoirs, provide important protection against floods and water levels up to a certain exceedance probability. However, despite their essential flood protective function, these structural measures come with inherent risks of failure and can result in an unintended increase of the opposite hydrological risk, drought (Ward et al., 2020).

For this reason, in recent years, attention has also been drawn towards the evaluation of alternative and additional mitigation measures for hydrologic extremes, referred to as **Nature-Based Solutions (NBS)** (Kumar et al., 2021; Gourevitch et al., 2020). While technical hard-engineered grey measures are often built with the single purpose of flood protection, NBS are an integral approach covering a range of services (Naturkraacht.org, 2023). The European Commission defined the term NBS as measures that are cost-effective, inspired, and supported by nature with the objective of addressing environmental, social,

and economic challenges while providing co-benefits, such as carbon storage, improved water quality, enhanced groundwater recharge, and increased biodiversity, ultimately helping to build resilience (Commission and Agency, 2023). NBS in the field of watershed management are, among others, river re-meandering and floodplain restoration, which focus on reconnecting the river with its floodplain, resulting in elasticity in river water storage and the potential for natural self-regulation of water flow dynamics, such as reducing the flow velocity and peak discharges during heavy rainfall events (Kumar et al., 2021; Baptist et al., 2004; Ruangpan et al., 2020). On the other hand, wetland preservation and land use changes such as afforestation and hedgerows are discussed as NBS, which are measures designed to create "sponge-landscapes" which enhance infiltration capacity of the soil, interfere and slow down runoff, consequently decreasing and attenuating peak discharges in the river, which reduces the flood impact (Penning et al., 2023; Calder et al., 2003).

Nevertheless, Rogger et al. (2017) highlights the necessity for gaining more quantitative insights into the effect of land use changes, such as afforestation on runoff generation and floods on the catchment scale, as different studies come to contradictory conclusions. The large sample analysis study of Bradshaw et al. (2007) on floods in developing nations showed that large-scale forest protection and more reforestation reduce the frequency and severity of floods. In contrast, other studies point out missing evidence for flood mitigating effect of forests at larger scales and large flood events because the processes of interception and evaporation by vegetative cover would be overwhelmed by precipitation (Calder et al., 2004; Calder, Smyle, and Aylward, 2007; Van Dijk et al., 2009).

This raises the need to further analyze the effect of afforestation for large flood events while also considering its impact on soil hydraulic properties. Besides evaluating the effect of scale and distribution of forest on flood magnitude at the catchment scale, also the state of the forest should be included in the analysis as the effect of vegetation on the top soil and consequently on infiltration is dynamic over time and is also influenced by the maturity of the forest (Archer et al., 2016; Zema et al., 2021).

Furthermore, while hedgerows influence local hydrology through enhancing infiltration and interfering with the overland flow, their effect on flood mitigation on catchment scale, especially for large flood events, is under current debate and needs to be further quantified (Webb, 2021; Naturkraacht.org, 2023). As the design of hedgerows ranges from grass strips to densely planted shrub and tree lines, the effect of differences in vegetation type should be included in the analysis (Holden et al., 2019).

Assessing the effectiveness of afforestation and hedgerows for mitigating floods could be done in real-world and large-scale experiments, but those are time-consuming and often physically not feasible. Another approach is the schematization and implementation of forests and hedgerows into hydrologic and hydrodynamic models. Whereas hydrological models are valuable tools in improving the understanding of hydrological systems and assessing the impact of climate and land cover changes on runoff, subsurface water storage

and evapotranspiration, hydrodynamic models can be used to represent overland flow and flow behavior in riverine zones and provide valuable information on flood levels and inundation extends (Dubey et al., 2021; Pechlivanidis et al., 2011).

Due to the above reasons, the main objective of this thesis is **the evaluation of the two Nature-Based Solutions afforestation and hedgerows on how effective they might have been when implemented in reducing the flooding in the Geul catchment for the heavy rainfall event in July 2021**.

An event-based modeling study is performed to assess the impact of the two measures on flood characteristics such as water levels, discharges, and flood extent. Because of its spatially distributed structure and the ability to account for the hydrology and hydrodynamic flow processes of each grid cell simultaneously, the physically based numerical model openLISEM is used for the analysis. As the state of a forest is dynamic in time and influenced by factors such as seasonality and forest maturity, the first sub-objective is the evaluation of the effect of different forest parameterizations, representing **temporal dynamic variations in forests**, which consider differences in summer and winter leaf coverage and forest age-dependent influence on soils bulk density (BD) and organic matter content (OMC).

Spatial scenarios, such as riparian afforestation, downstream vs. upstream afforestation, full catchment afforestation, and afforestation according to current policy resolutions, have the objective of assessing whether afforestation is effective in reducing floods during heavy rainfall events and if so, which of the **spatial forest distributions** is most effective.

While the effect of hedgerows on the floods of July 2021 will be evaluated, the third sub-objective is the evaluation of the **effect of hedgerows for a 20% and 50% reduction of the event rainfall** as the effect of the small scale measure, is expected to be minor. Finally, the last sub-objective is the evaluation of possible **differences in the effect of grass infiltration strips and dense shrub hedgerows** on flood characteristics.

The structure and complexity of hydrological and hydrodynamic models are influencing the outcome of the simulation (Van Kempen, Van Der Wiel, and Melsen, 2021). By assessing the effect of afforestation and hedgerows in openLISEM and exploring its sensitivity to parameterizations, this study contributes to a better understanding of the capabilities of openLSIEM and if it is fit for the purpose of adequately assessing those nature-based flood mitigation measures. Ultimately, the findings of this analysis can be used to support decision-making in flood management.

2

Study Area

The following chapter gives a general overview of the case study area, the Geul catchment, and the flood characteristics of the July 2021 event. This is important as it builds the basis for setting up the event-based openLISEM model. The catchment, including topography is displayed in figure 2.1.

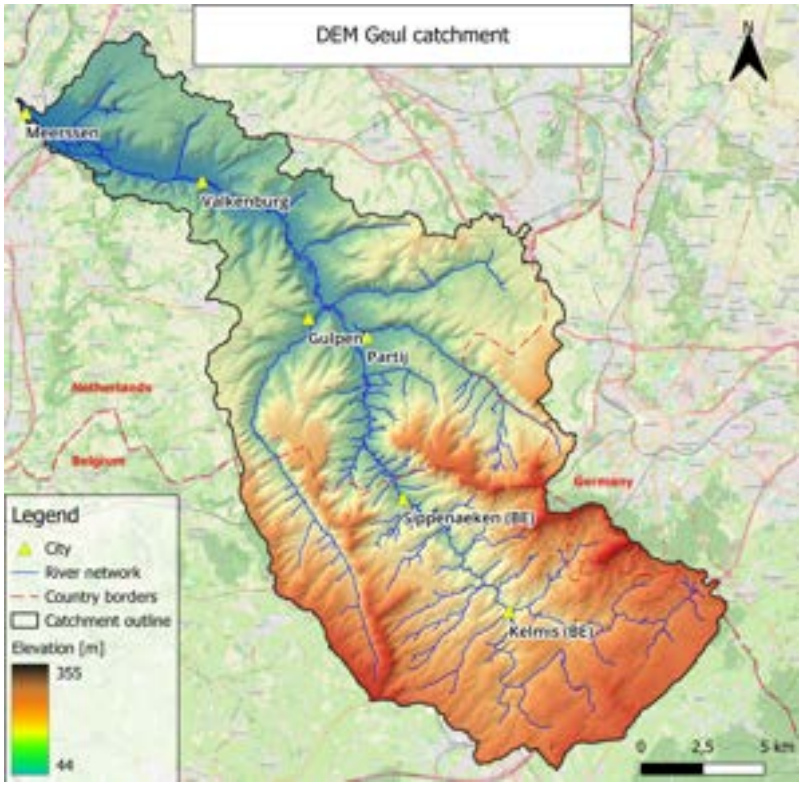

Figure 2.1: Topographic map of Geul catchment

2.1 Topography & Climate

The Geul catchment is a small river catchment with a size of about 340 km^2. The Geul River, with a total length of 56 km, is a major tributary of the Meuse River and stretches over Germany (6%), the region of Wallonia in Belgium (42%), and the south of Limburg in the Netherlands (52%) (Westeringh, 1980). With elevation changes from approximately 360 m above sea level in the Belgian source area to 50 m at the confluence with the Meuse a few kilometers north of Maastricht, the Geul presents steeper slopes and consequently higher flow velocities, compared to other catchments in the Netherlands (De Moor et al., 2008; Westeringh, 1980). This results in higher flow velocities in the Geul. The average discharge at the outlet is 3.4 $m^3 s^{-1}$ (De Moor et al., 2008). The main tributaries of the Geul are the Gulp, Eyserbeek, and Selzerbeek. The present landscape in the catchment area consists of large, flat plateaus into which asymmetrical river valleys with shallow floodplains are deeply carved (De Moor et al., 2008).

The total annual precipitation in the catchment ranges from 750 to 850 mmy^{-1} in the downstream area to more than 1000 mmy^{-1} in the upstream area (De Moor and Verstraeten, 2008). Evapotranspiration in the catchment is primarily constrained by energy rather than by water availability (Klein, 2022).

2.2 Hydrogeology & Soil Characteristics

The Geul River is cut into Paleozoic rocks, such as sandstones, shales, and limestones in the Belgian and southernmost part of Limburg. In the downstream Dutch area, the river is mainly cut into Cretaceous lime- and sandstones (De Moor et al., 2008). The overall catchment is covered by fertile loess (predominantly silt-sized sediment), which was deposited during the Saalian and Weichselian glacial period (Mücher, 1986). In the Dutch part, soils are thick and characterized mainly by moderate permeability, resulting in a high water storage volume. Conversely, in the Belgium part, soils are thinner with underlying impermeable rock and can consequently store less water (Naturkraacht.org, 2023). The plateaus are defined by coarse-silty soil texture with less clay content, whereas the floodplains and river valleys are of loamy and sandy texture with higher clay content in the subsoil (Westeringh, 1980).

The study of Klein (2022)) found that during and after the flood event of 2021, groundwater monitoring wells in the catchment showed different response times and drainage behaviors, indicating dual porosity and matrix flow and the existence of complex hydrogeology in the catchment with significant groundwater storage in the underlying aquifer system. Karstic structures are also present in the catchment.

2.3 Land Use

The landscape in the catchment can be described as a bocage landscape (Naturkraacht.org, 2023). On the plateaus often crops are cultivated, the steeper slopes are forested and in the valleys often grassland is present (Van Heeringen et al., 2022. The major land-use classes, such as built-up, grass- and cropland, water bodies, and forest are shown in figure 2.2

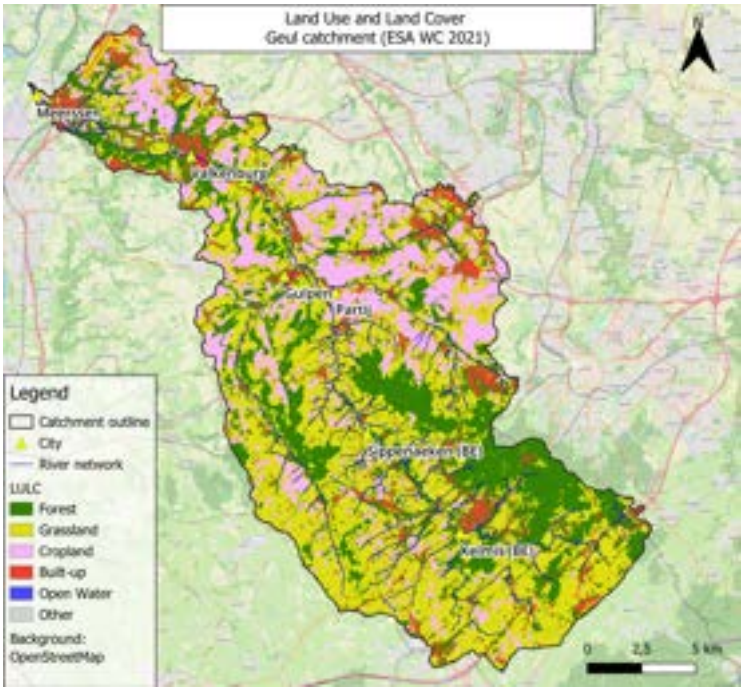

Figure 2.2: Land Use and Land Cover in the Geul catchment

2.4 Hydrology and July 2021 Flooding

The Geul is mainly rain-fed, so the river's discharge can vary rapidly after heavy thunderstorms (De Laat and Agor, 2003). Small-scale floods occur regularly on grasslands along the river but usually do not cause much damage. (De Moor et al., 2008). In July 2021, water levels along the Geul were the highest ever observed within the catchment, with an estimated probability of exceedance lying between 1/100 and 1/1000 per year (Strijker et al., 2023). The highest water levels occurred in the evening of 14th July and in the morning of 15th July. Peak discharge of the Geul near Valkenburg during the event is estimated to have been around 135 $m^3 s^{-1}$ (Strijker et al., 2023). Studies of Klein (2022) and Van Heeringen et al. (2022) found that the high rainfall intensity and the duration of rainfall, combined with local geology and antecedent moisture conditions, led to the high runoff generation. From a meteorological perspective, the heavy rainfall event could be linked to the phenomena of a low-pressure area with an upper-level cold pool of air,

which was cut off and decoupled from the jet stream, resulting in heavy spatially concentrated precipitation (ENW, 2021). Particularly, the Belgian upstream catchment, with its lower soil storage capacity, produced a rapid runoff response (Slager et al., 2022b) and contributed between 60% and 75% to the event discharge, despite representing only 42% of the catchment area (Klein, 2022; Van Heeringen et al., 2022). Figure 2.3 shows the cumulative rainfall over the event of the 13th to 17th of July based on KNMI reanalysis data (Overeem and Leijnse, 2021).

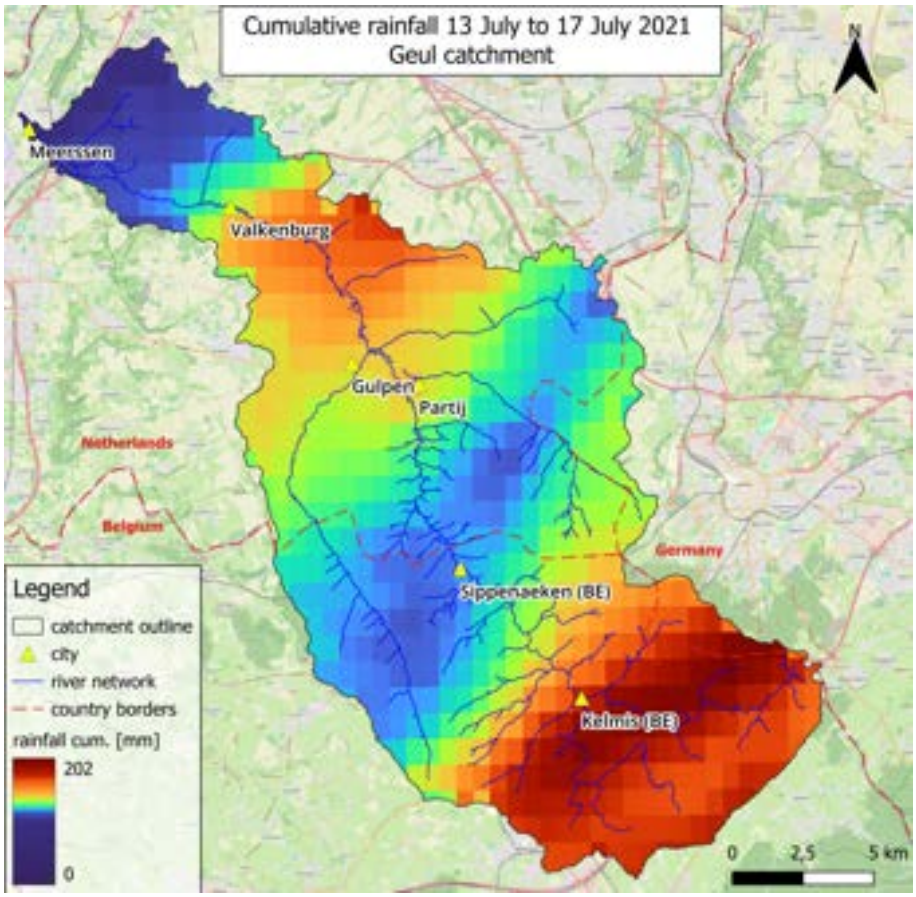

Figure 2.3: Cumulative rainfall in the Geul catchment between 13-17th of July 2021 based on KNMI reanalysis data

2.5 Flood Management Geul

In the Netherlands, primary flood defenses along the major rivers are managed by Rijkswaterstaat and financially supported by the government with safety standards varying from 1/100 to 1/100000 year failure probability (*Delta Decision for Flood Risk Management* 2023). For tributaries, flood defenses are often not present or significantly lower; in South Limburg, in urban areas, protection standards have a failure probability of 1 in 25 years (Strijker et al., 2023).

In the past 20 years, the waterboard of Limburg has constructed several rainwater buffers, which are often integrated into the landscape, such as in valleys or tributaries of the Geul, dry valleys (valleys without streams), and on slopes in the higher elevated areas (Van Heeringen et al., 2022). Their function is to capture rainwater, enhance infiltration, and consequently to delay the transport of water to the main river channel. In addition to the structural embankments, also other measures are discussed and being implemented.

Specific nature-based adaptation measures have been formulated by Naturkraacht.org (2023). Among others, these include afforestation along the plateau borders, converting cropland into natural grassland on steep slopes (>12%), and the implementation of infiltration zones along cropland and natural grasslands on medium slopes (7 to 12%). Moreover, on low to medium slopes (4-12%), the clearing of drainage systems has been proposed, as well as less extensive land use and brush development. Additionally, wetlands should be created in valleys and floodplains, and a widening and lowering of the floodplain for natural re-meandering of the river is suggested. In built-up areas, the sealed surfaces should be converted into vegetated areas to allow better infiltration and reduce runoff during rainfall.

2.5.1 Assessing NBS for flooding in the Geul catchment using hydrological and hydrodynamic models

In the following subsection, recent modeling studies of Deltares will be presented, which assessed the effect of afforestation on flooding in the Geul catchment. As their results will be used for comparison with the findings of this study, it is necessary to give a short overview of the used models and implementation approaches.

As a response to the flooding in 2021, a rapid assessment report was elaborated by Slager et al. (2022b). Among other subjects, it investigated the impact full catchment afforestation (without urban areas) would have had on flooding in the Geul catchment for the July 2021 rainfall. The analysis included a modeling study using the hydrological model wflow_sbm, which is developed and maintained by Deltares. The model is spatially distributed and allows the physically-based simulation of vertical processes, such as snow accumulation, interception, transpiration, and infiltration, and uses a kinematic wave model for river, overland, and lateral subsurface flow based on an eight-direction (D8) network (Verseveld et al., 2022). The soil in each grid cell is conceptualized as a bucket with

saturated and unsaturated store. Land use and soil properties are used to estimate input parameter values using PTFs. To each LULC class, such as a forest, different parameters are assigned, which are used in wflow_sbm, such as *Kext extinction coefficient for canopy gap* (-), *Manning's n*, *rooting depth* (mm), *paved fraction* (-), *storage leaves* (mm), and *wood storage (mm)*. The used resolution of the wflow_sbm model in the study of Slager et al. (2022a) was 1000 m and the timestep hourly, to capture the flashy behavior during the event. Afforestation was implemented in the study through a land use and land cover change (LUCC). Furthermore, the Manning's n coefficient, representing land surface roughness, was increased for the forest land use and land cover (LULC) class. This adjustment led to decreased flow velocity, allowing for more infiltration time. An additional expected effect of implementing the measure was increased interception and transpiration (Slager et al., 2022a).

What is important to mention in this context is that due to the model's structure, the influence of land cover does not directly affect the soil storage, e.g., through increased or decreased porosity. Moreover, the vertical saturated hydraulic conductivity is not influenced by land use changes. This is a significant difference to openLISEM, where the specific LULC directly influences the soil's saturated hydraulic conductivity and porosity. Nevertheless, due to the LULC parameterization in wflow_sbm, such as the rooting depth and wood storage, interception and evapotranspiration are described in higher detail compared to openLISEM.

Additionally, the wflow_sbm model was coupled to the SOBEK 1D and 2D hydrodynamic model, to account for floodplain storage and hydraulic flow, which resulted in a better representation of the peak discharges during the heavy rainfall event in 2021 (Slager et al., 2022a). In SOBEK, river branches and the main channel are represented in 1D, but the flood plain and flooding are modeled in 2D with a grid resolution of 25 m. By coupling the two models, the SOBEK model was completely forced with discharges from wflow_sbm (Slager et al., 2022a). River floodplain afforestation was implemented by increasing the floodplain roughness. The outcome of the study of Slager et al. (2022a) will be compared to this thesis' findings in the result section.

3

Methodology

The following chapter provides an overview of openLISEM and its event-based setup, which was used to answer the research questions. It includes the discussion of input data, the calibration and validation approach, and the elaboration of various afforestation and hedgerow scenarios. These scenarios will used to assess the effectiveness of afforestation and hedgerows in reducing flood impacts for the 2021 rainfall event in the Geul catchment. Figure 3.1 presents the workflow of the modeling study.

First, the required input data will be processed so that it can be used by the model. Subsequently, the model will be calibrated to the event discharge and water levels and validated to event water levels and flood extent. After adequate calibration and validation of the model, afforestation and hedgerow scenarios will be implemented through land use and land cover changes (LUCC) or by modifying the parameterizations of the LULC class. Additionally, for selected hedgerow scenarios, the amount of incoming rainfall will be decreased.

The effectiveness of these measures will be evaluated based on changes in channel discharges and simulated flood extent, which are the model's outputs.

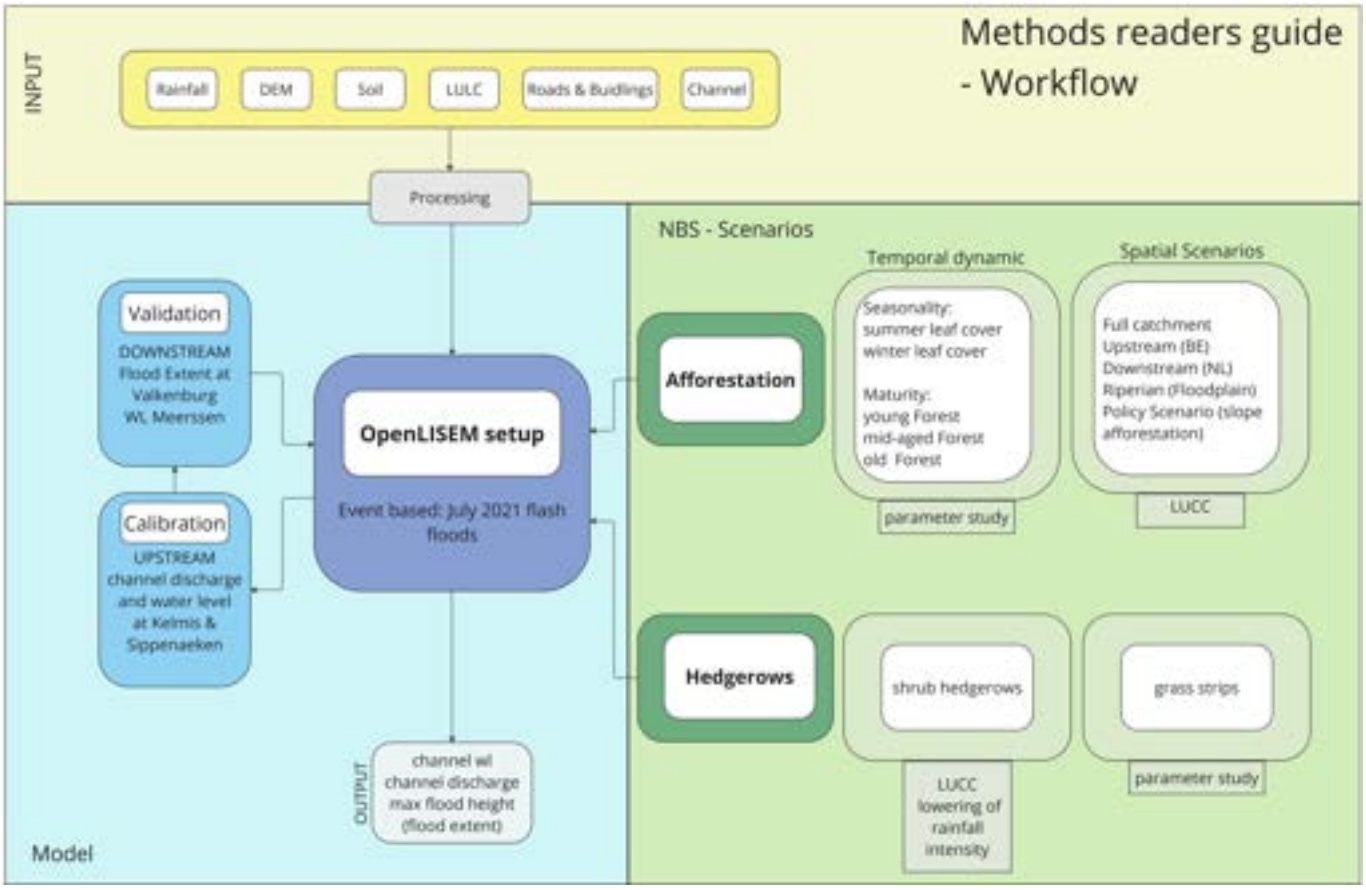

Figure 3.1: Flowchart Methodology

3.1 openLISEM

The following subsections give an overview of studies openLSIEM has been used for and which fundamental physical principles are applied in the model. Finally, the model setup for this study, which contains timestep, resolution, and simulation period, is presented.

3.1.1 General

The chosen model, openLISEM, was initially developed by the Universities of Utrecht, Wageningen, and Amsterdam under the lead of Prof. Ad de Roo and released in 1993 as LISEM (Limburg Soil Erosion Model) (De Roo, Wesseling, and Ritsema, 1996). Since its development as a tool to assess erosion and soil conservation measures in the province of Limburg (NL), it has been updated frequently. Currently, it allows the simulation of runoff, river flow, and flooding, groundwater flow, and sediment dynamics in all flows (Jetten and Bout, 2018). It has been used with resolutions between 1 m and 200 m and in catchment sizes of up to 5000 km^2 to support answering a wide range of scientific questions, such as for event-based quickflow simulation (Vieira et al., 2022; Kuiper, 2023), evaluation of land use changes on overland flow, runoff and flood extent (Jetten, 2022), and exploring effects of rainfall intensity and duration on soil erosion (Baartman et al., 2012). The model has been developed as an event-based model and is mostly applied in this manner, but continuous modeling of up to one year is also possible.

OpenLISEM is a spatially distributed, grid-based, integrated catchment model simulating the complete hydrology and flow. This means that within each grid cell runoff can be generated, leading to discharge and then eventually to flooding. The advantage of integrated catchment models over decoupled models is that runoff can result directly in flooding over open boundaries instead of via specified entry points, where source areas are separated from flood areas. This can lead to more accurate simulations, especially for flash floods, which are usually a combination of overflowing channels, overland flow, and direct rainfall (Jetten and Bout, 2018). Furthermore, its spatially distributed structure allows the provision of spatially varying rainfall data, and as the overland flow in the model follows topography, depressions in the landscape, such as integrated rainwater buffers and obstacles in the form of dikes, can be directly considered (Jetten, 2022). This is quite relevant as up-scaling of land use changes, such as afforestation, from plot to catchment scale has been proven to be complex because the spatial connectivity of flow processes is highly influencing the effect of land use changes (Rogger et al., 2017).

These characteristics of openLISEM should allow the exact evaluation of the impact of regional flood mitigation measures, such as afforestation and hedgerows. Nevertheless, the disadvantage of integrated catchment models is that they require more computation, which increases the model's runtime (Bout and Jetten, 2018).

3.1.2 Hydrological and hydrodynamic processes

The processes that are included in openLISEM are shown in figure 3.3. For this study, sediment fluxes and erosion are not simulated because no significant morphological changes have been observed in the riverbed in the Geul catchment after the July 2021 flash flood (Strijker et al., 2023). The hydrological response of each grid cell is based on land surface and soil characteristics and forcing data such as rainfall and temperature. However, due to high cloud cover during rainfall, the effect of evapotranspiration (ET) on event-based runoff and flood extent is considered less significant and is thus excluded from the simulation. Moreover, groundwater flow is characterized by slow flow velocities, therefore the increase in groundwater contribution to streamflow during a heavy rainfall event is considered to be minor, which is why a constant baseflow is chosen for the study reflecting the streamflow prior the event. This will be further discussed in the calibration section (3.3.1). Nevertheless, openLISEM generally allows the simulation of groundwater flow driven by accumulating water in the soil layer along a linear drainage direction network or as 2D flow resulting from pressure differences. Figure 3.2 shows the hydrological and hydrodynamic processes simulated by the model.

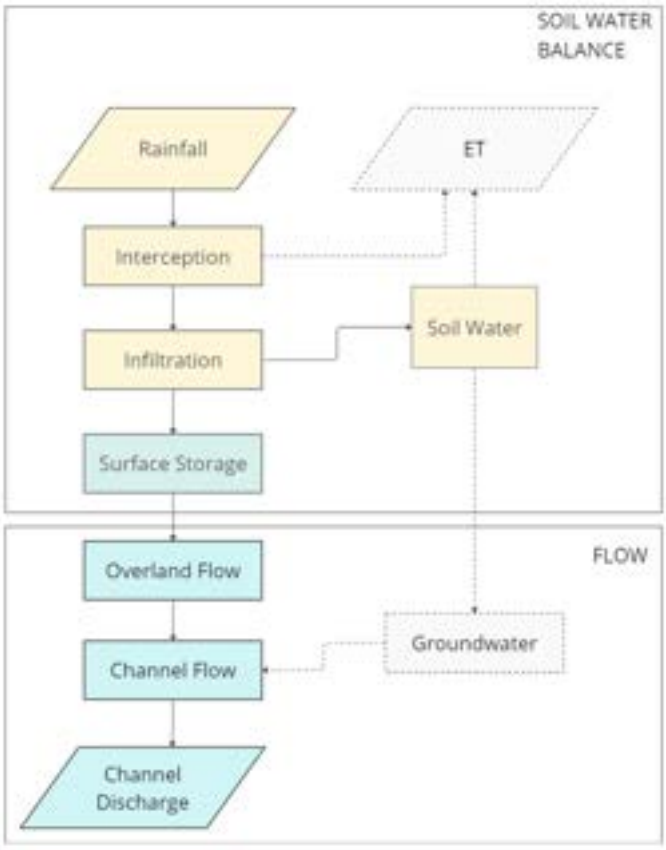

Figure 3.2: Most important hydrologic processes in openLISEM (adapted from Jetten and Bout, 2018.

In the following, the underlying physical assumptions and models are described, which are used in openLISEM for the simulation of runoff, channel flow, and flooding. Spatially distributed **rainfall** (mm/h) can be provided either through interpolated rainfall station measurements or radar images. Rainfall time intervals should be hourly or shorter. For this analysis hourly spatially dsitributed rainfall was used as will be described in section 3.2.8.

Interception can occur through roofs of buildings or vegetation in a grid cell. In openLISEM, the canopy interception is given by the following equation (3.1) of Aston (1979):

$$I_c = S_{max}\ (1 - e^{-k\frac{P_{cum}}{S_{max}}}) \tag{3.1}$$

$$k = 1 - e^{-(co\ LAI)} \tag{3.2}$$

where I_c is total intercepted storage at a given time (mm), k is parameter related to canopy openness (-), S_{max} is the maximum canopy storage (mm) and P_{cum} is the total precipitation (mm). The parameter related to canopy openness k (3.2) is dependent on canopy openness (-) and leaf area index (LAI) (-), which can be derived from NDVI satellite imagery as described later. S_{max} equations for different land covers, such as broad-leaved forest, cropland, and grassland, are taken from Hoyningen-Huene (1983) and presented in the appendix B.

The fraction of rainfall that hits a building is stored as long as there is storage. The storage can be defined by the user. The default roof interception storage of 10 mm was selected for this setup. Furthermore, as water hits the soil, infiltration occurs.

Infiltration can be simulated using the infiltration models of Smith and Parlange (1978), SWATRE (Bastiaanssen et al., 1996) and Green and Ampt (1911). For this study, the 2-layer infiltration model by Green and Ampt (1911) was chosen, which uses the overall assumption that soil above the wetting is fully saturated while beneath the front, the soil is completely dry. Moreover, it assumes that the wetting front moves downward in the soil parallel to the surface and that the water height above the soil surface is zero. This results in the following simplified Darcy equation for vertical water flow (3.3) given by Jetten (2022):

$$f_{pot} = -K_s \left(\psi\ \frac{\theta_s - \theta_i}{F} + 1 \right) \tag{3.3}$$

where f_{pot} is the potential infiltration rate ($m\ s^{-1}$), K_{sat} the saturated hydraulic conductivity of the soil ($m\ s^{-1}$), θ_s is the porosity (-), θ_i is the initial soil moisture content (m^3

m^{-3}), ψ is the matric pressure at the wetting front (m) and F is the cumulative infiltrated water (m). The infiltration rate varies between the first and second soil layer. Whereas the first layer is influenced by the type of land use, the infiltration rate of the second layer solely depends solely on soil properties. Moreover, for the openLISEM setup of this study, a closed boundary beneath the second soil layer is chosen, allowing water to accumulate. ψ, K_s and θ_s are based on empirical equations of Saxton and Rawls (2006).

The overland flow between grid cells is calculated based on the average hydrological response of a grid cell per time step and the resulting increase in water level in micro-depressions and different spatial surface water heights. The micro depressional **surface storage** (m) is mainly affected by the slope and standard deviation of the surface heights (cm), which is also called random roughens. The random roughness varies with each land use type.

Overland flow and flooding can be approximated through several options in openLISEM. Either overland flow follows the DEM-derived local drainage direction network as a 1D kinematic wave, where only runoff occurs and no flooding, or as a 1D kinematic wave combined with a 2D dynamic wave for flooding when the channel overflows. The third option, which is also used within this study, is a fully dynamic 2D wave following the DEM approximated by the Saint-Venant equations for shallow flooding using depth average velocity. This method does not differentiate in the calculation between runoff and flooding and is combined with 1 D kinematic channel flow.

Flooding is defined as runoff which exceeds the threshold of 0.05 m. The underlying governing physical principles are the conservation of mass, momentum, and motion. A semi-explicit finite volume solution with dynamic time-step is used for numerical solution based on the FullSWOF2D library (Jetten and Bout, 2018; Delestre et al., 2014).

The connection between 1D channel flow and 2D overland flow follows the assumption that the direction of overland flow in the cells containing the channels is perpendicular to the channel direction. Moreover, the channel is assumed to be in the middle. By utilizing the channel width and flow velocity, the proportion of runoff water that flows into the channel can be calculated using the following formula (3.4):

$$f_{qch} = \frac{d_t \cdot u}{0.5 \cdot (C_{xy} - B_c)} \tag{3.4}$$

where f_{qch} is the fraction of channel discharge, B_c is the channel width at the surface, C_{xy} is the resolution of the model, u (equation 3.5) is the flow velocity ($m \cdot ms^{-1}$) and dt is the timestep (s).

$$u = R^{\frac{3}{2}} \cdot \frac{\sqrt{S}}{n} \tag{3.5}$$

where S is the energy slope, the energy slope in each orthogonal direction is given by the difference in water levels between the adjacent cells divided by the distance between the cell centers. R is the hydraulic radius (m), and n is Manning's coefficient ($s \cdot m^{-1/3}$).

When the channel overflows, water is transformed into flooding water. If the channel has extra capacity, flooded water is transported to the channel. In the case of an already flooded cell, incoming water is added to the flood (Jetten and Bout, 2018). The velocity of flood water is recalculated using the conservation of kinetic energy. In this way, high quantities of runoff influence the flood velocity. The schematization of the order of processes simulated in openLISEM is shown in figure 3.3.

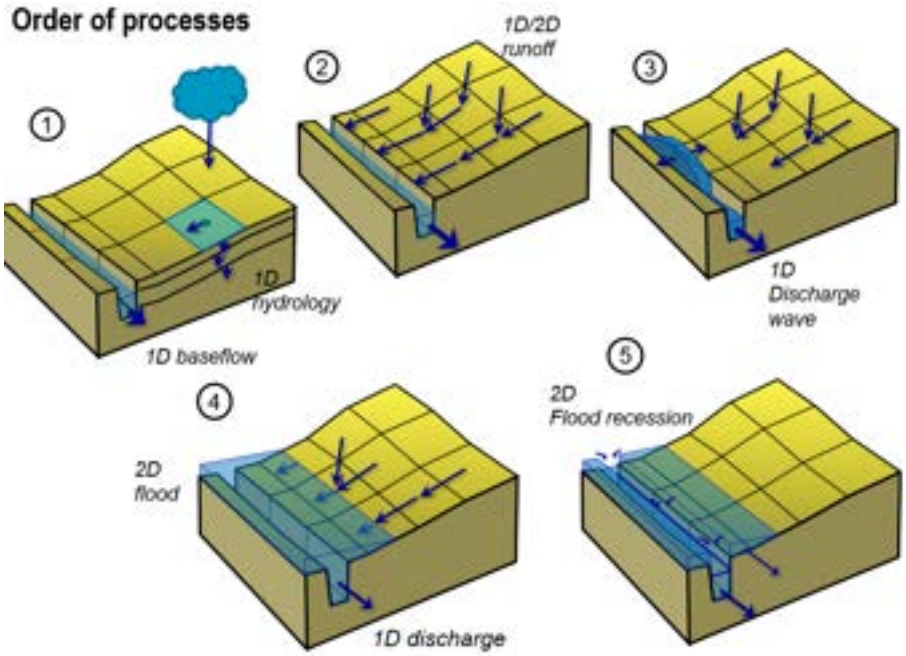

Figure 3.3: order of processes in openLISEM (source: Jetten and Bout, 2018)

In this context, it is important to mention that the channel discharge is very sensitive to the chosen time step because hydrological processes and kinematic flow are averaged over this timestep. A sensitivity analysis is included in figure 26 in the appendix.

3.1.3 Model setup

For this study openLISEM version 6.95 (2024) is used, which is embedded in a graphical user interface (GUI). Initial model runs for the entire Geul catchment using a resolution of 10 meter took over 48 hours to finalize (hardware setup is described in appendix A). Moreover, an increase in timestep led to a reduced channel discharge (figure 26). Therefore, in order to increase computational efficiency, the resolution of the model setup was reduced

to 20m. Furthermore, a time step of 60 seconds was chosen. Nevertheless, due to the numerical solution method, the model uses a non-iterative but dynamic timestep between 0.5 and 60 seconds for solving the 2D Saint Venant equations. The model setup is event-based and covers the period of the flood event, which was defined as the time between the 13th of July at 00:00 and the 16th of July at 23:00.

3.2 Input openLISEM

OpenLISEM uses spatially distributed raster maps as input layers, which contain the hydrological parameters required for numerical solutions of the governing equations, such as for flow and infiltration. The hydrological parameters are derived from input maps, which can be categorized into soil physical information, information on vegetation, information on buildings and roads, and channel data (figure 3.4).

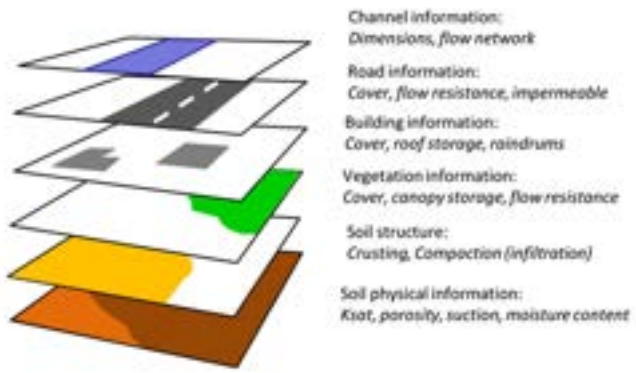

Figure 3.4: openLISEM input categories (source: Jetten and Bout, 2018).

Infrastructure and urban elements such as buildings and roads are given as a fraction of a grid cell, also vegetation and river channel dimensions can be provided on sub grid level. Ultimately, a grid cell could consist, e.g., of 20% channel, 15% vegetation and 10% buildings or roads, and 55% bare soil influenced by the above land cover. Moreover, information on compaction and crusting of soil can be supplied. Soil maps containing soil physical information build the base layer.

The creation of the required input maps in PCRaster format using the raw input data is partly guided and automated by preset and adjusted Python scripts which are embedded in the openLISEM database creator version 4.74 (2024). Other tools used for input processing are the GIS software QGIS (version 3.36.0), Nutshell (version 5.1.) and Pyhton. Table 3.1 shows an overview of the used input data

Table 3.1: Overview of used data

Category	Input Data	Year	File Type	Source
Buildings	Buildings Köln	2024	shapefile (polygon)	OSM (Geofabrik)
	Buildings Belgium	2024	shapefile (polygon)	OSM (Geofabrik)
	Buildings Limburg	2024	shapefile (polygon)	OSM (Geofabrik)
Channel	Waterways Köln	2024	shapefile (line)	OSM (Geofabrik)
	Waterways Belgium	2024	shapefile (line)	OSM (Geofabrik)
	Waterways Limburg	2024	shapefile (line)	OSM (Geofabrik)
DEM	Merged DEM	2023	GeoTIFF (5 m)	Deltares (AHN 4 Geoportail Wallonia Geoportal NRW)
Soil	SoilGrids Data	2020	GeoTIFF (250 m)	SoilGrids (soilgrids.org)
LULC	Land Cover Map	2021	GeoTIFF (10 m)	ESA WorldCover 2021
Satellite Imagery	Sentinel 2 Bands Geul Catchment	2021	GeoTIFF (10 m)	Copernicus (Sentinel Data)
Roads	Roads Köln	2024	shapefile (line)	OSM (Geofabrik)
	Roads Belgium	2024	shapefile (line)	OSM (Geofabrik)
	Roads Limburg	2024	shapefile (line)	OSM (Geofabrik)
Rainfall	KNMI Reanalysis Rainfall Data	2019-2021	.nc file	Deltares (KNMI)
Discharge	Q Kelmis & Sippenaeken	2019-2021	.xlsx file	Hydrometrie Wallonie
Water Level	WL Kelmis & Sippenaeken	2019-2021	.xlsx file	Hydrometrie Wallonie
Water Level	WL for selected locations along Geul	2021	.xlsx file	Deltares

The input data and processing will be described in the following subsections. The overall projection of the setup is Amersfoort EPSG: 28992.

3.2.1 Buildings

Buildings in the Geul catchment have been derived from Open Street Map (OSM) as polygons. OSM is based on governmental data, which is further completed by a community of users and considered to provide detailed, reliable, and recent information on land cover (Slager et al., 2022a). The fraction of polygon building cover is calculated for each grid cell. In openLISEM, the effect of buildings on surface water flow can be included in two ways. Either the cells containing buildings are assigned a high flow resistance, but buildings are practically permeable to flow, or cells containing buildings are added to the DEM as

obstacles where the fraction of buildings per grid-cell exceeds a certain threshold (e.g., 0.3). For this setup, the first option of assigning the buildings a high flow resistance is chosen. However, due to the fact that buildings are practically permeable, runoff might be transported quicker to the river channel. The final buildings in the catchment are presented in appendix E

3.2.2 Channel Network

In openLISEM, the river channel is assumed to be rectangular. Nevertheless, the channel dimensions should give a close approximation to the reality because the channel discharge and water level output is highly influenced by the channel cross-sectional dimensions at the specific location. By default, openLISEM allows the interpolation of the river depth and width based on start and outlet locations. Nevertheless, the river course of the Geul varies from wide, natural meandering bands to straightened canalized subsections. This is why cross-sections have been measured at specific locations, such as at Kelmis and Sippenaeken, and cross-sectional data has been taken from existing SOBEK model channel schematizations of Deltares for further interpolation and improved channel representation in the model (SOBEK model description in 2.5.1). Approximated rectangular dimensions of river cross-sections are presented in the appendix C. The river channel between those cross sections has been interpolated using the non-linear relation between channel width and total river length (equation 3.6) as derived by Allen and Pavelsky (2015) through observations of US rivers.

$$W = L^{0.459} \tag{3.6}$$

where W is river width (m) and L is river length (m).

The relation of channel depth to width is given by Jetten and Bout (2018) and based on earlier openLISEM simulations (equation 3.7):

$$D = W^{0.3} \tag{3.7}$$

where D is channel depth (m) and W is channel width (m).

The linear channel network has been derived from OSM waterways, which include linear water features such as rivers, canals, and streams. It has been further adjusted by combining it with a DEM-derived flow network at locations where channels and streams were connected to the main river channels through subsurface drainage pipes, which are not included in OSM. This is necessary to ensure that runoff water ends up in the main channel. Canalization can not be simulated within openLISEM.

Culverts were not included in the model setup since they can only be included in the model by limiting discharge at specific channel locations to a defined maximum. Extensive culvert descriptive data is needed to solve the equations describing culvert flow, such as the semi-empirical Chézy equation, which are needed to approximate maximum channel flow. This data was not fully available for this study, and the required effort was considered to contribute not significantly to the study's findings, so it was not included. The final river network and location of cross-sections used for interpolation are presented in figure 3.5.

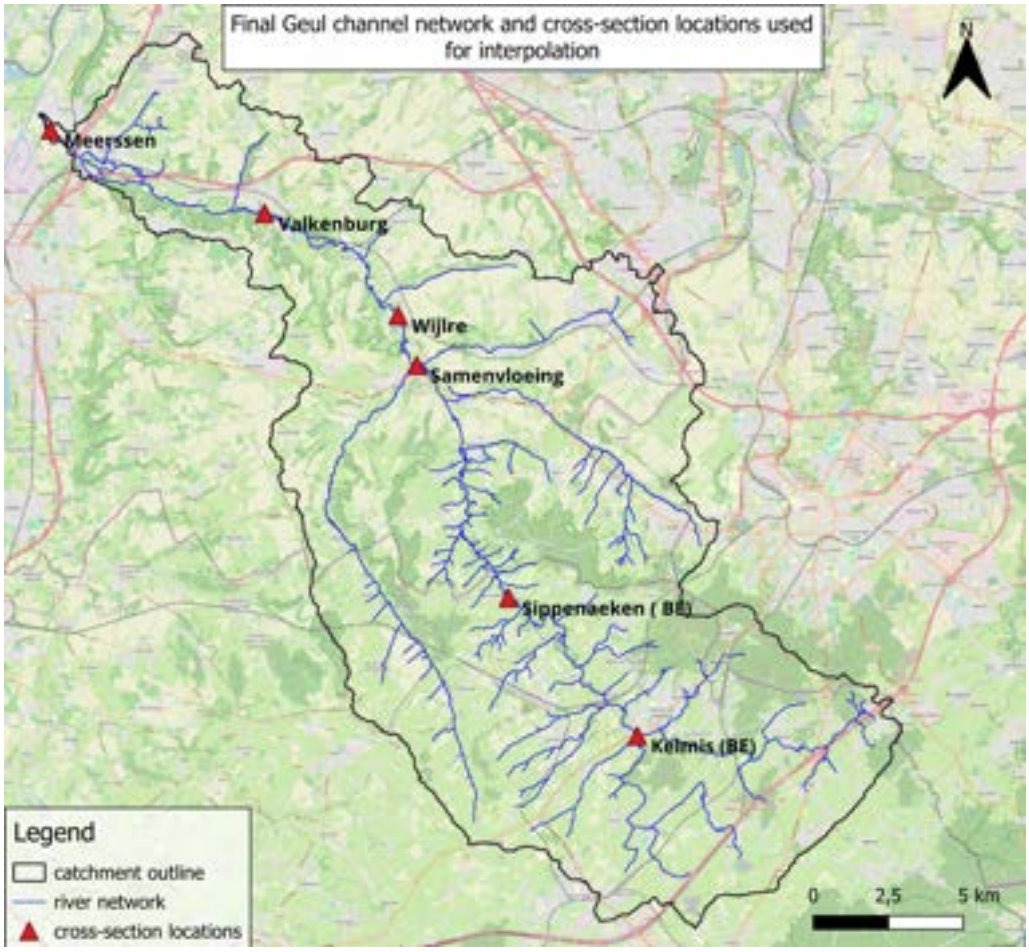

Figure 3.5: Geul river network and locations of cross-sections

3.2.3 Digital Elevation Model (DEM)

The Digital Elevation Model (DEM) is crucial in hydrological and hydrodynamic modeling. Changes in elevation determine flow gradients and, therefore, greatly affect flow velocities and discharges. The study of Xu et al. (2021) concluded that the source and resolution of the DEM can significantly alter the simulation of inundation height and extent. Simulations with higher spatial resolution resulted in increased flood inundation and extent compared

to coarser resolutions. Nevertheless, because high-resolution DEMs result in long runtimes for computationally extensive models, such as openLISEM, the initial input DEM with 5m resolution was resampled to a coarser 20 m resolution using the Cubic B Spline method in QGIS. Cubic b spline is a preferable interpolation method in this context due to the continuous nature of the elevation data and its smoothing effect (Minh et al., 2024). The input 5 m DEM was provided by Deltares and contains already harmonized and resampled elevation data for the Geul catchment. The initial sources were national DEMs derived from AHN 4 (NL), Geoportail Wallonia (BE), and Geoportal NRW (DE). Moreover, depressions in the DEM larger than 1 m were filled. In this way, the rainwater buffer depressions in the landscape should still be included. In the DEM, bridges and train tracks are included in the elevation. This lead in the test model runs to the stoppage of water at that location, although the river passes below the bridge or train tracks. This is why, at several locations, the DEM was manually altered to ensure correct water transport downstream. The final DEM is presented in figure 2.1 and the manual adjustments can be found in the appendix D.

3.2.4 Roads

Roads are derived from OSM roads. To account for the different road widths of the major OSM road classes, such as primary, secondary, tertiary, service, residential, motorway, and unclassified, measurements have been taken in QGIS using ESRI satellite imagery. For each major OSM road class, 30 samples were taken across the catchment, the samples were randomly chosen, and the population of each class was normally distributed. Therefore, each road class's mean width was taken (appendix E). Roads are provided as a fraction of a grid cell and are considered to be impermeable in the model; road drainage sinks were not included. The final roads in the catchment are presented in appendix E.

3.2.5 Soil

OpenLISEM allows the description of soil properties in high detail. The necessary spatial soil textural data was downloaded from SoilGrids, a global coverage database, which uses machine learning methods and global soil profile information and interpolation to provide soil properties on 250 m resolution for six layers up to a depth of 200 cm (Hengl et al., 2017). The derived soil properties are sand, silt, and clay content, bulk density (BD), gravel content, and soil organic matter content (OMC). Within the openLISEM database creator, these properties are used in pedotransfer functions of Saxton and Rawls (2006). The multiple regression pedotransfer functions calculate porosity, field capacity, wilting point, and pore size coefficient λ and transfer those characteristics into hydrological properties such as saturated hydraulic conductivity (ksat). The equations require a reference BD and initial soil moisture content. The reference bulk density is taken as default by the model,

which is 1350 kg/m^3. The determination of the initial soil moisture content is part of calibrating the model.

For the openLSIEM setup of this study, the 2-layer Green & Ampt infiltration model is used. Therefore, two soil layers with different depths were defined. The first layer represents the A-horizon of the soil, which is characterized by higher organic matter content. This first layer is also influenced by the type of land use, which is described in section 3.2.6. As mentioned in the introduction, soil depths vary within the Geul catchment. However, soils in the Belgian part are generally shallower than in the Dutch part, resulting in lower soil storage. The depth of the first layer is assumed to be constant throughout the catchment. The depth of the second soil layer also depends on the slope and the perpendicular distance to the river channel, with deeper soils close to the river and shallower soils on steeper slopes. Determining soil depths is part of the calibration and can be found in the result section of the calibration (4.1).

3.2.6 Land Use and Land Cover

Land Use and Land Cover (LULC) is an essential input of the model and this study since it influences runoff, infiltration, and interception. For this study, the global WorldCover project 2021 LULC product of the European Space Agency (ESA), which is based on Sentinel 1 and Sentinel 2 data, has been used. It contains 11 LULC classes, such as tree cover, shrub-land, grassland, cropland, built-up, bare/sparse vegetation, snow and ice, permanent water bodies, herbaceous wetland, mangroves and moss and lichen in a resolution of 10 m. Depending on the abundance of the LULC classes and for comparison to other studies, classes have been reclassified into five major groups, which are shown in table 3.2. Moreover, the LULC map has been reprojected to Amersfoort epsg:28992 and resampled from 10 m resolution to 20 m resolution using the nearest neighbor method. The LULC statistics have been compared to other analyses of the 2021 flood event in the Geul catchment, such as the studies of Slager et al. (2022a) and Klein (2022), which are presented in table 3.2.

Table 3.2: Table with parameters for July 2021 LULC

source	**This study ESA WC 2021**	**Slager et al. (RAR 2022) OSM (2022)**	**Klein (2022) Corine 2018**
LULC	[%]		
Forest	30.24	20	13
Grassland	44.09	46	27.5
Cropland	18.4	19	41.5
Built-up	7.16	10-15	17
Water	0.06	neglected	neglected
Other	0.04	neglected	neglected
Total	100	95-100	100

The comparison to Corine 2018 land cover data shows that big differences can be observed in the proportion of built-up area, grass- and cropland, and forest. The differences might be attributed to the differences in the resolution of the products, as Corine 2018 LC is provided in a resolution of 100 m. Moreover, the study of Slager et al., 2022a showed that urban areas in the catchment were over-represented in the Corine dataset. Slager et al. (2022a) used OSM data as input, which is considered to be of high accuracy, especially in urban environments. Generally, the ESA WC 2021 data is in range with the OSM data. Only the built-up area is less in ESA WC 2021, and the portion of forest is higher. Due to its high resolution and recent data in relation to the flood event, the ESA WC 2021 map serves as the LULC input for this study. Figure 2.2 shows the final reference LULC of 2021.

Each LULC class is represented by a set of parameters, such as random roughness (cm), Manning's n (-), plant cover (-), relative bulk density (-) and organic matter content (%), which influence hydrological and hydrodynamic processes, such as interception, infiltration, and overland flow. Final LULC parameterizations for each class are presented in table 3.3.

Table 3.3: Table with parameters for July 2021 LULC

LULC	RR [cm]	Manning's n [-]	Plant Cover [-]	rel. BD [-]	Smax	OMC [%]
Forest	2	0.1	0.9	0.9	6	4.5
Grassland	1	0.03	0.8	1	8	4.0
Cropland	1	0.04	0.7	1	1	3.0
Built-up	0.5	0.1	0.1	1.1	0	2.5
Water	1	0.03	0	0	0	1.5
Others	1	0.03	0.1	1	0	2.5

The initial values for the parameters random roughness (RR), relative bulk density (BD) and organic matter content (OMC) used for this study are taken from Jetten (2022) who performed a detailed analysis of two sub-catchments of the Geul. Values for Manning's n are taken from the HEC-RAS 2D manual U.S. Army Corps of Engineers (2024). Moreover, Smax refers to plant-species specific canopy storage equations, as explained in section 3.1.2. Their equations can be found in the appendix B. The land use-specific plant cover (canopy cover) is based on the average NDVI for each LULC class, which is explained in the following section.

3.2.7 NDVI

To account for the exact vegetation cover and consequently accurate interception during the event, a Normalized Difference Vegetation Index (NDVI) map was derived from Sentinel

2A satellite imagery with 10 m resolution. Furthermore, within openLISEM, the NDVI can also be used to determine micro relief (random roughness) and Manning's n through empirical equations. Nevertheless, for this analysis and to allow accurate comparison between reference and land use change scenarios, the NDVI is only used to determine the average canopy cover for the different land use classes. The image taken for the analysis dates to the 21st of July 2021, when cloud cover was less than 10%. The NDVI is calculated using information of the red and near-infrared spectrum (NIR), which is included in sentinel 2 satellite band 4 and band 8, respectively, using the following formula 3.8:

$$NDVI = \frac{NIR - Red}{NIR + Red} \tag{3.8}$$

Subsequently, the NDVI was resampled to a resolution of 20 m and reprojected to Amersfoort epsg:28992. The final average plant cover values for each LULC class are shown in table 3.3.

Plant cover (Cover) for each land use class was calculated using the following formula 3.9:

$$Cover = \min\left(0.99, \max\left(0.0, 4.257 \cdot NDVI^2 + 100.719 \cdot NDVI - 5.439\right)/100.0\right) \tag{3.9}$$

3.2.8 Rainfall

Precipitation, as the forcing data of the model, can be provided either in the form of rainfall data of multiple weather stations throughout the catchment, which are subsequently interpolated, or as spatially distributed radar data, satellite data, or reanalysis data.

For this study KNMI reanalysis spatial rainfall data has been used. The KNMI reanalysis data is based on radar data from radar stations in the Netherlands, Belgium, and Germany, automatic rain gauge measurements, and data from manual rain gauges. Since the KNMI reanalysis rainfall data is corrected to ground measurements, it is considered to be the most accurate data for the July 2021 event and is used for this study. The exact methodology of creating the KNMI reanalysis product can be found in Overeem and Leijnse, 2021. For this thesis, the rainfall product was provided by Deltares. However, the rainfall data presents hourly intensities (mm/h). This means that peak intensities are most certainly averaged out and underestimated. In the calibration process, this needs to be accounted for, e.g., by adjusting the saturated hydraulic conductivity of the soil.

Using the openLISEM database creator, the rainfall was reprojected from epsg:4326 to Amersfoort epsg:28992 and resampled to 20 m resolution using the nearest neighbor method. Since the provided dataset was already clipped to the Geul catchment but did not cover the full catchment extent used within this model setup, the missing rainfall

data at the catchment borders was extrapolated using the window average method with a window size of 10 by 10 pixels. In this way, dry cells were prevented. The sums of the input rainfall are shown in figure 2.3. Furthermore, the initial rainfall sums without application of the window average is shown in appendix 3.

3.3 Calibration and Validation

The Model has various outputs, including the spatial distribution of cumulative infiltration, interception, rainfall, overland flow, and maximum water levels. For this study, channel discharge, water level, and flood extent are the main parameters for evaluating the effect of NBS on flooding and are consequently used for calibrating and validating the model.

3.3.1 Calibration

As described in section 2.4, the sub-catchment with Sippenaeken as the outlet was the main contributor to the overall streamflow of the catchment, making up 60-75 % of the event discharge. Because of that and due to the openLISEMs computational requirements, calibration was performed for the upstream area with Sippenaeken as the outlet (figure 3.6).

The observed water level and discharge in Sippenaeken (BE) and Kelmis (BE) present the basis for calibration and have been provided by Hydrometrie Wallonia. The water levels at Sippenaeken and Kelmis are measured directly through a pressure sensor and transferred to discharge values using rating curves. The rating curve of Sippenaeken has been derived by the Walloon Water Authority through 58 discharge measurements using instruments such as flow meters and the Accustic Doppler current profiler (ADCP). The range of measurements at Sippenaeken lies between water levels of 0.45 m to 1.07 m, corresponding to a discharge of $0.171 m^3/s$ and $7.81 m^3/s$ respectively. This shows that higher uncertainty must be assigned to discharges higher than $7.81 m^3/s$, such as during the flood of 2021. This is why the measured water levels have been chosen as the main reference for the calibration.

Calibration can be performed using calibration coefficients, such as for Manning's n, Ksat, soil depth and initial moisture content. These coefficients provide values that can be directly multiplied with the input maps. For more detailed and local changes, the input maps must be adjusted manually. Moreover, when deriving soil maps from SoilGrids, reference bulk density and initial soil moisture content must be defined, whereas soil moisture can be set between wilting point and full saturation. Besides the initial water content, soil depths influence the water storage and were part of the calibration process.

The performance indicator was the Nash-Sutcliffe Efficiency coefficient (NSE), which describes how well the modeled discharge and water levels perform compared to the average observed water level and discharge.

The formula for calculating the NSE (3.10) is presented below :

$$NSE(o, \hat{o}) = 1 - \frac{\sum_{i=0}^{N-1}(o_i - \hat{o_i})^2}{\sum_{i=0} N - 1(o_i - mean(o))^2} \tag{3.10}$$

where o_i represents observed values at timestep i and $\hat{o_i}$ represent simulated values at timestep i.

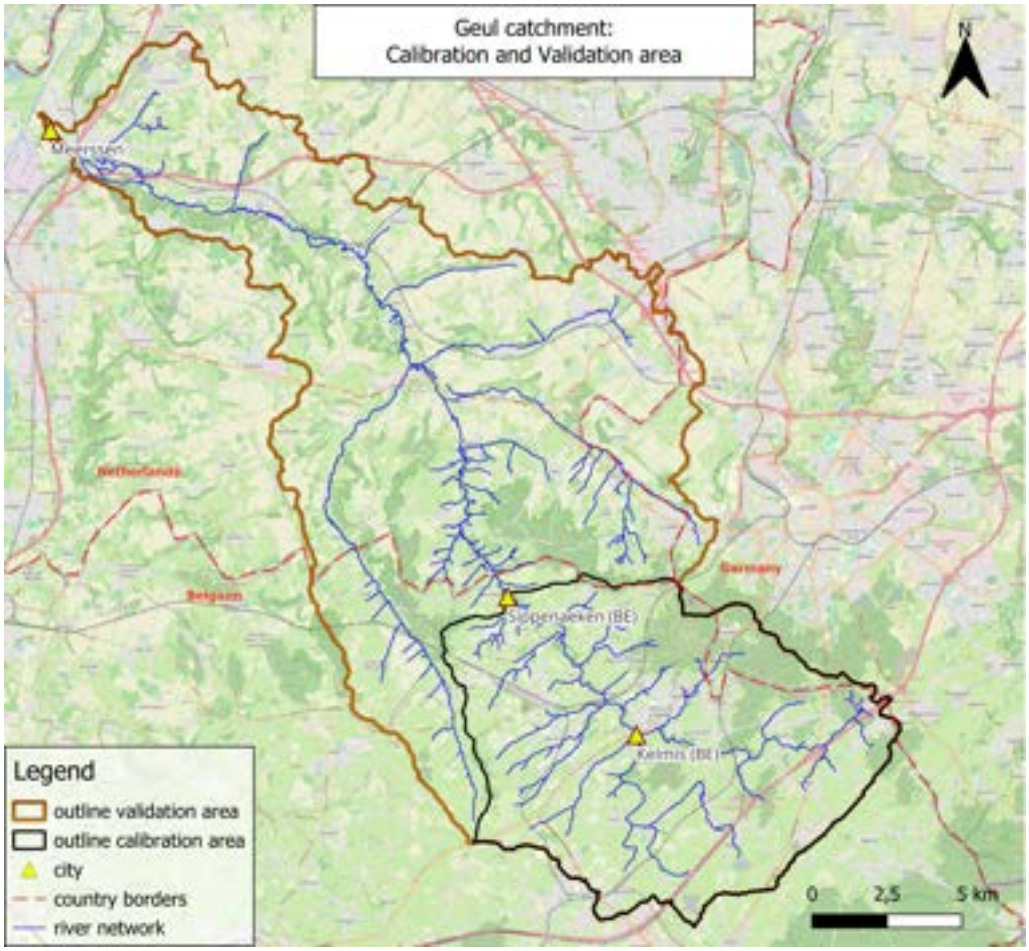

Figure 3.6: Calibration and Validation area

3.3.2 Validation

As the model calibration is event-based and requires an initial soil moisture content as input, which varies between events, the model will be validated to observed water levels close to the outlet of the Geul near Meerssen, which is not located in the calibration area,

and on zoomed-in flood extent along the channel encompassing the cities of Valkenburg, Schin op Geul, Gulpen and Partij as in those cities most of the structural damage occurred during the event. Since the observed flood extent is based on helicopter imagery closely after the event, which just focused on the main river channel in the Dutch part of the catchment, a 100 m buffer is created around the observed flood extent, which defines the area of comparison between simulated and observed flood extent. Within the defined flood extent area, hit rate, false rate, bias, and critical success index (CSI) will be calculated as performance metrics. Figure 3.6 shows the calibration and validation area.

3.4 Scenarios

The following subsections provide detailed information on the setup of various land use and land cover change (LUCC) scenarios and parameterization studies related to afforestation and hedgerows. These studies aim to enhance the understanding of how these two measures can mitigate flood impacts during extreme rainfall events. Table 3.4 gives an overview of all the scenarios that have been developed for this study.

3.4.1 Afforestation - Effect of temporal dynamics (maturity)

The following three scenarios aim to assess soil improvement through forests over time. The findings can contribute to a new perspective on how the impact of a forest on flooding changes over time and with the aging of the forest. Archer et al. (2016) investigated Scottish forests of different ages (6-year-old, 48-year-old, $>$ 1000-year-old forest) and found out that the saturated hydraulic conductivity increased over time. Zema et al. (2021) investigated the effect of forest age on saturated hydraulic conductivity in a Mediterranean environment and found an increasing relationship between age and increased ksat, driven by higher organic matter content (OMC) and lower bulk density (BD). The study presented soil properties at a depth of 5 cm for sandy clay loam under forest cover. Old forest ($>$80 years old) samples included 12% OMC, medium forest (20-80 years old) samples 8.5% OMC and young forest ($<$20 years old) samples 6 % OMC. Soil organic carbon (SOC) and thus also OMC decreases significantly with depth (Liu, Wang, and Dai, 2019).

Therefore, for this analysis, the chosen OMC for the first soil layer, which has a depth of 30 cm (shown in table 4.1), should be lower than literature values, which often just take the first 10 cm into consideration (Zema et al., 2021; Gonzalez-Sosa et al., 2010).

As forests are characterized by great heterogeneity, other factors might influence the change of saturated hydraulic conductivity over time, such as macropores through bioturbation and larger rootzones (Bouché and Al-Addan, 1997; Wang et al., 2022). Those factors are not directly included in the parameterization in openLISEM but can be indirectly accounted for by lowering the bulk density. Nevertheless, BD should not be decreased by

more than 10% as this can cause errors in the simulation (Jetten and Bout, 2018). Moreover, the assigned forest ages should not be taken as absolute values because multiple factors can cause variations in the associated temporal effect. Forest management practices and previous land use can result in varying timescales for improving soil conditions through afforestation (Archer et al., 2016).

This also holds true for forests in the Geul catchment, especially the larger forest area near Vijlen, which has been already managed for centuries but underwent large destruction during the Second World War and also suffered from overexploitation, which led to a degradation of the forest quality (Provincie Limburg, 2017). Due to the extensification of forest management and the afforestation of broadleaf trees, such as oaks and beeches, in the last decades, the forest quality near Vijlen has improved (Provincie Limburg, 2017). Jetten (2022) assigned forests in the Geul catchment an OMC of 4.5% and reduction of local BD by 10%, which corresponds to the "mid-aged" forest (20-80 years) parameterization of this study. This shows that historical and recent management influences the soil properties within a forest, and also, forests that have existed for centuries, such as the forest near Vijlre, can share parameterization with a more unmanaged "mid-aged" forest.

In summary, while the final forest parameterizations for "young" forest (<20 years), "mid-aged" forest (20-80 years), and "old" forest (>80 years) reflect plausible assumptions, such as that "young" forests locally lower bulk density by -5% and can be assigned an OMC of 4%, "mid-aged" forest locally lower bulk density by -10% and can be assigned an OMC of 4.5% and ultimately that "old" forest lower bulk density by -10% and can be assigned an OMC of 8%, it's essential to recognize that forest development is dynamic and therefore the age ranges (<20 years, 20-80 years, >80 years) should not be treated as rigid absolutes. Furthermore, as will be discussed later (section 4.3.1), due to the underlying assumptions in the model and derivation of PDFs, the "old" forest scenario represents the most extreme influence a LULC can have on soil hydraulic functions in the model. To see the biggest impact, full afforestation was assumed for the three scenarios. An overview of different forest parameterizations can be found in the appendix G.

3.4.2 Afforestation - Effect of temporal dynamics (seasonality)

This scenario aims to improve the understanding of the effect of seasonality on the flood impact of a broad-leaf forest. Since leaf cover is reduced during winter, the amount of interception is expected to change, ultimately influencing the generation of runoff (Andreasen et al., 2023). Therefore, two scenarios will be compared, reflecting summer and winter leaf cover. The determination of the summer leaf cover is already explained in section 3.2.7. In analogy, the winter leaf cover was determined using the NDVI map of the Geul catchment on the 21st of February, 2021. The average NDVI for the forest land use class was used and translated into plant cover as described in section 3.2.7. Final forest land use parameterization, including summer and winter plant cover values, are presented

in the appendix G. Both scenarios assume full catchment afforestation, which represents the conversion of grass- and cropland into forest, and "mid-aged" forest parameterization, which is representative of the current broad-leaf forest in the Geul catchment, as explained below.

3.4.3 Afforestation - spatial scenarios

The following scenarios aim to investigate the scale and spatial distribution at which afforestation is effective in reducing the flood impact in the catchment. All afforestation scenarios use summer leaf cover and the"mid-aged" forest parameterization. LULC maps and statistics for the different scenarios are included in the appendix

The **policy scenario** represents a scenario aligned with current policy resolutions regarding the planned expansion of forested areas. In the Limburg rural development strategy of 2023 ("*Limburgs Programma Landelijk Gebied*"), the strategy to increase current forest by an additional 35 km^2 is formulated (Limburg, 2023). This relates to a 10% increase of total forest cover in Limburg. The area of slopes larger than 10%, where either grass- or cropland is present, is approximately 12% of the Dutch catchment area and equals 22.6km^2. The study of Morbidelli et al. (2018) states that slopes are more vulnerable to erosion and can be associated with lower infiltration rates. This is why the selected 22.6 km^2 of slopes will be afforested in this scenario.

Riparian afforestation assess the effect of afforestation in the floodplain within 100 m distance to the river. This scenario particularly focuses on the effect of increased surface resistance and enhanced infiltration in the floodplain through forest vegetation. In the 100 m floodplain buffer area, grassland and cropland are converted into forest.

The **up- and downstream afforestation scenarios** aim to assess if afforestation is more effective upstream of Sippenaeken or downstream in terms of reducing the flood extend around the zoomed-in area (validation extent) and peak discharge close to the outlet at Meerssen. In both scenarios, the respective areas, grass- and cropland, are converted into forest.

The **full afforestation scenario** mirrors the one utilized to evaluate the impact of mid-aged forest parameterization.

In terms of spatial afforestation extent, higher forest cover is expected to result in larger flood peak and flood extent reduction due to increased infiltration (Johnen et al., 2020).

3.4.4 Hedgerows

A new LULC class with corresponding parameterization has been set up to implement hedgerows in the model. Multiple definitions can be found for hedgerows (Holden et al., 2019), but for this analysis, they will be considered as human-created systems of closely spaced shrubs. Infiltration zones are one of the suggested natural measures for flood mitigation by Naturkraacht.org (2023) for the Geul catchment. Their approach involves

implementing infiltration zones with 10-20 m widths parallel to the isolines at the end of hills and along streets. To allow comparison between the results of the studies and because a resolution of 20 m is used within this model setup, hedgerows will be assigned a width of 20 m. In analogy to the approach of Naturkraacht.org (2023), the hedgerows have been placed along isolines of 20 m increments, where land use was either grass- or cropland and on slopes larger than 7%. This selection process results in 21216 cells, which corresponds to an area of ca 8.5 km^2 with a total length of hedges of 424,32 km. In total this represents a LULC change of 2.5%. The LULC including hedgerows is presented in the appendix I.

Moreover, a Mannings'n of 1.2 reflects dense shrubs and is chosen for this LULC (U.S. Army Corps of Engineers, 2024). Furthermore, Holden et al. (2019) found out that the mean bulk density in the upper 50 cm of hedgerows was significantly lower, while organic matter content was higher in hedgerow soils than in surrounding arable fields. In alignment with findings of Holden et al. (2019), hedgerows have been further parameterized by locally lowering bulk density by 5% and are assigned an OMC of 4.5%. Herbst et al. (2006) investigated the interception of rainfall by hedgerows in southern England and derived a canopy storage capacity, S (mm), of 2.56 mm, which is also used as parameterization within this study. This approach might slightly overestimate interception since the storage capacity is directly assigned to the LULC class without accounting for the specific plant cover.

The effect of hedgerows will be tested for three rainfall scenarios: the July 2021 event rainfall, a 20% reduction of the event rainfall, and a 50% reduction of the event rainfall. This aims to analyze whether the effectivity of hedgerows increases for lower-intensity rainfall events.

Moreover, the fourth hedgerow scenario analyses how a different vegetation type, such as grassy field margins, influences the impact of a hedgerow. The scenario is implemented by solely changing Manning's n of the hedgerow LULC class to 0.06 (U.S. Army Corps of Engineers, 2024) and by keeping the rest of the parameters equal to the shrub hedgerow parameterization. Additionally, 50% reduced event rainfall is applied, as the expected effect is to be the most significant for the different rainfall scenarios. The different hedgerow LULC parameterizations are included in the appendix J.

The effect of hedgerows is expected to result in less runoff because of locally enhanced infiltration. Furthermore, the effect is expected to increase for less intensive rainfall events (Richet, Ouvry, and Saunier, 2017). Since expected annual damages can mainly be attributed to less intense flood events with high probability, their mitigation could result in a high economic benefit (Merz, Elmer, and Thieken, 2009). Furthermore, grass infiltration strips are expected to be less effective compared to dense shrub hedgerows as they are characterized by lower surface roughness, which is expressed in a lower Manning's n coefficient, resulting in higher flow velocities, ultimately decreasing the time for infiltration.

Table 3.4: Table with general overview of Scenarios

Scenario		Description	Study Type	Rainfall
	reference scenario	land use of 2021 used, (30% forest cover)	base scenario	July 2021
Afforestation broadleaf forest				
Temporal Dynamics	**winter forest cover**	full afforested catchment 92% with winter leaf cover,based on forest NDVI of Feb 2021, will be compared to summer leaf cover of mid-aged forest	parameter	July 2021
	mid-age forest	92% forest cover, plant cover based on NDVI July 2021, BD -10%, OMC 4.5%	parameter	July 2021
	young forest	92% forest cover, plant cover based on NDVI July 2021, BD -5%, OMC 4%	parameter	July 2021
	old forest	92% forest cover, plant cover based on NDVI July 2021, BD -10%, OMC 8%	parameter	July 2021
Spatial analysis	**full catchment**	same scenario as mid-age forest	LUCC	July 2021
	upstream afforestation	upstream of Sippenaeken afforested, additional 20% forest, mid-age forest parameterization used	LUCC	July 2021
	downstream afforestation	downstream of Sippenaeken afforested, additional 43% forest, mid-age forest parameterization used	LUCC	July 2021
	riparian afforestation	afforestation in river floodplain (100m buffer), additional 9% forest, mid-age forest parameterization used	LUCC	July 2021
	policy scenario	afforestation on slopes larger 10% in Dutch downstream catchment area, additional 7% forest, mid-age forest parameterization used	LUCC	July 2021
Hedgerows (Infiltration zones)				
	hedgerows ref	hedgerows, representing dense shrub (Manning's 1.2) along isolines with 20 m increments, where slope is larger 7%, (2.5% total catchment cover), BD - 5%, OMC 4.5%	LUCC	July 2021
	hedgerows -20% rain	hedgerows, representing dense shrub (Manning's 1.2) along isolines with 20 m increments, where slope is larger 7%, (2.5% total catchment cover), BD - 5%, OMC 4.5%	lower rainfall	0.8* July 2021
	hedgerows -50% rain	hedgerows, representing dense shrub (Manning's 1.2) along isolines with 20 m increments, where slope is larger 7%, (2.5% total catchment cover), BD - 5%, OMC 4.5%	lower rainfall	0.5* July 2021
	hedgerows grass -50% rain	hedgerows, representing grass stripes (Manning's 0.6) along isolines with 20 m increments, where slope is larger 7%, (2.5% total catchment cover), BD - 5%, OMC 4.5%	parameter & lower rainfall	0.5* July 2021

4

Results

In this section results of Calibration and Validation of the model will be discussed as well as the outcomes of the different afforestation and hedgerow scenarios. The findings will also be compared to findings of other studies and their plausibility and implications discussed.

4.1 Calibration

Final calibration choices included the lowering of initial saturated hydraulic conductivity (ksat) of the first soil layer by 30% and the ksat of the second soil layer by 70%. Soil layer depths were also part of the calibration and are shown in table 4.1. The SoilGrid's horizon reflects the layer in the database, which provided information on soil textural data. The ksat of the first layer was lowered, as rainfall peaks are not fully captured in the hourly rainfall data, which would have caused more runoff due to Horton overland flow. The decrease in ksat of the second soil layers is explained by the shallow soil conditions that are present in the upstream catchment area. This is also why a closed boundary is present in the model below the second soil layer where water can accumulate. The initial soil moisture was set exactly between field capacity and full saturation, which reflects the antecedent wet soil conditions prior to the event. Klein (2022) describes that in the month before the event on average 50 % more rainfall was recorded in the Geul catchment than the long-term average. Constant base flow was assumed, corresponding to the measured discharge at Sippenaeken before the flood event (11th of July 2021), which was 0.85 m^3/s. The calibrated spatial ksat distribution of the first and second soil layer as well as soil depths of the second soil layer are included in the appendix K.

Table 4.1: Soil layer depth properties

Area	Layer	max. soil depth (cm)	avg. soil depth (cm)	soilgrids horizon (cm)
Upstream (BE+DE)	Layer 1	30	30	15 - 30
	Layer 2	300	238	15 - 30
Downstream (NL+DE)	Layer 1	30	30	15 - 30
	Layer 2	500	411	15 - 30

The below figures 4.1 and 4.2 show simulated and observed water level hydrographs at the sub-catchment outlet in Sippenaeken and at Kelmis, which is located further upstream in the calibration domain (figure 3.6). The different calibration steps leading to the best simulation are presented in the appendix L.

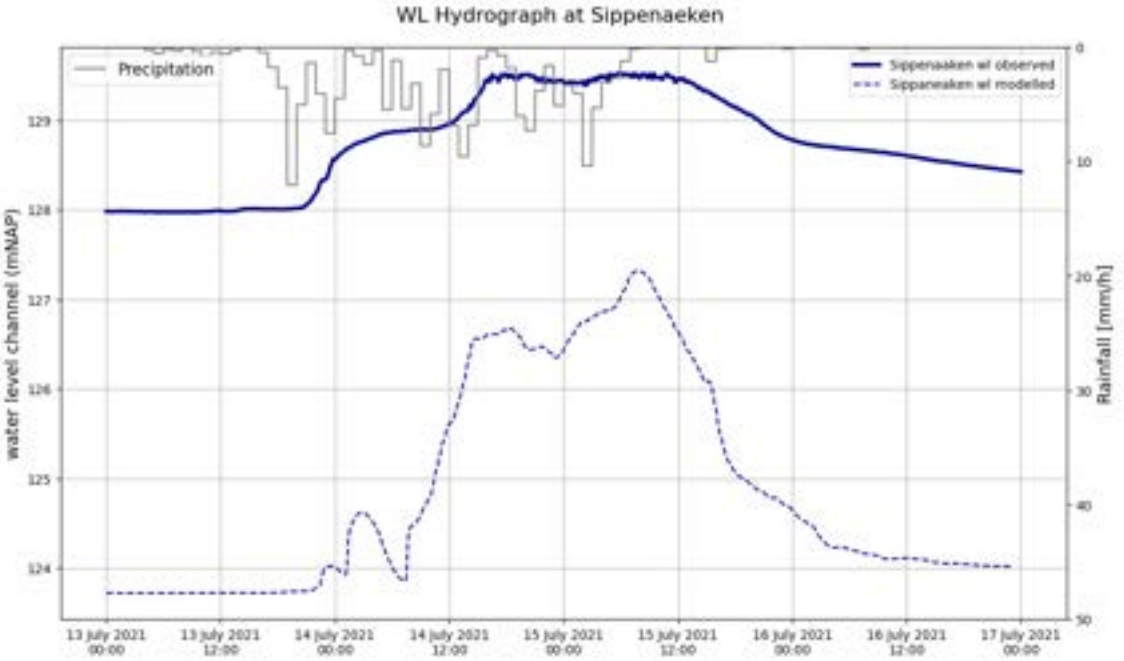

Figure 4.1: Comparison of observed and simulated channel discharge at Kelmis Sippenaeken

Figure 4.1 shows, that the simulated channel water levels at Sippenaeken are underestimated. Furthermore, the simulated increase in discharge by approximately 3 m differs strongly compared to the observed water level increase by 1.5 m, which results in a NSE of -0.91 (0 is the same predictability as the average, 1 is the perfect fit). The reasons for the deviations are discussed below.

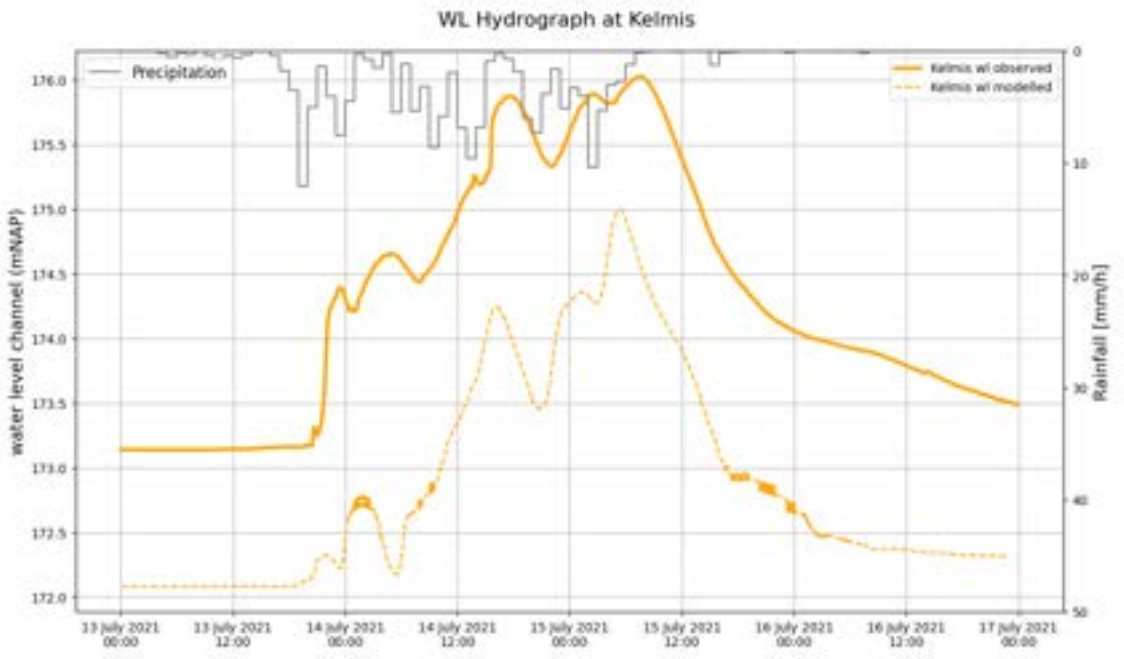

Figure 4.2: Comparison of observed and simulated channel discharge at Kelmis Sippenaeken

The simulated water levels at Kelmis, presented in figure 4.2 are generally underestimated, which results in a NSE of 0.53. Nevertheless, the changes in water levels are captured well by the model. Both simulated and observed water levels show a maximum increase of approximately 3 m.

The differences and underestimation of simulated and observed total water levels might be attributed to some extent to elevation differences in the used DEM and the real elevation at the observation stations. Those differences arise from resampling the DEM to a larger resolution (5m to 20m) and consequently averaging elevation values over a larger area. Moreover, the cubic b spline resampling method causes smoothing of the DEM, which is beneficial for simulating hydrodynamic processes in the model but might further be an explanation for the offset between simulated and observed water absolute water level. Furthermore, during a field visit in May 2024 at the measurement station in Sippenaeken, it was observed that the present flow dynamics at the measurement locations are complex and cannot be fully transferred to the simplicity of the models' channel network representation. At the measurement location in Sippenaeken, water is dammed up in the river in a little reservoir. Also, a second channel exists leading to a historic mill, which was closed during the visit but can potentially overflow at high rainfall events or be opened. This would increase the river width by a factor of approximately 1.5 and explains why the initial observed water increases relatively less over the event compared to the simulated water

level. The validity of the measurement data at Sippenaeken at those high water levels could also not be fully confirmed.

The below figure 4.3 shows simulated and observed discharge hydrographs at Sippenaeken and at Kelmis for the final calibration.

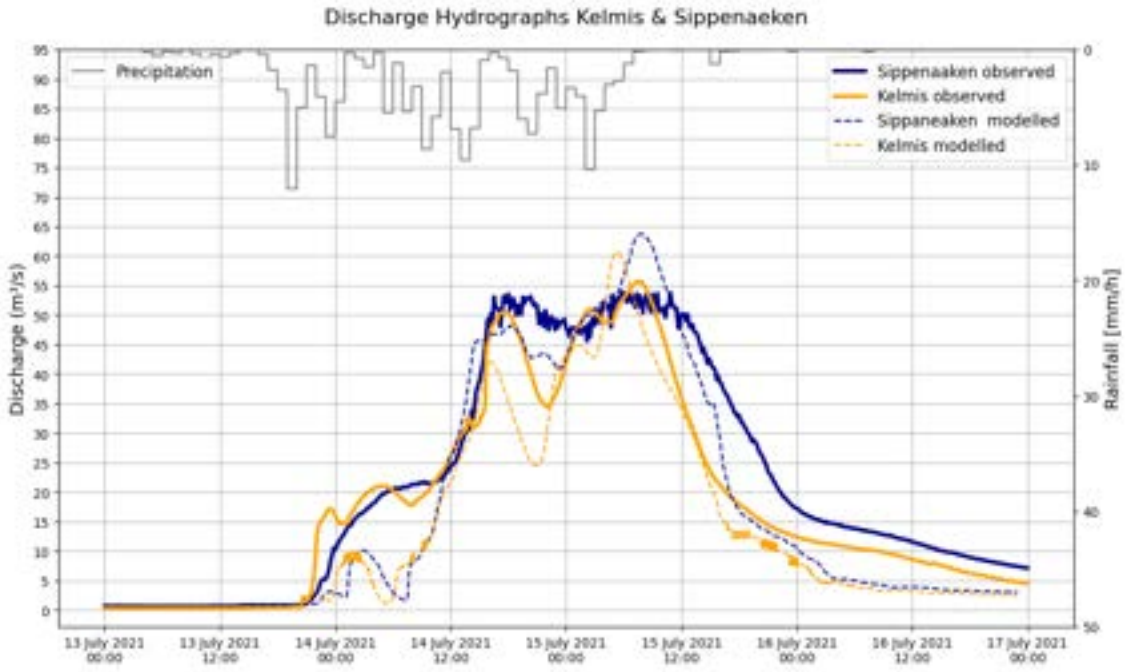

Figure 4.3: Comparison of observed and simulated channel discharge at Kelmis Sippenaeken - final calibration

The final chosen calibration performs well in simulating changes in discharges at Kelmis and Sippenaeken during the event, resulting in a NSE of 0.82 and 0.83, respectively. It can be observed that for both Kelmis and Sippenaeken, the first peak is underestimated. This means that some processes leading to the quick initial catchment response are not fully captured by the model. Moreover, the first larger peak discharge is underestimated for both locations and simulations, and the maximum flood peak is slightly overestimated. Nonetheless, as described before, observed discharges must be considered carefully since the used rating curves are assigned with uncertainty for extreme discharges.

Ultimately, the accuracy of the simulated and measured discharge and water levels at Kelmis is weighted with higher confidence than the water levels and discharge at Sippenaeken. Especially the change in water level at Kelmis is captured in the simulation well, despite the general offset. This resulted in the conclusion that the above-presented calibration setup should be proceeded with for the further analysis.

4.2 Validation

For validation, the calibration setup of the upstream catchment was applied to the full catchment extent of the Geul. In contrast to the calibration setup the maximum depth of the second soil layer in the downstream part of the catchment was increased to 5m to account for deeper soils present in that part of the catchment (final soil depths shown in appendix K). Furthermore, constant baseflow at the outlet near Meerssen was assumed to be 1.5 m^3/s. This corresponds to the measured discharge at Meerssen on July 12 in 2021. Figure 4.4 shows simulated and observed water levels during the rainfall event at the outlet in Meerssen.

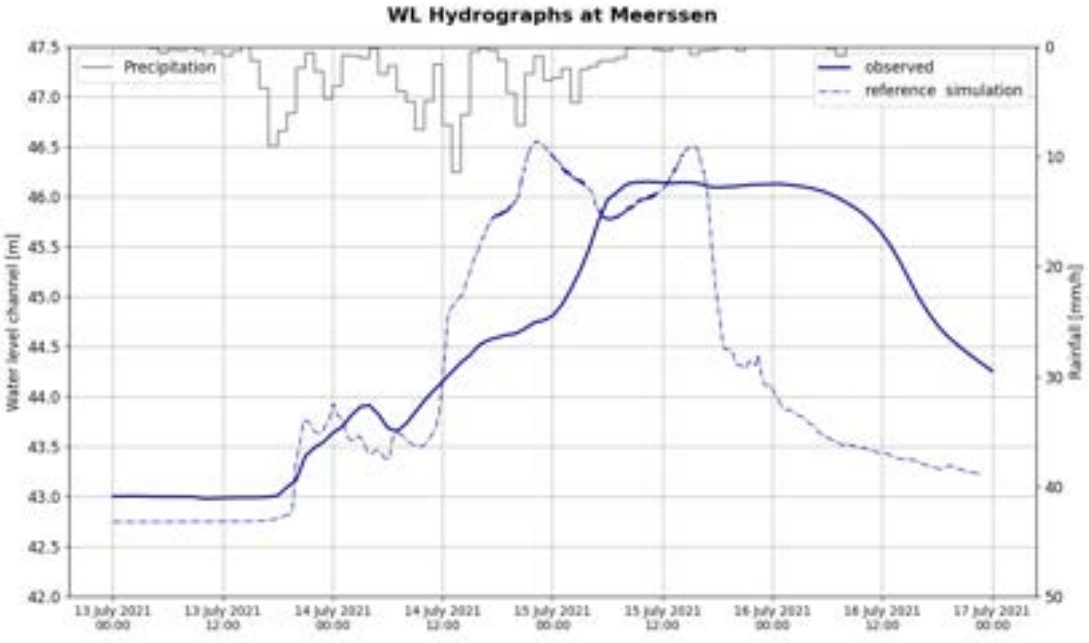

Figure 4.4: Comparison of observed and simulated channel water levels at Meerssen

The NSE of the simulation of water levels at Meerssen for the event is -0.0397. It can be observed that the flood wave arrives quicker in the simulation than in reality. This might be attributed to the resolution of the model, which reduces the natural re-meandering of the river, ultimately transporting the water quicker downstream than in reality. The simulated peak water levels are slightly overestimated. At the end of the event, the simulated WL drops very quickly, compared to the observation, which shows a rather gradual decrease. This might be explained by the partly blocked culvert close to Meerssen during the event, where a diver guides the channel below the Juliana Canal, which ultimately resulted in less water flow through the diver. Moreover, the backwater effect from the Meuse River is not

accounted for in the simulation. The flood peak of Meuse and Geul arrived simultaneously at the confluence of the two rivers Van Heeringen et al. (2022).

For validation and later analysis, a zoomed-in flood extent along the Geul encompassing the cities of Valkenburg, Schin op Geul, Gulpen, and Partij was also considered. The comparison of simulated and observed flood extent for that area is shown in figure 4.5. The threshold for flooding is set at surface water levels larger than 5 cm.

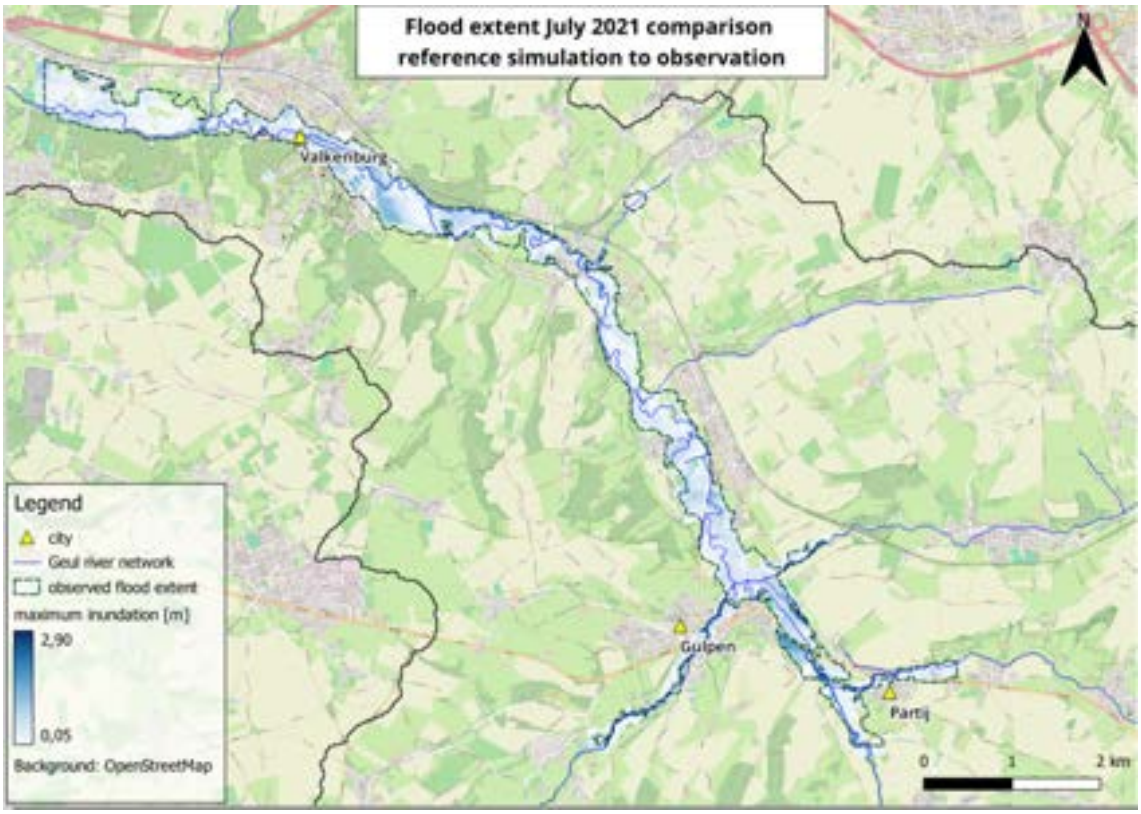

Figure 4.5: Comparison of simulated and observed flood extent

The following performance metrics for the simulation of flood extent could be determined, which are presented in table 4.2.

Table 4.2: Performance metrics simulation for zoomed-in flood extent

Hit rate	80.62
False rate	14.94
CSI	84.37
Bias	0.73

The hit rate of over 80 % suggests that the largest portion of observed flooding is cap-

tured by the model. The false rate (false positives) is low, indicating that 14 % of the simulated flooded area is not included in the observations. The bias of 0.7, representing the ratio of false positives to false negatives, illustrates that the model is more likely to underestimate the flood extent than overestimate it. The CSI of about 84, which puts the hit rate and false rate into perspective, is high and indicates an overall good performance of the flood extent simulation (a CSI of 100 would be a perfect fit).
Despite the offset in simulated water level compared to the observations, in the zoomed-in area, the simulated flood extent is quite accurately predicted, suggesting that the model captures the flow processes during the event quite well. Consequently, the applied calibration parameters will be used for further analysis. Simulated flood extent and discharge will be used to evaluate the effect of afforestation and hedgerow measures. The assessment of afforestation and hedgerows based on event discharges allows the comparison to other modeling studies. Nevertheless, simulated discharges at Meerssen could not be validated to observations as discharge data for the flood event is not available because of malfunctions of measurement stations (Klein, 2022; Van Heeringen et al., 2022; Slager et al., 2022a).

4.3 Results afforestation

In this section, the results of the temporal dynamic and spatial afforestation scenarios will be presented. Additionally, their plausibility will be evaluated and findings be compared to those from other studies. Ultimately, the implications of the results will be discussed.

4.3.1 Temporal dynamic afforestation scenarios

Figure 4.6 shows the event discharge time series for different afforestation parameterizations at Meerssen, which reflect temporal dynamic differences as they can be observed between "young", "mid-aged", and "old" forests. All three parameterizations represent 92% forest cover. Also, the simulated discharge of the reference scenario with 30% forest cover, which uses the "mid-aged" forest parameterization and represents the actual LULC in 2021, is visualized. Exact peak discharge volumes and timing for Meerssen and Valkenburg are given in table 4.3

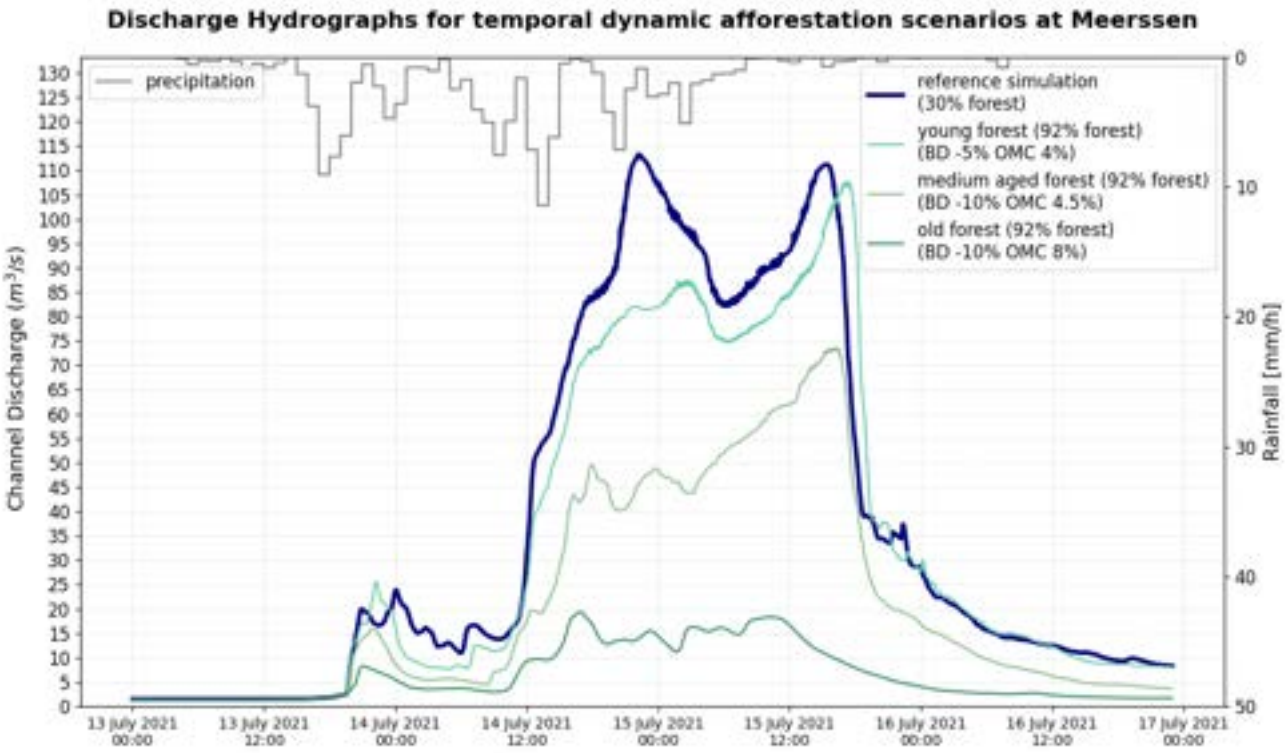

Figure 4.6: Simulated discharges at Meerssen for different forest parameterizations reflecting temporal dynamics

Before discussing the differences in discharges between the different forest parameteriza-

tions, it is important to point out the effect of increased forest cover between the reference scenario and "mid-aged" forest parameterization, which use the same forest parameterizations and solely differ in forest extent.

For the **"mid-aged" forest** scenario, reflecting the conversion of all crop- and grassland into forest, the peak discharge at Meerssen reduces by 34.89 % from 113.23 m^3/s to 73.51m^3/s (table 4.3). Moreover, the peak discharge is delayed by approximately 18 hours because the first of the larger peaks on the night of the 14th of July is significantly lowered by approximately 65 m^3/s (figure 4.6 and table 4.3). Ultimately, the zoomed-in flood extent is lowered by 27.9% from 4.84 km^2 to 3.49 km^2, and on the catchment scale, the flood extent decreases by 35.08 % from 24.43 km^2 to 23.21 km^2 (table 4.4).

Table 4.3: Effect of temporal dynamic afforestation scenarios on peak flow at Meerssen and Valkenburg

Scenario	**Location**	**Peak Discharge Q [m^3/s]**	**Time**	**Q Diff. to "mid-aged"** ΔQ[%]	**Q Diff. to reference** ΔQ[%]
reference (30% forest)	Meerssen	113.23	14.07.21 22:19	-	-
(-10% BD 4.5% OMC)	Valkenburg	92.24	14.07.21 19:12	-	-
winter leaf cover (92% forest)	Meerssen	73.72	15.07.21 16:25	+ 0.29	-34.89
(-10% BD 4.5% OMC)	Valkenburg	76	15.07.21 09:07	+0.70	-18.02
"mid-aged" (92% forest)	Meerssen	73.51	15.07.21 16:13	-	-35.08
(-10% BD 4.5% OMC)	Valkenburg	75.47	15.07.21 14:18	-	-18.18
"young" (92% forest)	Meerssen	108	15.07.21 17:18	+46.92	-5.03
(-5% BD 4% OMC)	Valkenburg	90.19	15.07.21 14:24	+19.50	-2.22
"old" (92% forest)	Meerssen	19.32	14.07.21 15:21	-73.72	-82.94
(-10% BD 8% OMC)	Valkenburg	17.85	15.07.21 09:07	-76.35	-80.65

However, simulated discharges at Meerssen vary significantly for different parameterizations. This is why discharges at Meerssen and flood extents in the catchment of "young" and "old forest" scenarios will be compared to the "mid-aged" forest scenario. The **"young" forest** parameterization, representing solely a 5% reduction in BD instead of 10% for the "mid-aged" scenario and an OMC of 4% instead of 4.5%, results in a peak discharge of 108 m^3/s, which is approximately 47% higher than the peak discharge of the "mid-aged" scenario (table 4.3). Furthermore, the flood extent for the "young" forest scenario, with 4.83 km^2 for the zoomed-in extent and 23.21 km^2 on the total catchment scale, is significantly larger compared to the "mid-aged" forest scenario with an increase

of approximately 38% and 46% respectively (table (4.4). With a maximum discharge of 19.32 m^3/s, the peak flow at Meerssen for the **"old" forest** scenario, representing solely an increase in OMC by 3.5% compared to the "mid-aged" scenario, is approximately 76% lower than the "mid-aged" forest scenario (figure 4.7). Moreover, the simulated zoomed-in flood extent is 0.83 km^2 and thus 76% lower than the "mid-aged" forest scenario's flood extent (table 4.4). Visualizations of the reduction of zoomed-in flood extent for "young", "mid-aged" and "old" afforest scenarios can be found in the appendix M.

Table 4.4: Flood extents for temporal dynamic afforestation scenarios

Scenario	**Flood Extend "zoome-in" [km²] [%]**	**Diff. to "mid-aged" [%]**	**Diff. to reference [%]**	**Flood Extend Catchment [km²]**	**Diff. to "mid-aged" [%]**	**Diff. to reference [%]**
reference (30% forest) (-5% BD 4% OMC)	4.84	-	-	24.43	-	-
winter leaf cover (92% forest) (-10% BD 4.5% OMC)	3.50	+0.29	-27.83	15.89	0.00	-34.95
"mid-aged" (92% forest) (-10% BD 4.5% OMC)	3.49	-	-27.90	15.89	-	-34.95
"young" (92% forest) (-5% BD 4% OMC)	4.83	+38.40	-0.38	23.21	+46.01	-5.01
"old" (92% forest) (-10% BD 8% OMC)	0.83	-76.22	-82.78	4.47	-71.87	-81.71

Furthermore, it was also analyzed how **seasonality** influences the effect of a broad-leaf forest on flooding as canopy cover is reduced in winter. Table 4.5 shows the catchment totals for rainfall, interception, infiltration, outflow and runoff ratio for the different temporal dynamic afforestation scenarios.

It can be observed that afforestation assuming summer leaf cover, which is used for all of the scenarios except the winter scenario, leads to a reduction in total interception from 1.49mm to 1.38 mm (table 4.5). In contrast to this simulated reduction, Zhong et al. (2022) state that, generally, forests can intercept more water as short vegetation due to their larger canopy storage and wood storage. The differences can be linked back to the calculation of canopy interception within openLISEM, which is governed by NDVI-derived LAI and plant-specific empirical leaf storage according to Hoyningen-Huene (1983) as explained in chapter 3. Because wood storage is not accounted for in openLISEM, the model seems

to underestimate the interception of broadleaf forests. Other models, such as wflow_sbm, account for the effect of wood storage (Verseveld et al., 2022).

Table 4.5: Total simulation stats for forest parameterization scenarios

Scenario	Rainfall, P [mm]	Outflow, Q [mm]	Q/P [%]	Interception [mm]	Infiltration [mm]
reference scenario (30% forest) (-10% BD) (4.5% OMC)	141.14	35.22	24.98	1.49	93.54
winter leaf cover(92% forest) (-10% BD) (4.5% OMC)	141.14	19.73	13.98	0.05	115.42
"mid-aged" forest (92% forest) (-10% BD) (4.5% OMC)	141.14	19.48	13.8	1.38	114.3
"young" forest (92% forest) (-5% BD 4% OMC)	141.14	16	22.58	1.38	98.11
"old" forest (92% forest) (-10% BD) (8% OMC)	141.14	5.08	3.60	1.38	131.91

Furthermore, it can be observed that for the **winter leaf cover** scenario with "mid-age" forest parameterization, interception decreases to 0.05 mm. Nonetheless, the effect on peak discharge and outflow are minor, as shown in table 4.5 and table 4.3. Peak discharge increases from 73.51 m^3/s for summer leaf cover to 73.72 m^3/s for winter leaf cover and total outflow, from 19.48 mm to 19.73 mm. Moreover, the zoomed-in flood extent only increased slightly by 0.29% for winter leaf cover (table 4.4). This shows that interception and, thus, seasonal changes in leaf cover do not significantly influence peak flow magnitudes and flood extents for this event. This confirms the expectations as Rogger et al. (2017) state that during intense rainfalls, the effect of interception is overwhelmed by the amount of incoming precipitation.

In summary, it can be concluded that different forest parameterizations reflecting forest maturity, result in quite significantly different simulated discharges and flood extents. This shows that the outcome of the simulation for full afforestation is highly sensitive to the choices in parameterization. The biggest influence can be attributed to increased infiltration through higher organic matter content and lowering of the bulk density in the first soil layer. This alters soil hydraulic properties such as porosity and saturated hydraulic conductivity (ksat), as can be seen in table 4.6, which displays the average porosity and ksat of the first soil layer in the catchment for the different scenarios. For the "young" forest scenario, the average porosity lies at 55% and average ksat at 22.77 mm/hr (table 4.6), for a further decrease of 5% in BD and additional 0.5% OMC reflecting "mid-aged" forest, the average porosity in the catchment increases to 58% and the average ksat to

33.39 mm/hr. The "old" forest scenario shows the highest average porosity and ksat, with 66% and 62.24 mm/hr, respectively.

It can be observed that the lowering of BD and increase in OMC increases average porosity and ksat in the catchment. Ultimately, this leads to increased water storage in the soil and larger infiltration capacity, which is reflected in the change in infiltration ratios, representing the ratio of total infiltration to total incoming rainfall, which are visualized in the appendix O for the different forest parameterizations. Table 4.5 also shows that increased infiltration reduces the runoff ratio (Q/P), consequently lowering the overland flow volume contributing to stream flow.

Especially the increase in OMC from 4.5% to 8% caused a large increase in total infiltration. For the derivation of the within openLISEM applied pedotransfer functions by Saxton and Rawls, 2006, soil samples with OMC higher than 8% were excluded. Therefore, an OMC 8% represents the largest value that can be used for simulations using that method. In addition, the relative decrease in BD by 10% also defines the maximum value for this parameter, as further lowering can cause erroneous results (Jetten and Bout, 2018). This means that the "old" forest scenario represents the most extreme influence a LULC can have on soil hydraulic functions in the model.

Table 4.6: Catchment averages of porosity and ksat for forest parameterization scenarios

Scenario	**Average Porosity** [-]	**Average Ksat** [mm/hr]
reference (30% forest) (-10% BD 4.5% OMC)	0.54	20.26
"mid-aged" (92% forest) (-10% BD 4.5% OMC)	0.58	33.39
"young" (92% forest) (-5% BD 4% OMC)	0.55	22.77
"old" (92% forest) (-10% BD 8% OMC)	0.66	62.24

Kuiper (2023) used openLISEM to analyze the effect of afforestation in the upper Geul sub-catchment, with Kelmis as the outlet, for the 2021 rainfall event. There, the simulated event peak discharge at Kelmis decreased from 59.9 m^3/s to 22.3 m^3/s for full afforestation (grass- and cropland to forest), which reflects a peak discharge reduction of 37 %. Within the here presented study, the simulated effect of full afforestation on discharge at Kelmis shows a reduction of 5.2% from 58 m^3/s to 55 m^3/s for "mid-aged" forest parameterization, which has also been used by Jetten (2022) and represents current forest characteristics in the catchment (explained in 3). Nevertheless, due to the aforementioned reasons, the magnitude of simulated peak flow reduction at Kelmis changed for "young" and "old" forest parameterization. For "young" forest parameterization, the peak discharge at Kelmis lies at 57.8 m^3/s, and for "old" forest parameterization, the peak streamflow Kelmis is $11 m^3/s$

under full catchment afforestation. The discharge hydrographs at Kelmis for different forest parameterizations are presented in the appendix N. This further confirms that the effect of afforestation on discharge is highly sensitive to its parameterization, which was also pointed out by Kuiper (2023). For comparison, the forest parameterization of Kuiper (2023) is shown in table 4.7.

Table 4.7: Forest parameterization used by Kuiper (2023)

LULC	RR [cm]	Manning's n [-]	rel. BD [-]	additional OMC [%]
Forest	2	0.1	0.9	1

The only difference in forest parameterization can be observed in OMC. The study of Kuiper (2023) followed the approach to use OMC data derived from SoilGrids and to add 1% OMC, where forest is present. In contrast, this study follows the approach of Jetten (2022) where each LULC class is assigned directly an absolute OMC value dependent on literature and local observations. The latter method guarantees that the maximum OMC of 8% in the soil is not exceeded as otherwise, the used PTFs are not valid anymore (Saxton and Rawls, 2006). Other differences in the results to Kuiper might arise from differences in soil depths, as Kuiper (2023) assigned the first soil layer a thickness of 40 cm, which would cause a larger increase in soil storage as porosity changes due to afforestation. This points out that the by openLISEM simulated effect of afforestation also depends on the thickness of the first soil layer, whose soil hydraulics and storage are influenced by the respective LULC, such as a forest.

The improvement of soil hydraulic functions through increased OMC is also reported in studies of Nijpels (2018), Rutgers and al. (2014), and Osman (2013). Hudson (1994) state that due to its influence on soil aggregation and pore space distribution, an increase in OMC enhances the water retention in the soil and the hydraulic conductivity. Nevertheless, the soil-improving functions of a forest and associated timescales depend on previous land use and also on tree species (Hüblová and Frouz, 2021).

Ultimately, the study of the temporal dynamics in forests demonstrates the general potential of improving the organic matter content in soils to reduce floods. Besides afforestation, which needs a long time to establish improved soil functions, also alternative measures should be considered, e.g., through the improvement of agricultural management techniques, such as no-tillage management (Faiz et al., 2022; He et al., 2009. Furthermore, also the addition of biochar has been reported to improve carbon sequestration in the soil and to increase infiltration through improving soil hydrological functions (Novak et al., 2016). Agricultural production could also benefit from enhanced fertility through higher OMC. Nonetheless, the effect of soil organic matter levels on the nutrient balance is complex and also influenced by sand and clay soil composition (Luske et al., 2014).

The strong sensitivity of openLISEM and its modeled infiltration to an increase in OMC has not been reported by the literature so far and represents one of this study's novel findings.

4.3.2 Results for spatial afforestation scenarios

Figure 4.7 shows simulated discharges at Meerssen for different spatial afforestation scenarios in the Geul catchment during the heavy rainfall event from July 13 to 17 in 2021. The impacts of the different spatial scenarios on catchment flood extent and zoomed-in flood extent, which encompasses the cities of Valkenburg, Schin op Geul, Gulpen, and Partij, is displayed in table 4.9. For the spatial afforestation scenarios, the "mid-age" forest parameterization is used, reflecting a lowering of BD by 10% and OMC of 4.5% and represents current forest characteristics in the catchment.

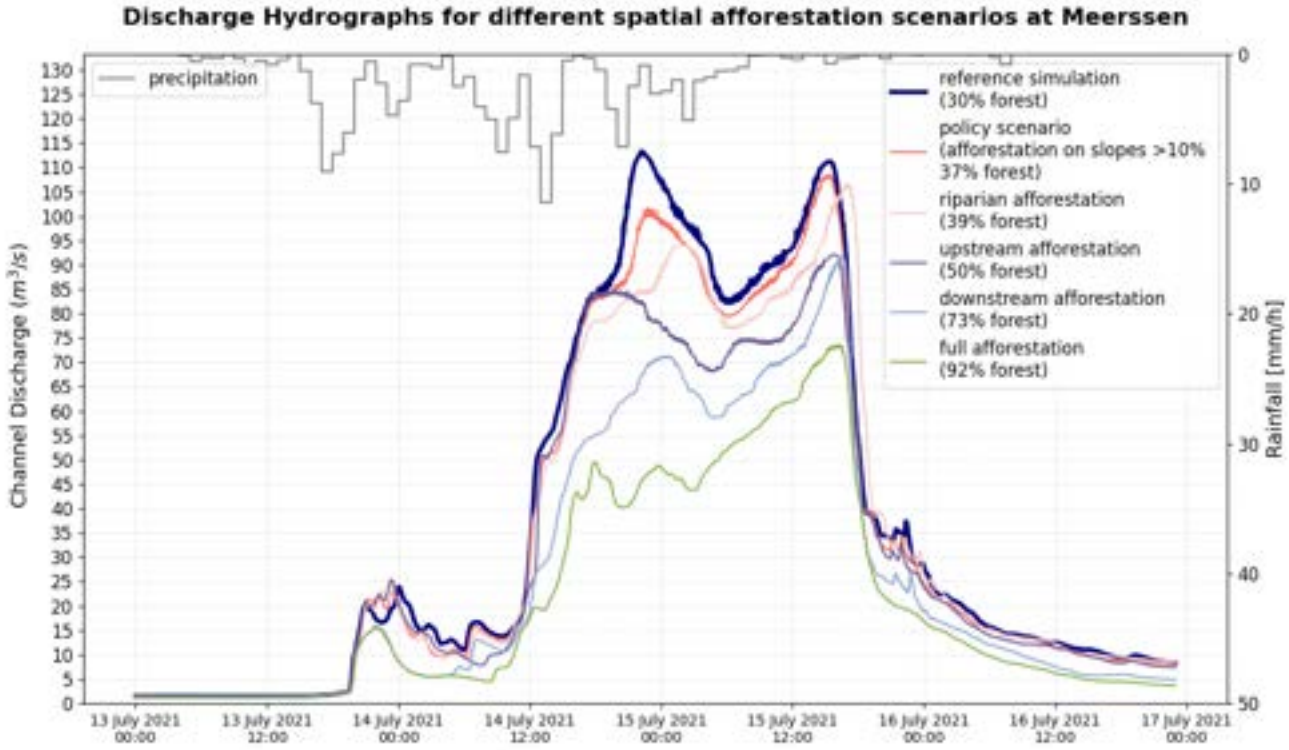

Figure 4.7: Simulated discharges at Meerssen for different spatial afforestation scenarios

In general, it can be observed that each of the afforestation scenarios lowers the peak discharge at Meerssen (figure 4.7). Moreover, for all of the examined scenarios, the first of the two larger peak flows, which occurred during the night of the 14th, is lowered more significantly than the second peak during the night of the 15th. This is quite relevant as in the simulated discharge under current land use (reference scenario), the first of the two larger peaks shows the highest flow rates, whereas, for the afforestation scenarios, the second of the two high peaks represents the maximum flow rates. This causes a delay in

flood peak of at least 17 hours for all of the afforestation scenarios, as can be derived from figure 4.7 and table 4.8.

Figure 4.7 shows that the smallest peak flow reduction is caused by the **policy scenario**, where slopes larger than 10% are afforested in the Dutch part of the catchment, increasing total forest cover by 7% to 37%. This results in a peak discharge reduction of 4% (table 4.8). Moreover, in the policy scenario, per kilometer change of forest cover, peak discharge decreases on average by 0.19%. This relationship is outlined in table 4.8 under the term "land use and land cover change (LUCC) efficiency".

Table 4.8: Effect of different spatial afforestation scenarios on peak flow

Scenarios*	**Location**	**Peak Discharge** $Q_p[m^3/s]$	**Time**	**Diff. to Ref.** ΔQ_p [%]	**LUCC efficiency**** $\Delta Q_p/A$ [%/km^2]
reference scenario	Meerssen	113.23	14.07.21 22:19	-	-
(30% forest)	Valkenburg	92.24	14.07.21 19:12	-	
policy scenario (slopes)	Meerssen	108.4	15.07.21 15:22	-4.27	-0.19
(37% forest)	Valkenburg	90.37	15.07.21 12:43	-2.03	
riparian afforestation	Meerssen	107	15.07.21 17:02	-5.91	-0.20
(39% forest)	Valkenburg	89.49	15.07.21 14:24	-2.98	
upstream afforestation	Meerssen	92.1	15.07.21 15:50	-18.66	-0.28
(50% forest)	Valkenburg	82.81	14.07.21 18:03	-10.22	
downstream afforestation	Meerssen	91.88	15.07.21 16:34	-18.86	-0.13
(73% forest)	Valkenburg	83.59	15.07.21 01:23	-9.38	
full afforestation	Meerssen	73.51	15.07.21 16:25	-34.89	-0.17
(92% forest)	Valkenburg	75.47	15.07.21 09:07	-18.02	

* "mid-aged" forest parameterization used ** Decrease in peak discharge (Q_p)per area (A) of new converted forest

Furthermore, the zoomed-in flood extent decreases by 3.29 % to 4.69 km^2 as shown in table 4.9. Instead of planting forest on hill-slopes, the **riparian afforestation** scenario represents the afforestation in a buffer zone of 100 m width next to the river, which represents its floodplain. This results in a forest cover increase by 9 % to 39 %, which is comparable to the policy scenario. As a consequence, peak discharge at Meerssen reduces by 5.91 % to 107 m^3/s compared to the reference scenario. The LUCC efficiency is almost the same as for the policy scenario and lies at a reduction of 0.20 % of peak discharge

per square kilometer increase in forest cover. Nevertheless, the zoomed-in flood extent decreases just by 1.16 %, which is less than for the policy scenario. This phenomenon can also be observed for the full catchment flood extent, which reduces by 0.85 % for riparian afforestation compared to a reduction of 3.12 % for the policy scenario (table 4.9).

This shows that although floodplain afforestation is more effective in reducing the peak flow, afforestation on slopes is more effective in reducing the overall flood extent in the catchment. Differences arise because floodplain afforestation increases surface resistance next to the river, which lowers the flow velocity but can also lead to a local increase in water height. This has also been observed in the study of Kiss et al. (2019), which found that the removal of invasive plant species in the floodplain reduced peak flood stages. Also, the study of Chow (1959) shows that channel and floodplain roughness changes flow conditions. This indicates that it is important to consider both flood extent and peak flow in the analysis of the effect of land use changes.

Table 4.9: Flood extents for different spatial afforestation scenarios

Scenarios*	**Flood Extent Selection** [km^2]	**Diff. to ref.** [%]	**Flood Extent Catchment** [km^2]	**Diff. to ref.** [%]
reference (30% forest)	4.84	-	24.43	-
policy scenario (slopes) (37% forest)	4.69	-3.29	23.67	-3.12
riparian afforestation (39% forest)	4.79	-1.16	24.27	-0.85
upstream afforestation (50% forest)	4.34	-10.40	22.35	-8.55
downstream afforestation (73% forest)	3.90	-19.57	17.96	-26.52
full afforestation (92% forest)	3.50	-27.90	15.89	-34.95

* "mid-aged" forest parameterization used

The rapid assessment study of Slager et al. (2022b) for the July 2021 event also investigated the flood mitigating effects of afforestation on hill-slopes and in the floodplain using the coupled wflow_sbm Sobek model as described in section 2.5.1. In wflow_sbm the re-

forestation on hills and plateaus (+10 to +20% of the basin) resulted in a simulated peak discharge decrease at Valkenburg of 1-2%. Moreover, afforestation in the central floodplain (+10 to +20% of the river valley) led to a simulated reduction in peak discharge of 4-7%. Both findings are in range with the results of this openLISEM modeling study, with a 2% peak discharge decrease at Valkenburg for slope afforestation in the policy scenario and a 3% decrease in peak discharge for riparian afforestation (table 4.8). Nevertheless, as the rapid assessment simulation does not account for flood extent, the conclusions differ. So does the study of Slager et al. (2022b) assign riparian afforestation a higher flood mitigating effect than hill-slope afforestation because it reduces the peak discharge more significantly. But this study showed that hill-slope afforestation can actually have slightly larger flood-mitigating impacts compared to riparian afforestation on a regional scale as it reduces the flood extent more significantly in the zoomed-in area (table 4.9).

However, floodplain afforestation might be effective if applied at a further distance to urban areas, where larger flood extents due to increased surface resistance do not result in damage but allow more water to infiltrate the floodplain. This should be part of further research. It is also important to mention that the larger flood peak reduction through riparian afforestation is more effective in reducing the stream flow contribution of the Geul to the Meuse, which means that the conclusion of Slager et al. (2022b) is valid, in regards to the downstream Meuse basin.

Besides the spatial distribution of forest, upstream and downstream afforestation also differ in forest extents, which results in different catchment totals 4.10.

Table 4.10: Total simulation stats for spatial afforestation scenarios

Scenarios*	**Rainfall, P** [mm]	**Outflow, Q** [mm]	**Q/P** [%]	**Interception** [mm]	**Infiltration** [mm]
reference scenario (30% forest)	141.14	35.22	24.98	1.49	93.54
policy scenario (37% forest)	141.14	33.26	23.59	1.48	95.70
riparian afforestation (39% forest)	141.14	32.84	23.29	1.47	96.07
upstream afforestation (50% forest)	141.14	30.06	21.32	1.46	99.78
downstream afforestation (73% forest)	141.14	24.58	17.43	1.40	107.96
full afforestation (92% forest)	141.14	19.48	13.8	1.38	114.3

* "mid-aged" forest parameterization used

Downstream afforestation results in enhanced total infiltration of 107.96 mm, which causes a reduction in total outflow from 35.22 mm to 24.58 mm, compared to the reference simulation, ultimately decreasing the runoff coefficient to 17.43 % (table 4.10). For the **upstream afforestation** scenario the runoff coefficient lies at 21.32 %, because total catchment infiltration is less compared to the downstream scenario. This difference can be attributed to the variation in forest extent, which results in a larger area where infiltration and soil storage is enhanced. The peak discharges at Meerssen in the two scenarios are almost equal, as both upstream and downstream afforestation lower the peak discharge by approximately 19% to 92 m^3/s.

Nevertheless, due to the spatial and temporal variations in rainfall, the runoff in the Dutch downstream part mainly contributes to the first large flood peak, while the Belgian upstream part mainly contributes to the second large flood peak. This is also reflected in the effect of the afforestation scenarios; as for the upstream afforestation scenario, the discharge curve follows the reference discharge curve until approximately the 14th of July at 20:00 (figure 4.7). For the downstream afforestation scenario, the effect is immediate, but after the 15th of July, around 6:00, the increase in discharge is stronger compared to the upstream afforestation scenario, which reflects the unchanged contribution of runoff from the upstream catchment.

The LUCC efficiency in table 4.8 of -0.28 $\%/km^2$ reflects that upstream afforestation is more effective in terms of lowering the discharge peak at Meerssen per square kilometer increase in forest cover in the catchment, than downstream afforestation where the LULC efficiency lies at -0.13 $\%/km^2$. The higher LUCC efficiency for the upstream afforestation can be attributed to the fact that during the 2021 rainfall scenario, most of the rainfall occurred in the upstream Belgian part of the catchment as visualized in figure 2.3 and the highest proportion of runoff was generated there. Thus, an increase in infiltration capacity through afforestation in the upstream catchment has a more significant impact. Nonetheless, the lower LUCC efficiency does not necessarily indicate a lower return on investment for the downstream scenario, as described below.

Table 4.9 shows the comparison of the flood extents of the two scenarios. It can be observed that the decrease in flood extent on the catchment scale, but also for the zoomed-in area, decreases for the downstream afforestation scenario by 26.52% to 17.96 km^2 and by 19.57% to 3.90 km^2 respectively. On the other hand, upstream afforestation reduces flooding on the catchment scale by 8.55% to 22.35 km^2 and in the zoomed-in extent by 10.40% to 4,34 km^2. Because measured peak discharges are almost equal, it is important to explain why the differences in flood extent between the two scenarios occur. Therefore, the exact flood extent for the zoomed-in area covering the cities of Valkenburg, Schin op Geul, and Gulpen has been visualized in figure 4.8.

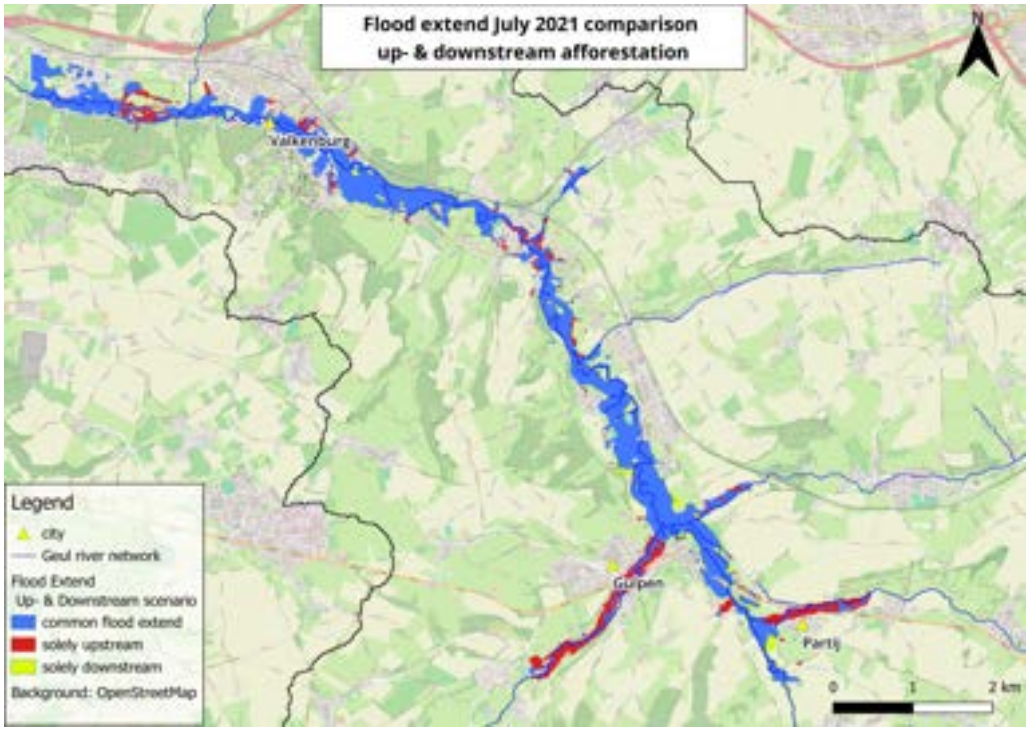

Figure 4.8: Comparison of flood extents for up & downstream afforestation

The most significant differences can be observed in the area of Partij and Gulpen, where the tributaries Selzerbeek and Gulp join the Geul. Here, downstream afforestation reduces the incoming water of the tributaries and, consequently, the flood extent. Upstream afforestation does not affect the Gulp and Selzerbeek sub-catchments, and therefore, significantly more flooding occurs in proximity to the outlet of the two tributaries. In the floodplain along the main channel, differences are smaller and probably caused by locally changed surface roughness and infiltration behavior in the floodplain.

The comparison shows that the contribution of water from the upstream area is quite significant, as the flood extent along the main channel is quite similar, which also corresponds to findings of Klein (2022). Nevertheless, the contribution of other tributaries, such as the Gulp and Selzerbeek, is still significant, and afforestation in those sub-catchments also has the potential to reduce flooding in populated areas such as Gulpen and Partij adjacent to tributaries of the Geul. More detailed scenarios should be evaluated by looking at the effect of upstream afforestation within the specific sub-catchments individually. Nevertheless, the impact of afforestation is also largely influenced by the distribution of incoming rainfall.

The largest effect can be observed for the **full catchment afforestation**, where around 60% of the catchment cover is altered to forest, resulting in a final forest cover of 92% of the catchment area, which was already elaborated on in the previous section. Besides the

increased water uptake of the soil, the delay in peak discharge can also be attributed to larger surface roughness in the catchment, which reduces the overland flow velocity and increases the time for infiltration.

As mentioned in section 2.5.1 the study of Slager et al. (2022a) also assessed the effect of full afforestation (excl. urban) on stream flow for the rainfall event in 2021 in the Geul catchment. The authors used the hydrological model wflow_sbm and simulated at Meerssen a peak discharge reduction of 27 % from 166 m^3/s to 121 m^3/s for full catchment afforestation. Moreover, at Schin op Geul (ca. 4km upstream of Valkenburg), the simulated discharge decreased also by 27 % to 157 m^3/s to 114 m^3/s. The authors of the study of Slager et al. (2022a) noted that due to its structure, the wflow_sbm model was not capable of accounting for floodplain storage as a consequence of flooding and, therefore, potentially overestimated the event stream-flow.

Using openLISEM, floodplain storage can be simulated, as the model accounts for hydrological and hydrodynamic processes simultaneously. By comparing the findings of Slager et al. (2022a) to this study, it can be observed that the simulated discharges are generally higher for wflow_sbm than openLISEM, which simulated a peak discharge reduction of approximately 35 % from 113 m^3/s to 74 m^3/s at Meerssen (table 4.8). At Valkenburg, the simulated peak discharge after full afforestation was higher than at Meerssen, with approximately 75.5 m^3/s, reflecting a reduction of 18% compared to the reference scenario (table 4.8). This leads to the conclusion that storage occurred in the floodplain between Valkenburg and Meerssen, which could be simulated with openLISEM but not with the model wflow_sbm.

In the study of Slager et al. (2022a) the model wflow_sbm was also coupled to the hydraulic SOBEK model, to account for floodplain storage and hydraulic flow (section 2.5.1). As a result, the simulated discharge peak at Schin op Geul was 140 m^3/s for the event rainfall of 2021. The conversion of crop- and grassland into forest resulted in a peak flow reduction by 11 % to 125 m^3/s (Slager et al., 2022a). The coupling of the two models, reduced the peak discharge for the flood event in 2021 at Schin op Geul, nevertheless, the relative reduction is lower and absolute peak discharge after afforestation is still higher than for the openLISEM simulation. This might be explained by the structure of the models.

As described in section 2.5.1 LUCC in wflow_sbm does not cause a change in vertical saturated hydraulic conductivity. The influence of a forest is mostly expressed in changes in interception and evapotranspiration and increased surface roughness. In contrast, the soil's hydraulic conductivity is altered within openLISEM through LUCC, which provides a possible explanation for the larger reduction in discharge at Valkenburg after catchment afforestation. Nevertheless, as elaborated in the previous subsection, the simulated effect of afforestation by openLISEM is highly sensitive to the parameterization of a forest and particularly to the assigned OMC.

In summary, the analysis of various spatial afforestation scenarios indicates that large-scale afforestation is necessary to significantly reduce flood impacts, primarily due to increased infiltration from larger forest cover. Nonetheless, despite total larger forest cover and greater peak flow reduction, riparian afforestation was less effective in reducing flood extent in the catchment than afforestation of slopes (policy scenario), which means that the locations for implementing floodplain afforestation should be at a distance of the urban areas and further assessed by future research. Upstream afforestation was most effective in reducing peak discharge per square kilometer of forest cover due to higher rainfall in the upstream area. However, thinner soils in the upstream area limited its effectiveness, reducing peak discharge at Kelmis by 5.2 % compared to 18 % at Meerssen. Downstream afforestation showed a greater overall flood extent reduction in the catchment. This shows that despite the larger rainfall sums in the upstream area of the catchment in July 2021 (figure 2.3), which corresponds to historical observations that, on average, more precipitation occurs in that area (De Moor et al., 2008), afforestation should be considered for each sub-catchment rather than focusing solely on upstream areas. Further research should explore more detailed sub-catchment afforestation scenarios and the impact of varying rainfall patterns.

4.4 Results - Hedgerows

Within this section, the results of the implementation of hedgerows will be presented and discussed. Discharge hydrographs of the Geul near Meerssen will be presented, which are relevant as they indicate the discharge contribution of the Geul to the Meuse (figure 4.9, figure 25 and figure 4.9). Moreover, flood extent variations will also be shown (table 4.12). The spatial extent of hedgerows is equal for each hedgerow scenario and represents about 2.5% of the catchment area. Details can be found in the methodology 3. The scenarios using shrub hedgerow vegetation cover have also been applied with a 20% and 50% reduction of the event rainfall of 2021. Moreover, the effect of grass hedgerows compared to shrub hedgerows for 50% reduced event rainfall will be discussed.

4.4.1 Impact of hedgerows on flooding for different rainfall scenarios

Figure 4.9 shows the discharge hydrograph at Meerssen for the simulated reference scenario, with initial land use, and discharge hydrograph after implementation of shrub hedgerows.

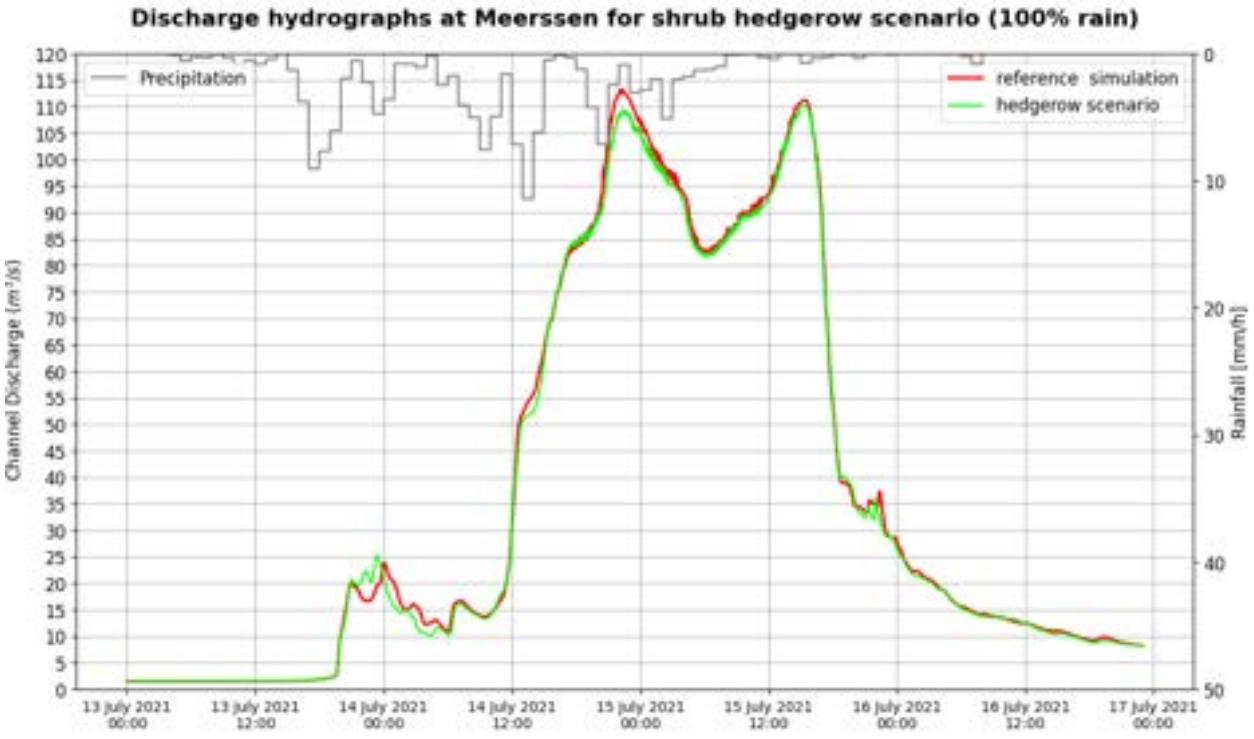

Figure 4.9: Effect of hedgerows for 100% of event rainfall

It can be observed that the peak discharge at Meerssen is lowered by 2.7%, from $113.2 m^3/s$ to 111.6 m^3/s. The discharge curve of the hedgerow scenario follows mostly the same pattern as the reference scenario. The reduction of the first peak on the night

of the 14th results in the second flood peak on the afternoon of the 15th becoming the maximum flood peak, which results in a maximum discharge peak delay of approximately 17 h. Nevertheless, the peaks are almost equally large and differ by approximately 2 m^3/s. The effect of peak discharge at Valkenburg is smaller and lies at around -1% (table 4.11).

Table 4.11: Effect of hedgerows on peak discharge at Meerssen and Valkenburg for different rainfall intensities

Scenarios	**Location**	**Peak Discharge** $Q_p[m^3/s]$	**Time**	**Diff. to Ref.*** ΔQ_p [%]
reference scenario	Meerssen	113.23	14.07.21 22:19	-
(100% rain)	Valkenburg	92.24	14.07.21 19:12	-
hedgerow scenario	Meerssen	110.6	15.07.21 15:24	-2.71
(100% rain)	Valkenburg	91.27	15.07.21 12:30	-1.05
reference scenario	Meerssen	61.91	14.07.21 18:58	-
(80% rain)	Valkenburg	60.19	14.07.21 17:45	-
hedgerow scenario	Meerssen	59.42	14.07.21 19:12	-4.02
(80% rain)	Valkenburg	58.52	14.07.21 17:31	-2.77
reference scenario	Meerssen	8.20	15.07.21 16:34	-
(50% rain)	Valkenburg	8.22	15.07.21 01:23	-
hedgerow scenario	Meerssen	7.22	15.07.21 11:28	-12.17
(50% rain)	Valkenburg	7.23	15.07.21 09:22	-12.04
hedgerow scenario	Meerssen	7.22	15.07.21 11:28	-12.17
grass (50% rain)	Valkenburg	7.23	15.07.2109:22	-12.04

*always refers to the difference to the reference simulation with the same amount of rainfall

Flood extents are presented in table 4.12. It can be observed that the implementation of hedgerows reduces the zoomed-in flood extent, which was also used for model validation, from 4.84 km^2 by 1.4 % to 4.77 km^2. On the catchment scale, the effect is even less, with a reduction of 1 % of the overall flood extent. The reduction is caused by a slight increase in interception by 0.01 mm and an increase in infiltration of 0.5 mm on the catchment scale. This leads to a runoff ratio reduction from 24.98 % to 24.58 % (table 4.13).

Table 4.12: Effect of hedgerows on flood extent

Scenario	**Flood Extent** "zoomed-in" [km^2]	**Diff. to Ref.*** [%]	**Flood Extent** Catchment [km^2]	**Diff. to Ref.*** [%]
reference scenario (100% rain)	4.84	-	24.43	-
hedgerow scenario (100% rain)	4.77	-1.44	24.18	-1.03
reference scenario (80% rain)	3.14	-	15.40	-
hedgerow scenario (80% rain)	3.04	-3.16	14.93	-3.08
reference scenario (50% rain)	0.37	-	1.92	-
hedgerow scenario (50% rain)	0.31	-14.00	1.76	-7.96
hedgerow grass scenario (50% rain)	0.31	-14.00	1.76	-7.96

*always refers to the difference to the reference simulation with the same amount of rainfall

Ultimately, shrub hedgerows show only a minor effect on the 2021 flooding, which can be attributed to the high intensity and amount of rainfall and the small spatial extent of the measure. This is why the same scenario was also analyzed for different rainfall intensities.

Before discussing the effect of hedgerows for 20% and 50% reduced rainfall, it is important to evaluate the effect of those rainfall reductions on stream flow and flooding without any LUCC. By reducing the event rainfall by 20%, representing a cumulative rainfall of 141.14mm for the duration of the event, peak discharge at Meerssen reduced from 113.23 m^3/s to 61.91 m^3/s (table4.13 and table 4.11).

The 50% reduction of event rainfall further reduced the channel discharge at Meerssen to 8.2 m^3/s, which only resulted in minor flooding on the catchment scale with a total area of 1.92 km^2 flooded. (table4.13, table 4.11 and table 4.12). Nevertheless, a 50% reduction of the event rainfall represents a cumulative rainfall of 70.57 mm on the catchment scale, which can still be considered as an extreme rainfall event.

The simulated discharge of 8.22 m^3/s at Valkenburg seems to underestimate the actual discharge for such an event. The visualization of the flood extent for 50% reduced rainfall is included in the appendix P. The study of Penning et al. (2024) simulated, among others, streamflow at Schin op Geul (about 4 km upstream of Valkenburg) for different rainfall intensities and dry and wet initial soil moisture conditions. The used coupled model

wflow_sbm, which was described in section 2.5.1, simulated for wet initial conditions and the actual land use of 2021 for a cumulative rainfall of 72.9 mm in 24 hours a discharge of 200 m^3/s at Schin op Geul. This is most certainly an overestimation because floodplain storage and hydraulics are not included in wflow_sbm as described in section 2.5.1 and pointed out in the previous subsection.

In addition, also the coupled model wflow-SOBEK was used for the rainfall scenario, resulting in peak discharges at Schin op Geul of 167 m^3/s. The spatial rainfall distribution and initial soil moisture conditions used by Penning et al. (2024) vary compared to this study, and also, the rainfall duration is less, representing higher rainfall intensities (up to 6.5 mm/h compared to 5 mm/h).

However, it shows that the magnitude of stream flow should be higher than the outcome of the openLISEM simulation for the same amount of rainfall. This finding is also supported by historic peak discharges at Hommerich (about 12 km upstream of Valkenburg), presented in the study of Klein (2022). A possible explanation would be that certain runoff processes were not captured sufficiently by openLISEM as the runoff ratio is just 1.14 % for a cumulative rainfall of 70.57 mm over the duration of the still extreme rainfall event (table 4.13), ultimately showing an uncertainty associated with the event-based setup of the model.

Table 4.13: Influence of hedgerows on catchment totals for different rainfall intensities

Scenarios	**Rainfall, P** [mm]	**Outflow, Q** [mm]	**Q/P** [%]	**Interception** [mm]	**Infiltration** [mm]
reference scenario (100% rain)	141.14	35.22	24.98	1.49	93.54
hedgerow scenario (100% rain)	141.14	34.69	24.58	1.5	94.03
reference scenario (80% rain)	112.91	17.16	15.2	1.49	88.74
hedgerow scenario (80% rain)	112.91	16.58	14.68	1.5	89.21
reference scenario (50% rain)	70.57	1.14	1.61	1.49	67.00
hedgerow scenario (50% rain)	70.57	1.03	1.46	1.5	67.1
grass hedgerow scenario (50% rain)	70.57	1.03	1.46	1.5	67.1

Therefore, the simulated effect of hedgerows on flooding for reduced rainfall must be considered conditionally. For **20% reduced rainfall**, the implementation of hedgerows

would have lowered the peak discharge at Meerssen by 4% from 61.91 m^3/s to 58.5 m^3/s (table 4.11). Moreover, the zoomed-in flood extent would have been reduced by 3.16% from 3.14 km^2 to 3.04 km^2. This is explained by a 0.5 mm increase in total infiltration between the reference and hedgerow scenario from 88.74 mm to 89.21 mm. Furthermore, also interception slightly increases by 0.1 mm. The hydrograph at Meerssen for this scenario is shown in the appendix Q.

The strongest effect of peak flow reduction through hedgerows can be observed for **50% reduced rainfall**, with peak flow reduction from 8.2 m^3/s to 7.22 m^3/s, representing a decrease of 12% (figure 4.10. Moreover, the flood extent in the zoomed-in area reduces by 12% to 0.31 km^2 4.10. The flood mitigating effect can be attributed to increased infiltration and interception (4.13).

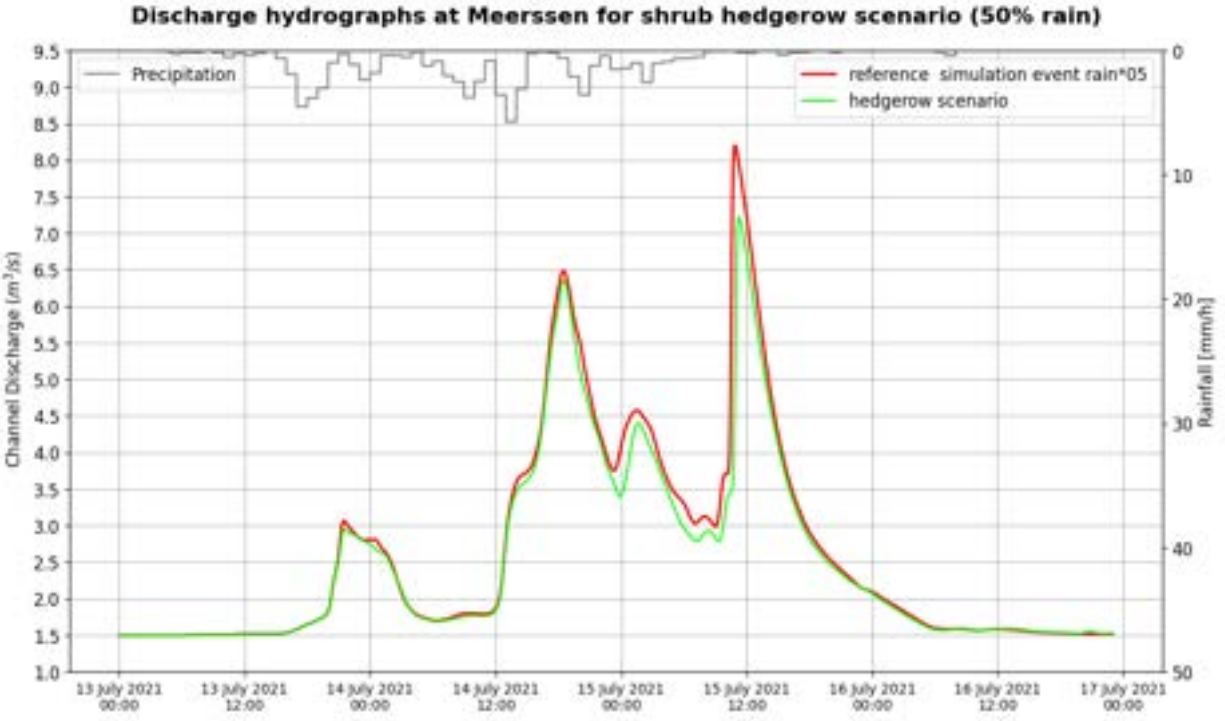

Figure 4.10: Effect of hedgerows for 50% of event rainfall

The study of Naturkraacht.org (2023) analyzed the potential flood mitigating effect of infiltration zones with 10-20 m width in the Selzerbeek sub-catchment of the Geul for the 2021 rainfall event, using the hydrological model SWAT+ (Bieger et al., 2017). The observed effect was a reduction of the tributary's peak discharge from 9.8 m^3/s to 9.3m^3/s, which represents a 5% decrease. Nevertheless, the authors emphasize that due to the model's structure, using hydrological response units, the effect of infiltration strips is potentially underestimated. As no supportive information was available on the exact

implementation of hedgerows by Naturkraacht.org (2023) and as no discharge data for the outlet of the Selzerbeek was derived for this study, the results of the studies are not comparable. Moreover, the study of Naturkraacht.org (2023) used a daily timestep, which is not sufficient to capture the flashy dynamics of the 2021 flood event.

In summary, the implementation of hedgerows showed an effect on peak discharges for the July 2021 rainfall event, which increased for a 20 % and 50 % reduction of the event rainfall. Nevertheless, the effect was very minor and would most certainly not lead to a reduction in flood damages.

4.4.2 Effectivity of grass-hedgerows

The change in Manning's roughness coefficient from 0.12 to 0.6 reflects the difference between shrub and grass hedgerows and reflects a lower surface roughness associated with grass strips. Nevertheless, for the analyzed 50% reduced rainfall event, both parameterizations showed the same effects (table 4.13, table 4.12, table (4.11). This means that different hedgerow vegetation types would not have influenced the flood-mitigating impact for an event of this rainfall magnitude. Nevertheless, as the simulated discharge is underestimated, the result must be considered conditionally.

5

Discussion

In the previous section (results 4), the results of this study have been compared to the findings of other studies to evaluate their plausibility, discuss differences, and ultimately point out their implications. This section first addresses the sensitivity of the model and uncertainties associated with the model setup. Additionally, it discusses the potential impact of afforestation on the other hydroclimatic extreme, drought, and the extent to which openLISEM could potentially be used to assess this impact.

5.1 Model sensitivity

An in-depth sensitivity analysis of the final openLISEM setup to changes in calibration factors or land cover parameters was not performed due to time constraints and long simulation run times (about 10h). Previous studies, such as those by Jerszurki et al. (2022) and Wu et al. (2021), have performed sensitivity analyses for different environments as part of calibrating openLISEM. These studies identified key parameters affecting total discharge, such as random roughness (RR), saturated hydraulic conductivity (ksat), and Manning's n. They also highlighted the nonlinearity of the model's response to input changes and the dependency on initial parameter values. For instance, a low initial parameter value might remain low even after a 100% increase and, therefore, might not be considered sensitive in that case.

In this study, while a quantitative sensitivity analysis was not performed, qualitative observations were made during the calibration process and in the analysis of afforestation and hedgerow scenarios. Increased initial soil moisture and reduced first soil layer depth significantly raised simulated discharge (Appendix L). Conversely, changes in Manning's n, intended to compare shrub and grass hedgerows' impact on flooding, had no effect. This could be explained by the underestimation of runoff for that scenario, decreasing the overall impact of surface roughness in the catchment. Reducing bulk density and increasing organic matter content (OMC) enhanced infiltration, thus lowering discharge rates. Notably, OMC appeared to be a critical parameter, as significant differences were

observed between the "mid-aged" and "old" forest scenarios, which varied solely in OMC levels (Figure 4.6). The parameterization for the "old" forest scenario, involving a 10% reduction in bulk density and an 8% OMC, demonstrated the most extreme influence of a land cover type on enhancing infiltration while remaining consistent with the Green and Ampt (1911) infiltration model's assumptions. However, the model's sensitivity to OMC is interrelated with soil depth of the first layer, which is directly influenced by the LULC; greater depths would amplify the effect of higher OMC due to increased porosity and enhanced saturated hydraulic conductivity, allowing more water storage in the soil.

Also the used timestep influences the simulated discharge as shown in the appendix in figure 26. A 50% reduction of the timestep to 30 seconds increased the discharge by 4.4%, whereas a 50% increase of the timestep to 90 seconds lowered the simulated peak discharge by 2.7%. An increase of the timestep to 1 h (3600 seconds) lowered the peak discharge by 65% to 35 m^3/s.

In summary, those findings and observations highlight the parameters that had the strongest influence on the results and thus should be chosen with strong justification within openLISEM modeling studies.

5.2 Uncertainties related to the model setup

OpenLISEM accurately predicts the hydrologic response of a catchment setup based on empirically derived and physical equations. However, this system only approximates reality based on plausible reasoning. Such reasoning is necessary because, often, not all the required information is sufficiently available or harmonized on larger scales. This is particularly true for the representation of the subsurface, such as soil depths and soil data. A more detailed representation of soil depths in the catchment would improve certainty in the results of afforestation and hedgerows for the Geul catchment. Additional field surveys would be necessary to reduce the inherent uncertainty of globalized soil databases, which are often not feasible in a short time on the catchment scale. Future studies should assess how different soil depths, particularly of the first soil layer, affect the simulated effect of forests and hedgerows on flooding. Consequently, this study's chosen catchment system representation is not the only plausible approximation of reality; different modelers might argue for different setups, e.g., in terms of soil depths, ultimately influencing the outcome. This phenomenon, reported by many studies, is one of the challenges of hydrologic and hydrodynamic modeling and is described by the term equifinality (Pechlivanidis et al., 2011). It refers to the phenomenon that different parameter setups can produce similar results. This is especially relevant for event-based setups, such as with openLISEM, where no spin-up period is used, and the model is solely calibrated to high flood discharges and not for low flow conditions.

Within the analysis of the effect of hedgerows, it could be observed that simulated discharges for reduced event rainfall were underestimated. This might indicate that certain runoff processes are not captured sufficiently by the model. Eventually, urban areas are underrepresented in the model setup, which could explain an underestimation of runoff. The used input LULC data of ESA World Cover 2021 showed a deviation from other LULC data sources, such as OSM data and Corine 2018 LULC, with respect to built-up area and forest (table 3.2). Due to the 10 m resolution of the ESA World Cover 2021 LULC data, single trees in built-up areas might be misclassified as forest. Nevertheless, the effect of potential under-representation of urban runoff might be unintentionally balanced for the event rainfall through the calibration choices, such as the decrease of saturated hydraulic conductivities of the first and second soil layer (the reasoning behind calibration choices is presented in 4.1). Nonetheless, lower rainfall intensity might allow a higher ratio of the incoming water to percolate in the deeper soil layer, which could explain the reduced runoff.

Concluding, despite the reasonably well-simulated discharges at Sippenaeken and Kelmis after calibration, with NSE values of 0.83 and 0.82, respectively, and a simulated flood extent with a CSI of 84.37, which suggests an accurate representation of the actual flow dynamics during the event, this modeling study should be regarded as a a realistic simulation but not as the only possible and absolute reconstruction of the processes during the heavy rainfall event of 2021. Moreover, it functions as an impact assessment for evaluating the effects of afforestation and hedgerows on flooding in similar situations.

5.3 Effect of afforestation on droughts

Afforestation can enhance storage and infiltration in the soil through processes that have been discussed previously, such as an increase in porosity and saturated hydraulic conductivity. Nevertheless, evapotranspiration was neglected within the analysis as it is expected to play a minor role during extreme rainfall events. However, solutions for flood mitigation should also always be evaluated in terms of their implications for the opposite hydrologic extreme, droughts, before they find practical application. This is necessary because droughts are also increasing in frequency and severity due to climate change, and the underlying meteorological processes are interconnected to floods (Rodell and Li, 2023). As many studies found that afforestation increases evapotranspiration, this section will therefore discuss the possible impacts of large-scale afforestation on stream-flow conditions during periods with rainfall deficits. Moreover, suggestions for assessing the effect of afforestation on droughts using openLISEM will be presented.

In a multiple scenario modeling study of Buechel, Slater, and Dadson (2022) using the land-surface model JULES with a resolution of 1 km^2 to investigate the effect of widespread

broad-leaf afforestation in Great Britain, results showed that medium and low streamflow decreased on median by 2.57 % and 4.42 % respectively per 10% increase in forest cover.

In the study of Penning et al. (2024), the previously introduced wflow_sbm model setup (section 2.5.1) was used to assess the influence of afforestation in the Geul catchment, for the summer drought of 2020. The presented discharge at Schin op Geul for the month of September in 2020 reflected a reduction in simulated base flow from approximately 1.8 m^3/s to 1.6 m^3/s on average, which was linked to increased interception and evapotranspiration. Nevertheless, the authors point out that due to the structure of the model with maximum soil depths of 2.5 m, deeper groundwater levels could not be simulated, which is a limitation of the model.

Filoso et al. (2017) stated that the effect of forest restoration on local water availability shows contrasting effects. A recent study by Tuinenburg, Bosmans, and Staal (2022) examined the global potential of forest restoration for mitigating drought. The study found that, on average, over two-thirds of the increased land evapotranspiration - approximately 10 mm — would precipitate over land under current climate conditions. They state a significant potential for drought mitigation in regions such as eastern Africa, southern Central Africa, Madagascar, the edges of the Amazon rainforest, China, northern Southeast Asia, France, and central Europe (Tuinenburg, Bosmans, and Staal, 2022). Those findings underline the relevance to locally assess nature-based flood mitigation measures, such as afforestation, in terms of their impact on droughts.

5.3.1 Drought analysis using openLISEM

In this study, the effect of afforestation on drought in the Geul catchment was not investigated with openLISEM since it requires a substantially new model setup, which will be described below.

To accurately analyze droughts, instead of an event-based set-up, a continuous simulation is required. The used openLISEM model version 6.95 (2024) allows continuous simulations of up to one year, which limits its drought application capabilities. Moreover, it would be necessary to decrease the runtime of the model. For the current analysis and model setup, a full catchment simulation took approximately 10 hours to finish (hardware specifications are presented in appendix A). Reducing the runtime for full catchment simulations could be done by increasing the timestep or decreasing the resolution of the model. Despite improving computational efficiency, the suggested options come with disadvantages, such as loss of detail in LULC and elevation, which could change flow hydrodynamics. Nevertheless, as some of the input can be provided in sub-grid detail, e.g., roads and buildings and channel dimensions, the loss of detail in land use and land cover might be minor for assessing large-scale afforest. As hedgerows are a small-scale measure, their implementation in model setups with larger resolutions is not possible. Furthermore, increasing the timestep alters

the channel discharge, as it reacts sensitively to it (appendix 26). The aforementioned changes explain why a new calibration would be necessary.

During the setup of the openLISEM model for this study, enabling the models' groundwater module did not show any effects on the simulation. This is probably due to slow reaction time and the needed accumulation of water in the second soil layer. Still, the functionality of the groundwater module has not been fully approved yet by other studies, which would make it an interesting subject for further research. Moreover, leakage to deeper layers and aquifers must be accounted for, which are present in the Geul catchment (Klein, 2022; De Moor et al., 2008). In openLISEM, this can be done by defining a groundwater loss to deep percolation in the model (mm/h). Furthermore, the representation of the subsurface is simplified, and outcomes of the simulations are strongly influenced by the soil depths on which information is not always available on the catchment scale. As mentioned by Penning et al. (2024), this limits the representation of groundwater level fluctuations exceeding the defined maximum soil depths.

As shown in the results (4), simulated interception decreased for the full afforestation scenarios. This might be explained by the fact that openLISEM does not account for wood storage and solely uses the plant-specific canopy storage for calculating interception through vegetation, which is also influenced by the LAI but higher for crops and grassland as shown in the appendix B. Nevertheless, the plant-specific canopy storage equations can be adjusted in the openLISEM database creator, allowing improvement, e.g., by adding wood storage. Moreover, on longer timescales and due to seasonality, the plant cover changes. Those seasonal changes can not be represented in openLISEM in a continuous simulation as it uses static plant cover parameters. Evapotranspiration can be included by providing spatial information on potential evapotranspiration (ET_p), which must be calculated beforehand. Nevertheless, ET_p can also be provided on daily intervals, and under consideration of the average catchment latitude, the model adjusts the ET_p internally to account for differences in sun angle (*OpenLISEM Wiki* n.d.). Snow routines are not included in the model, which further limits its applicability for continuous modeling.

Given the above-mentioned current functionality and consequent limitations of openLISEM regarding continuous modeling, it does not seem to be a suitable tool for assessing the effect of afforestation on droughts for longer periods (>1 year) and in catchments where snowmelt might be a relevant factor. This might also be the reason why there are no published studies yet on the application of openLISEM for assessing droughts. Nevertheless, for shorter simulation periods, with a short spin-up sequence, it would be interesting to test the performance and functionality of openLISEM for simulating low-flow conditions while accounting for dynamic baseflow contributions.

6

Conclusion

This study investigated whether two nature-based solutions, afforestation and hedgerows, could have reduced flooding in the Geul catchment during the heavy rainfall event in July 2021. A modeling study using the hydrologic and hydrodynamic model openLISEM was conducted to address this question.

Results showed that the effect of afforestation is highly sensitive to its parameterization. Using the parameterization reflecting current forest characteristics in the catchment ("mid-aged" scenario), the simulated peak discharge at Meerssen was 73.51 m^3/s for full afforestation (92% forest cover). In addition, the flood extent in the catchment was 15.89km^2. For the "young" forest parameterization, the peak discharge increased by about 47%, and flood extent increased by 46 % compared to the "mid-aged" scenario. Conversely, the "old" forest parameterization decreased peak discharge at Meerssen by about 74% and lowered the catchment flood extent by 72%. Adjusting the summer leaf cover of the "mid-aged" forest to winter leaf cover resulted in only a 0.3% increase in peak discharge, with no change in flood extent. In conclusion, this parameterization study showed that seasonality did not significantly affect the impact of a broad-leaf forest on flooding and that "old" forests most effectively reduced the flood impact, highlighting that flood mitigating effect of forests has the potential to increase over time and that openLISEM is sensitive to changes in organic matter content.

Spatial afforestation scenarios, using the "mid-aged" forest parameterization, showed that large-scale afforestation would be necessary to significantly reduce flooding. Increasing the forest cover by 7 % (policy scenario) reduced peak discharge at Meerssen by about 4% and catchment flood extent by about 3 %. Furthermore, a 9 % increase in forest cover (riparian scenario) lowered peak discharge by about 6 % and reduced flood extent by approximately 1 %. The riparian scenario's greater flood extent, despite the larger forest cover and reduction in peak discharge, suggests that increased vegetation in floodplains might be more effective at a distance from urban areas, where larger flood extents allow more water to infiltrate without causing damage.

The comparison of upstream and downstream afforestation, with forest cover increases of 20 % and 43 %, respectively, showed that both measures reduced peak flow at Meerssen by about 19 %. This could be attributed to the spatial and temporal rainfall pattern during the event, showing the largest rainfall sums in the upstream catchment. However, downstream afforestation more significantly reduced catchment flood extent (26.5 %) compared to upstream afforestation (8.6 %), indicating that flood mitigation should also include sub-catchments of the Geul, such as Gulp and Selzerbeek, where flooding also occurred. Ultimately, full catchment afforestation (92 % forest cover), representing a 62 % increase in forest cover, reduced the peak discharge at Meerssen and the flood extent in the catchment by about 35 %. These findings demonstrate that large-scale afforestation could have mitigated flooding during the 2021 event, but it would not have fully prevented it.

The implementation of shrub hedgerows resulted in a peak flow reduction at Meerssen by about 3% and a flood extent reduction of 1%. This effect increased under reduced rainfall scenarios, with a 50% reduction in event rainfall (70.57 mm cumulative) leading to a 12% decrease in peak discharge and an 8% reduction in flood extent. Grass hedgerows had the same effect as shrub hedgerows for the 70.57 mm rainfall scenario. However, the simulated streamflow for the reference land use under 50% reduced event rainfall seemed to be underestimated with a peak discharge at Meerssen of 8.2 m^3/s. This demonstrated, on the one hand, that hedgerows were not effective in reducing the flood impact for the heavy rainfall event in July 2021, but also that some uncertainty must be assigned to the event-based model setup and the simulated catchment response of the reduced rainfall (still extreme rainfall) with openLISEM.

In evaluating the impact of afforestation and hedgerows on mitigating floods in the Geul catchment, this study also assessed openLISEM's suitability for this purpose. One of the model's strengths is its ability to account for the influences of land use changes on saturated hydraulic conductivity and porosity, which other hydrological models, such as wflow_sbm, don't. Its integrated catchment structure allows realistic simulation of water routing and evaluation of local measures' effects. Furthermore, its various outputs, such as hydrographs of channel discharges and water levels, inundation maps, and spatial infiltration and runoff maps, improve the understanding of catchment processes during heavy rainfall events. Nevertheless, it is sensitive to the parameterization of the LULC, especially the OMC, which can be quite heterogeneous on a catchment scale and within the same land use category. This can lead to local underestimation or overestimation of infiltration. Also, the event-based approach presents an uncertainty, as described before. Ultimately, the model is capable of simulating the effect of land use changes, such as the implementation of afforestation and hedgerows on flooding, in great detail with a specific focus on infiltration under defined conditions, such as soil depths and initial soil moisture conditions. Still, this simulation should not be seen as an absolute and the only possible reconstruction of the processes during the heavy rainfall event of 2021.

In summary, the openLISEM modeling study showed that afforestation and hedgerows on a smaller scale could not significantly prevent flooding in the Geul catchment after the heavy rainfalls in July 2021. Despite this, the implementation of those measures should still be considered as they inhere various co-benefits, such as carbon sequestration, increased biodiversity, and improved soil quality. Nevertheless, their impact on other hydrologic extreme droughts should be evaluated in future research before they find practical application.

Bibliography

Allen, George H and Tamlin M Pavelsky (2015). "Patterns of river width and surface area revealed by the satellite-derived North American River Width data set". In: *Geophysical Research Letters* 42.2, pp. 395–402.

Andreasen, Mie et al. (2023). "Seasonal dynamics of canopy interception loss within a deciduous and a coniferous forest". In: *Hydrological Processes* 37.4, e14828.

Archer, Nicole AL et al. (2016). "Rainfall infiltration and soil hydrological characteristics below ancient forest, planted forest and grassland in a temperate northern climate". In: *Ecohydrology* 9.4, pp. 585–600.

Asselman, N and Klaas-Jan Van Heeringen (2023). "Een watersysteemanalyse-wat leren we van het hoogwater van juli 2021? Inzichten in het functioneren van beeksystemen bij grote hoeveelheden neerslag en het effect van verschillende typen maatregelen". In.

Aston, AR (1979). "Rainfall interception by eight small trees". In: *Journal of hydrology* 42.3-4, pp. 383–396.

Baartman, Jantiene EM et al. (2012). "Exploring effects of rainfall intensity and duration on soil erosion at the catchment scale using openLISEM: Prado catchment, SE Spain". In: *Hydrological processes* 26.7, pp. 1034–1049.

Baptist, Martin J et al. (2004). "Assessment of the effects of cyclic floodplain rejuvenation on flood levels and biodiversity along the Rhine River". In: *River Research and Applications* 20.3, pp. 285–297.

Bastiaanssen, Wim GM et al. (1996). "Modelling the soil-water-crop-atmosphere system to improve agricultural water management in arid zones (SWATRE)". In: *Dutch experience in irrigation water management modelling*, pp. 13–30.

Bieger, Katrin et al. (2017). "Introduction to SWAT+, a completely restructured version of the soil and water assessment tool". In: *JAWRA Journal of the American Water Resources Association* 53.1, pp. 115–130.

Bouché, Marcel B and Fathel Al-Addan (1997). "Earthworms, water infiltration and soil stability: some new assessments". In: *Soil biology and biochemistry* 29.3-4, pp. 441–452.

Bout, VB and VG Jetten (2018). "The validity of flow approximations when simulating catchment-integrated flash floods". In: *Journal of hydrology* 556, pp. 674–688.

Bradshaw, Corey JA et al. (2007). "Global evidence that deforestation amplifies flood risk and severity in the developing world". In: *Global change biology* 13.11, pp. 2379–2395.

Buechel, Marcus, Louise Slater, and Simon Dadson (2022). "Hydrological impact of widespread afforestation in Great Britain using a large ensemble of modelled scenarios". In: *Communications Earth & Environment* 3.1, p. 6.

Calder, Ian et al. (2004). "Forest and Water Policies. The need to reconcile public and science perceptions". In: *Geologica Acta*, pp. 157–166.

Calder, Ian R, James Smyle, and Bruce Aylward (2007). "Debate over flood-proofing effects of planting forests". In: *Nature* 450.7172, pp. 945–945.

Calder, Ian R et al. (2003). "Impact of lowland forests in England on water resources: Application of the Hydrological Land Use Change (HYLUC) model". In: *Water Resources Research* 39.11.

Chow, Ven Te (1959). "Open-channel hydraulics: New York". In: *US Army Corps of Engineers, Hydrologic Engineering*.

Commission, European and European Research Executive Agency (2023). *Nature-based solutions – EU-funded nbs research projects tackle the climate and biodiversity crisis*. Publications Office of the European Union. DOI: doi/10.2848/879543.

De Laat, P and MLC Agor (2003). "Geen toename piekafvoer Geul". In: *H2O* 9, pp. 25–27.

De Moor, JJW and Gert Verstraeten (2008). "Alluvial and colluvial sediment storage in the Geul River catchment (The Netherlands)—combining field and modelling data to construct a Late Holocene sediment budget". In: *Geomorphology* 95.3-4, pp. 487–503.

De Moor, JJW et al. (2008). "Human and climate impact on catchment development during the Holocene—Geul River, the Netherlands". In: *Geomorphology* 98.3-4, pp. 316–339.

De Roo, APJ, CG Wesseling, and CJ Ritsema (1996). "LISEM: a single-event physically based hydrological and soil erosion model for drainage basins. I: theory, input and output". In: *Hydrological processes* 10.8, pp. 1107–1117.

Delestre, Olivier et al. (2014). "FullSWOF: A software for overland flow simulation". In: *Advances in Hydroinformatics: SIMHYDRO 2012–New Frontiers of Simulation*, pp. 221–231.

Delta Decision for Flood Risk Management (2023). Delta Programme. URL: https://english.deltaprogramma.nl/three-topics/flood-risk-management/delta-decision.

Dottori, Francesco et al. (2023). "Cost-effective adaptation strategies to rising river flood risk in Europe". In: *Nature Climate Change* 13.2, pp. 196–202.

Dubey, Amit Kumar et al. (2021). "Flood modeling of a large transboundary river using WRF-Hydro and microwave remote sensing". In: *Journal of Hydrology* 598, p. 126391.

ENW (Sept. 2021). *Hoogwater 2021 Feiten en Duiding. Expertise Netwerk Waterveiligheid*. https://www.enwinfo.nl/publish/pages/183541/211102_enw_hoogwater_2021-dv-def.pdf. Version 2. Accessed: 2024-06-10.

Faiz, Mukhtar Ahmad et al. (2022). "Zero tillage, residue retention and system-intensification with legumes for enhanced pearl millet productivity and mineral biofortification". In: *Sustainability* 14.1, p. 543.

Filoso, Solange et al. (2017). "Impacts of forest restoration on water yield: A systematic review". In: *PloS one* 12.8, e0183210.

Gonzalez-Sosa, E et al. (2010). "Impact of land use on the hydraulic properties of the topsoil in a small French catchment". In: *Hydrological processes* 24.17, pp. 2382–2399.

Gourevitch, Jesse D et al. (2020). "Spatial targeting of floodplain restoration to equitably mitigate flood risk". In: *Global Environmental Change* 61, p. 102050.

Green, W Heber and GA Ampt (1911). "Studies on Soil Phyics." In: *The Journal of Agricultural Science* 4.1, pp. 1–24.

He, Jin et al. (2009). "Soil physical properties and infiltration after long-term no-tillage and ploughing on the Chinese Loess Plateau". In: *New Zealand Journal of Crop and Horticultural Science* 37.3, pp. 157–166.

Hengl, Tomislav et al. (2017). "SoilGrids250m: Global gridded soil information based on machine learning". In: *PLoS one* 12.2, e0169748.

Herbst, Mathias et al. (2006). "Measuring and modelling the rainfall interception loss by hedgerows in southern England". In: *Agricultural and Forest Meteorology* 141.2-4, pp. 244–256.

Holden, Joe et al. (2019). "The role of hedgerows in soil functioning within agricultural landscapes". In: *Agriculture, ecosystems & environment* 273, pp. 1–12.

Hoyningen-Huene, J. von (1983). *Die Interzeption des Niederschlags in landwirtschaftlichen Pflanzenbeständen. In DVWK (Ed.), Einfluss der Landnutzung auf den Gebietswasserhaushalt (Vol. 57, pp. 1-53).* Verlag Paul Parey. URL: https://books.google.nl/books?id=j1SWnQEACAAJ.

Hüblová, Lucie and Jan Frouz (2021). "Contrasting effect of coniferous and broadleaf trees on soil carbon storage during reforestation of forest soils and afforestation of agricultural and post-mining soils". In: *Journal of environmental management* 290, p. 112567.

Hudson, Berman D (1994). "Soil organic matter and available water capacity". In: *Journal of soil and water conservation* 49.2, pp. 189–194.

IPCC (2021). "Summary for Policymakers". In: *Climate Change 2021: The Physical Science Basis. Contribution of Working Group I to the Sixth Assessment Report of the Intergovernmental Panel on Climate Change*. Ed. by V. Masson-Delmotte et al. Cambridge, United Kingdom and New York, NY, USA: Cambridge University Press, 332. DOI: 10.1017/9781009157896.001.

Jerszurki, Lucas et al. (2022). "Sensitivity analysis of the OpenLISEM model: calibration for an unpaved road in Southern Brazil". In: *Modeling Earth Systems and Environment*, pp. 1–14.

Jetten, Victor (2022). *Evaluatie van potentiële veranderingen in landgebruik op oppervlakte afvoer Een model analyse met openLISEM van de stroomgebieden Ransdaal en de*.

Jetten, Victor and Bastian van den Bout (2018). *OpenLISEM Multi-Hazard Land Surface Process Model Documentation User Manual*.

Johnen, Gregor et al. (2020). "Modelling and Evaluation of the Effect of Afforestation on the Runoff Generation Within the Glinščica River Catchment (Central Slovenia)". In: *Nature-Based Solutions for Flood Mitigation: Environmental and Socio-Economic Aspects*. Springer, pp. 215–231.

Kiss, Tímea et al. (2019). "(Mis) management of floodplain vegetation: The effect of invasive species on vegetation roughness and flood levels". In: *Science of the Total Environment* 686, pp. 931–945.

Klein, Angela (2022). "Hydrological Response of the Geul Catchment to the Rainfall in July 2021". MSc Thesis.

Kuiper, J. (2023). "Flash Floods in the Geul Catchment: To What Extent Could Potential Mitigation Measures In the Boven Geuldal Belgium Reduces the Effects?" MSc Thesis. University of Twente.

Kumar, Prashant et al. (2021). "Nature-based solutions efficiency evaluation against natural hazards: Modelling methods, advantages and limitations". In: *Science of the Total Environment* 784, p. 147058.

Limburg, Provincie (June 2023). *Eerste concept Limburgs Programma Landelijk Gebied*. Accessed: 2024-07-27. URL: https://www.limburg.nl/onderwerpen/natuur-en-landschap/limburgs-programma-landelijk-gebied/.

Liu, Ling, Haiyan Wang, and Wei Dai (2019). "Characteristics of soil organic carbon mineralization and influence factor analysis of natural Larix olgensis forest at different ages". In: *Journal of forestry research* 30, pp. 1495–1506.

Luske, Boki et al. (2014). *Een indicatorsysteem voor ecosysteemdiensten van de bodem: Life support functions revisited. Beworteling van grasland en droogtetolerantie. Maatregelen voor een diepere beworteling. Root development of grasslands and drought tolerance. Measures to increase root depth. English summary page 9.* URL: http://www.louisbolk.n.

Merz, Bruno, Florian Elmer, and AH Thieken (2009). "Significance of" high probability/low damage" versus" low probability/high damage" flood events". In: *Natural Hazards and Earth System Sciences* 9.3, pp. 1033–1046.

Minh, Nguyen Quang et al. (2024). "Impacts of Resampling and Downscaling Digital Elevation Model and Its Morphometric Factors: A Comparison of Hopfield Neural Network, Bilinear, Bicubic, and Kriging Interpolations". In: *Remote Sensing* 16.5, p. 819.

Morbidelli, Renato et al. (2018). "Role of slope on infiltration: A review". In: *Journal of Hydrology* 557, pp. 878–886. ISSN: 0022-1694. DOI: https://doi.org/10.1016/j.jhydrol.2018.01.019. URL: https://www.sciencedirect.com/science/article/pii/S0022169418300192.

Mücher, Herman Jozef (1986). *Aspects of loess and loess-derived slope deposits: an experimental and micromorphological approach*. Koninklijk Nederlands Aardrijkskundig Genootschap.

Naturkraacht.org (2023). *Onderzoeksrapport: Water vasthouden en vertragen in het Geuldal*. https://natuurkracht.org/nieuws/2024/onderzoeksrapport-water-vasthouden-en-vertragen-in-het-geuldal. Accessed: 2024-06-07.

Nijpels, E. (2018). *Ontwerp van het Klimaatakkoord*. The Hague. URL: https://www.klimaatakkoord.nl/documenten/publicaties/2018/12/21/ontwerp-klimaatakkoord.

Novak, Jeff et al. (2016). "Biochars impact on water infiltration and water quality through a compacted subsoil layer". In: *Chemosphere* 142, pp. 160–167.

OpenLISEM Wiki (n.d.). https://github.com/vjetten/openlisem/wiki/History. Accessed: July 3, 2024.

Osman, Khan Towhid (2013). "Organic matter of forest soils". In: *Forest soils: Properties and management*, pp. 63–76.

Overeem, Aart and Hidde Leijnse (2021). "Evaluatie & verbetering radarneerslagproducten: Casestudie extreme neerslag Zuid-Limburg 13–15 juli 2021". In: *RD Waarnemingen en Datatechnologie*. URL: [1](https://www.knmi.nl/over-het-knmi/nieuws/evaluatie-verbetering-radarneerslagproducten-casestudie-extreme-neerslag-zuid-limburg-13-15-juli-2021).

Pechlivanidis, IG et al. (2011). "Catchment scale hydrological modelling: A review of model types, calibration approaches and uncertainty analysis methods in the context of recent developments in technology and applications". In: *Global NEST journal* 13.3, pp. 193–214.

Penning, Ellis et al. (2023). "Nature-based solutions for floods AND droughts AND biodiversity: Do we have sufficient proof of their functioning?" In: *Cambridge Prisms: Water* 1, e11.

Penning, Ellis et al. (2024). *Sponswerking van Landschappen in Nederland*. Technical Report 11209224-003. Deltares. URL: https://publications.deltares.nl/11209224_003_0001.pdf.

Provincie Limburg, cluster Natuur en Water (2017). *Natura 2000 Gebiedsanalyse voor de Programmatische Aanpak Stikstof (PAS)*. https://www.natura2000.nl/gebieden/limburg/geuldal/geuldal-gebiedsanalyse.

Richet, Jean-Baptiste, J-F Ouvry, and M Saunier (2017). "The role of vegetative barriers such as fascines and dense shrub hedges in catchment management to reduce runoff and erosion effects: Experimental evidence of efficiency, and conditions of use". In: *Ecological Engineering* 103, pp. 455–469.

Rodell, Matthew and Bailing Li (2023). "Changing intensity of hydroclimatic extreme events revealed by GRACE and GRACE-FO". In: *Nature Water* 1.3, pp. 241–248.

Rogger, Madgalena et al. (2017). "Land use change impacts on floods at the catchment scale: Challenges and opportunities for future research". In: *Water resources research* 53.7, pp. 5209–5219.

Ruangpan, L. et al. (2020). "Nature-based solutions for hydro-meteorological risk reduction: a state-of-the-art review of the research area". In: *Natural Hazards and Earth System*

Sciences 20.1, pp. 243–270. DOI: 10.5194/nhess-20-243-2020. URL: https://nhess.copernicus.org/articles/20/243/2020/.

Rutgers, M. and et al. (2014). *Een indicatorsysteem voor ecosysteemdiensten van de bodem: Life support functions revisited*. RIVM Rapport 2014-0145. RIVM.

Saxton, K. E. and W. J. Rawls (Sept. 2006). "Soil Water Characteristic Estimates by Texture and Organic Matter for Hydrologic Solutions". In: *Soil Science Society of America Journal* 70 (5), pp. 1569–1578. ISSN: 0361-5995. DOI: 10.2136/sssaj2005.0117.

Slager, K. et al. (2022a). *Rapid assessment study on the Geul river basin: Appendices with background material*. Tech. rep. Deltares.

— (2022b). *Rapid assessment study on the Geul river basin: screening of flood reduction measures*. Tech. rep. Deltares.

Smith, RE and J-Y Parlange (1978). "A parameter-efficient hydrologic infiltration model". In: *Water Resources Research* 14.3, pp. 533–538.

Strijker, Bart et al. (2023). "The 2021 flood event in the Dutch Meuse and tributaries from a hydraulic and morphological perspective". In: *Journal of Coastal and Riverine Flood Risk* 2, p. 6.

Tradowsky, Jordis S et al. (2023). "Attribution of the heavy rainfall events leading to severe flooding in Western Europe during July 2021". In: *Climatic Change* 176.7, p. 90.

Tuinenburg, Obbe A, Joyce HC Bosmans, and Arie Staal (2022). "The global potential of forest restoration for drought mitigation". In: *Environmental Research Letters* 17.3, p. 034045.

U.S. Army Corps of Engineers (2024). *HEC-RAS User's Manual*. URL: https://www.hec.usace.army.mil/confluence/rasdocs/r2dum/latest/developing-a-terrain-model-and-geospatial-layers/creating-land-cover-mannings-n-values-and-impervious-layers.

Van Dijk, Albert IJM et al. (2009). "Forest–flood relation still tenuous–comment on 'Global evidence that deforestation amplifies flood risk and severity in the developing world'by CJA Bradshaw, NS Sodi, KS-H. Peh and BW Brook". In: *Global Change Biology* 15.1, pp. 110–115.

Van Heeringen, K et al. (2022). *Analyse overstorming Volkenburg - Watersysteemevaluatie Waterschap Limburg*. Tech. rep. Deltares.

Van Kempen, Gijs, Karin Van Der Wiel, and Lieke Anna Melsen (2021). "The impact of hydrological model structure on the simulation of extreme runoff events". In: *Natural Hazards and Earth System Sciences* 21.3, pp. 961–976.

Verseveld, Willem J van et al. (2022). "Wflow_sbm v0. 6.1, a spatially distributed hydrologic model: from global data to local applications". In: *Geoscientific Model Development Discussions* 2022, pp. 1–52.

Vieira, DCS et al. (2022). "Event-based quickflow simulation with OpenLISEM in a burned Mediterranean forest catchment". In: *International Journal of Wildland Fire* 31.7, pp. 670–683.

Wang, Haofei et al. (2022). "Assessing the effects of plant roots on soil water infiltration using dyes and hydrus-1D". In: *Forests* 13.7, p. 1095.

Ward, Philip J. et al. (Dec. 2020). "The need to integrate flood and drought disaster risk reduction strategies". In: *Water Security* 11. ISSN: 24683124. DOI: 10.1016/j.wasec.2020.100070.

Webb, Bid (2021). *Investigating the impact of trees and hedgerows on landscape hydrology*. Bangor University (United Kingdom).

Westeringh, W Van de (1980). "Soils and their geology in the Geul Valley". In: *Mededelingen van de Landbouwhogeschool Wageningen* 80.8, pp. 1–25.

Wu, Jinfeng et al. (2021). "Testing the impacts of wildfire on hydrological and sediment response using the OpenLISEM model. Part 1: Calibration and evaluation for a burned Mediterranean forest catchment". In: *Catena* 207, p. 105658.

Xu, Kepeng et al. (2021). "The importance of digital elevation model selection in flood simulation and a proposed method to reduce DEM errors: a case study in Shanghai". In: *International Journal of Disaster Risk Science* 12, pp. 890–902.

Zema, Demetrio Antonio et al. (2021). "Influence of forest stand age on soil water repellency and hydraulic conductivity in the Mediterranean environment". In: *Science of the Total Environment* 753, p. 142006.

Zhong, Feng et al. (2022). "Revisiting large-scale interception patterns constrained by a synthesis of global experimental data". In: *Hydrology and Earth System Sciences* 26.21, pp. 5647–5667.

Appendix

A Hardware details of Computer used for modeling

To have a representative understanding of the mentioned model run times throughout the report, it is necessary to mention the hardware used for modeling during the study. The details are presented in table A.

Table 1: Hardware information of Computer used for the modeling study

Processor	Intel(R) Xeon(R) Gold 6246R CPU @ 3.40GHz 3.39 GHz (4 processors)
Installed RAM	16.0 GB

B Interception

In the following, the equation is presented, which was used to calculate the land use and landcover specific LAI, which is derived from plant cover and NDVI as described in 3.2.7. Moreover, the plant-specific canopy storage equations are shown, based on the study of Hoyningen-Huene (1983).

Leaf Area Index (LAI) $[m^2/m^2]$:

$$LAI = \frac{\ln(1 - \min(0.95, Cover))}{-0.4} \tag{1}$$

S_{max} 1: (Cropland) [mm]:

$$S_{max} = 1.412 \cdot LAI^{0.531} \tag{2}$$

S_{max} 6: (Broadleaf Forest) [mm]:

$$S_{max} = 0.2856 \cdot LAI \tag{3}$$

S_{max} 8: (Grassland) [mm]:

$$S_{max} = 0.59 \cdot LAI^{0.88} \tag{4}$$

C Channel Network

The start channel dimensions, shown in table 2, are based on field observations but might vary since not all of the tributaries' start locations could be visited during the field trip. This means that the channel dimensions of the tributary streams of the Geul are less accurate than the main river channel dimensions. Cross-sections for Kelmis and Sippenaeken were measured in the field. The others are derived from the SOBEK Geul setup (model described in section 2.5.1).

Table 2: Table with channel cross-sections used for interpolation

cross-section location	**Channel width (m)**	**Channel depth (m)**
Start	0.8	0.5
Kelmis	6.8	1.5
Sippenaeken	10	2.5
Samenvloeing Gulp, Selzerbeek, Eyserbeek	8.35	2.25
Wijlre	13	2.75
Valkenburg	11	3
Outlet (Meerssen)	13	3

D DEM

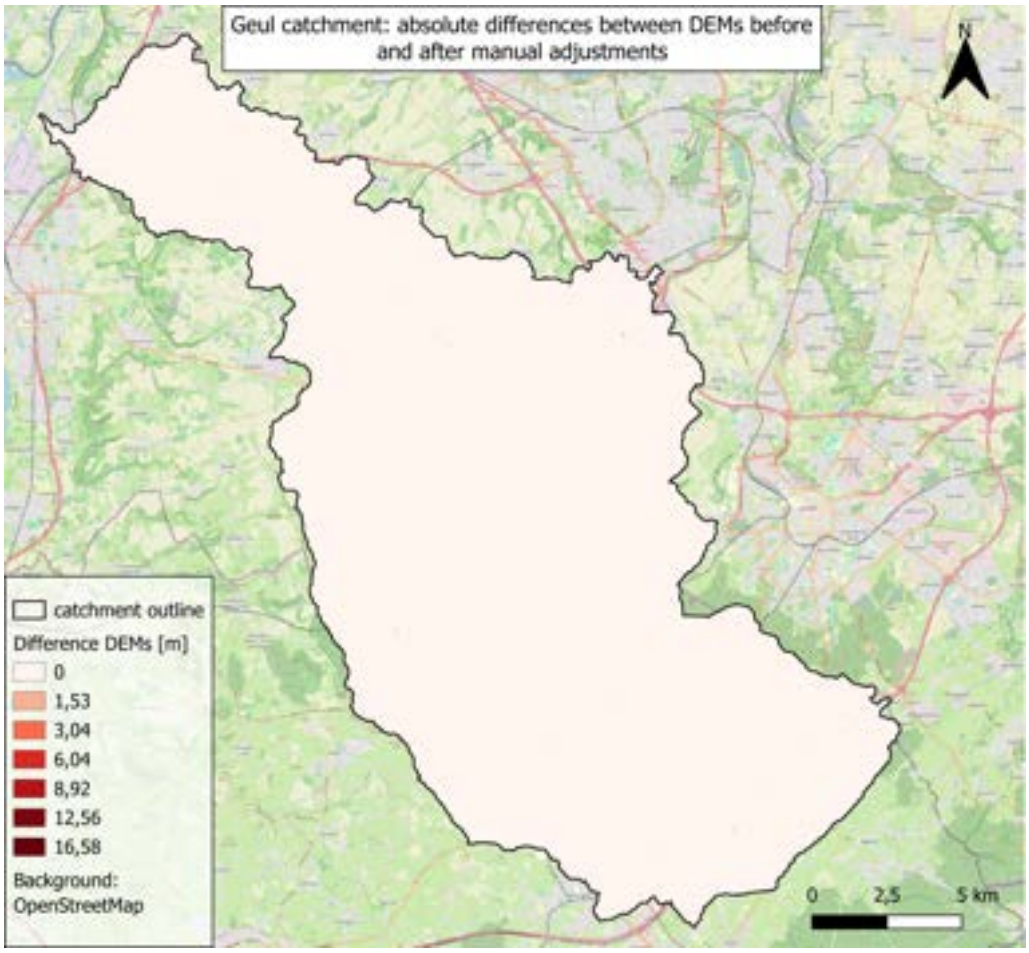

Figure 1: Differences in DEM after manual adjustments

E Roads & Buildings

Table 3: Summary statistics for OSM road categories

OSM road category	Count	Mean width (m)	Median width (m)	Stdev (m)
Primary	30	7.71	7.25	1.96
Secondary	30	6.43	6.34	1.12
Tertiary	30	5.87	5.50	0.90
Service	30	5.01	4.26	2.15
Residential	30	5.95	6.09	1.29
Motorway	30	11.05	10.98	2.32
Unclassified	30	4.16	3.62	1.27

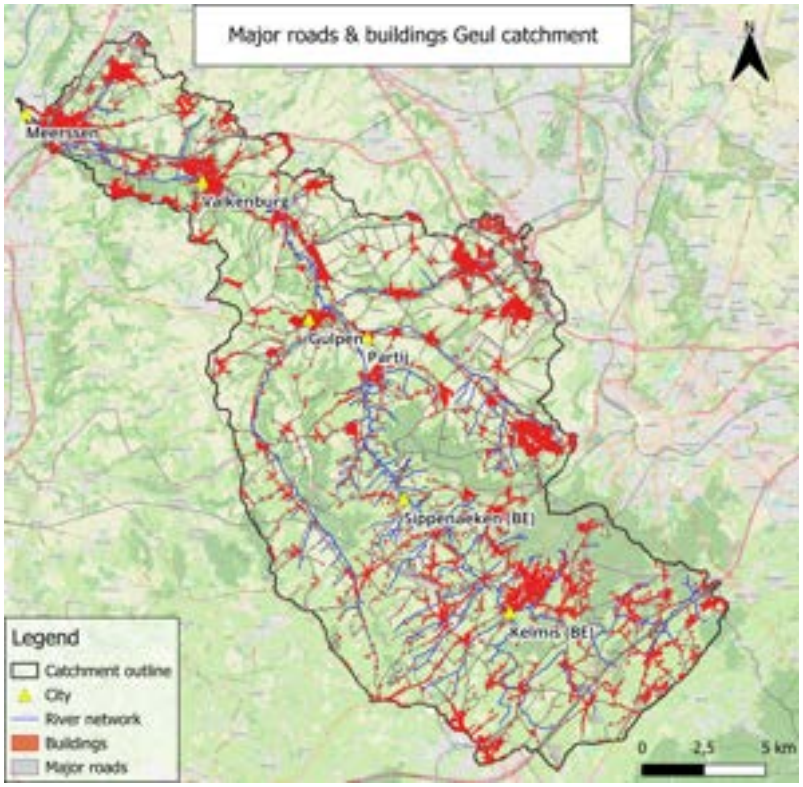

Figure 2: Roads & Buildings used in openLISEM

F Rainfall

The below figure 3 shows the raw cumulative rainfall sums without the application of the window average for the empty cells near the catchment outline. The final interpolated cumulative rainfall is shown in figure 2.3.

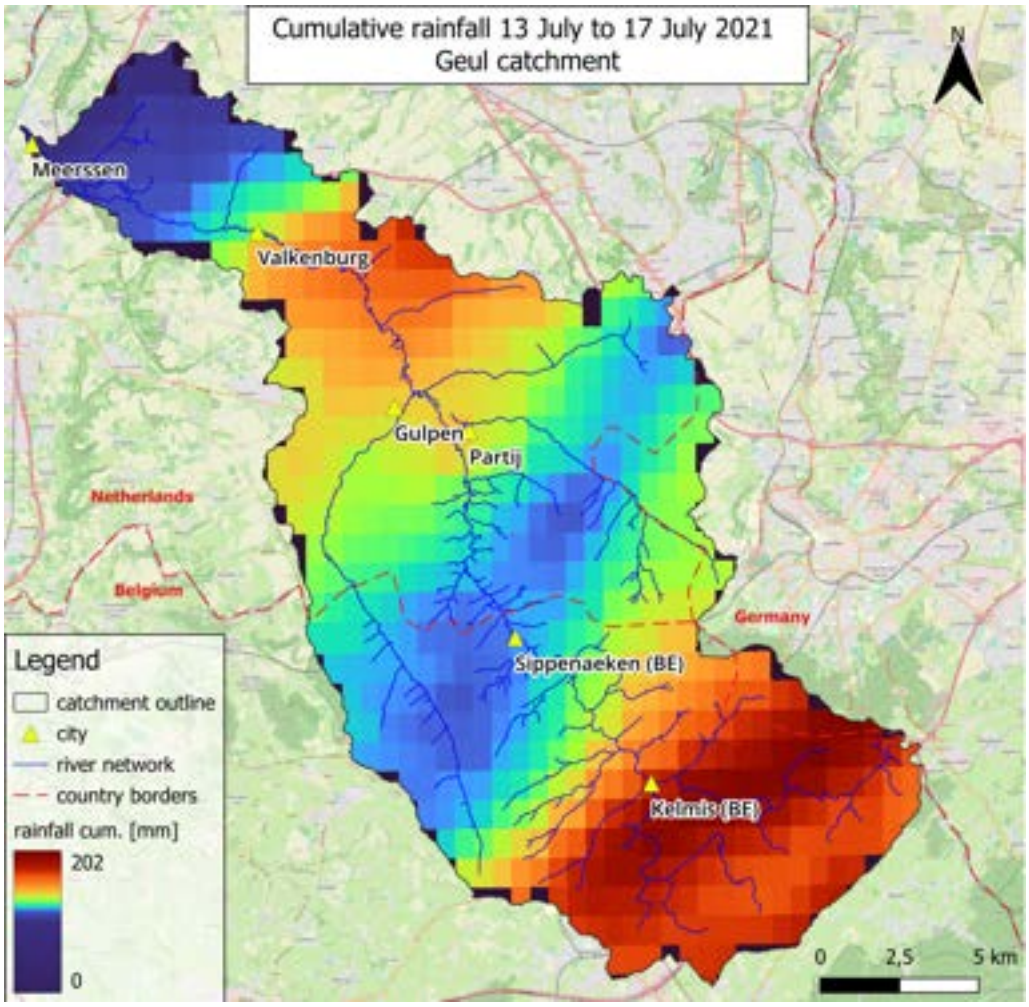

Figure 3: Raw cumulative event rainfall based on KNMI reanalysis data

G Forest parameterizations

Table 4: Different Forest parameterizations used in the scenarios

LULC	RR [cm]	Manning's n [-]	Plant Cover [-]	rel. BD [-]	Smax	OMC [%]
Forest "winter cover"	2	0.1	0.25	0.9	6	4.5
Forest "mid-aged"	2	0.1	0.9	0.9	6	4.5
Forest "young"	2	0.1	0.9	0.95	6	4.0
Forest "old"	2	0.1	0.9	0.9	6	8.0

H LULC maps & LULC statistics spatial afforestation scenarios

Table 5: Different spatial forest LULC stats

LULC	Reference scenario [%]	full afforestation [%]	policy scenario [%]	riparian afforestation [%]	upstream afforestation [%]	downstream afforestation [%]
Forest	30.24	92.73	38.91	36.96	50.03	72.95
Grassland	44.09	0	36.44	38.31	26.23	17.86
Cropland	18.40	0	17.38	17.46	16.47	1.93
Built-up	7.16	7.16	7.16	7.16	7.16	7.16
Water	0.06	0.06	0.06	0.06	0.06	0.06
Others	0.04	0.04	0.04	0.04	0.04	0.04
Total [%]	100	100	100	100	100	100

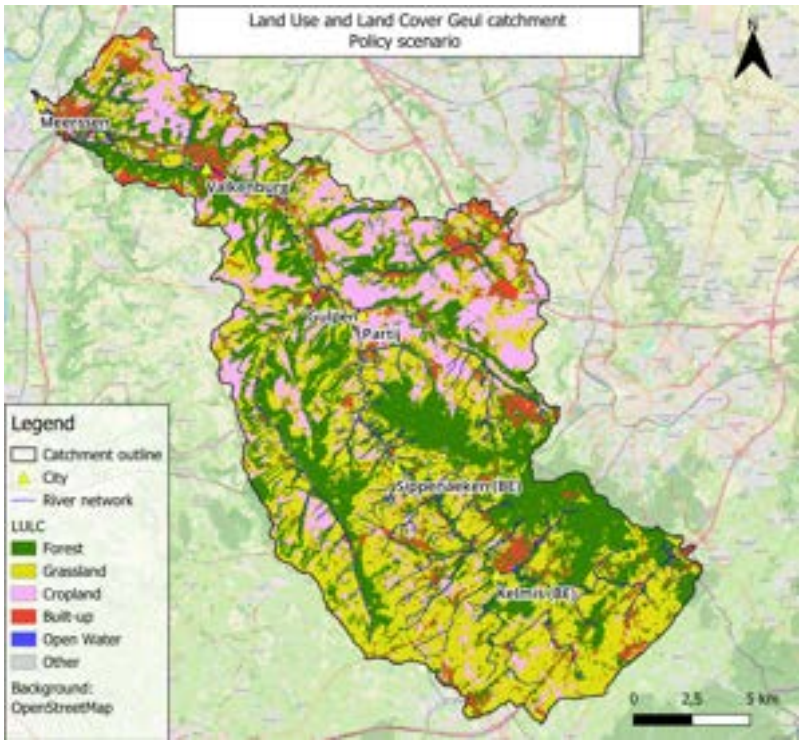

Figure 4: LULC policy scenario

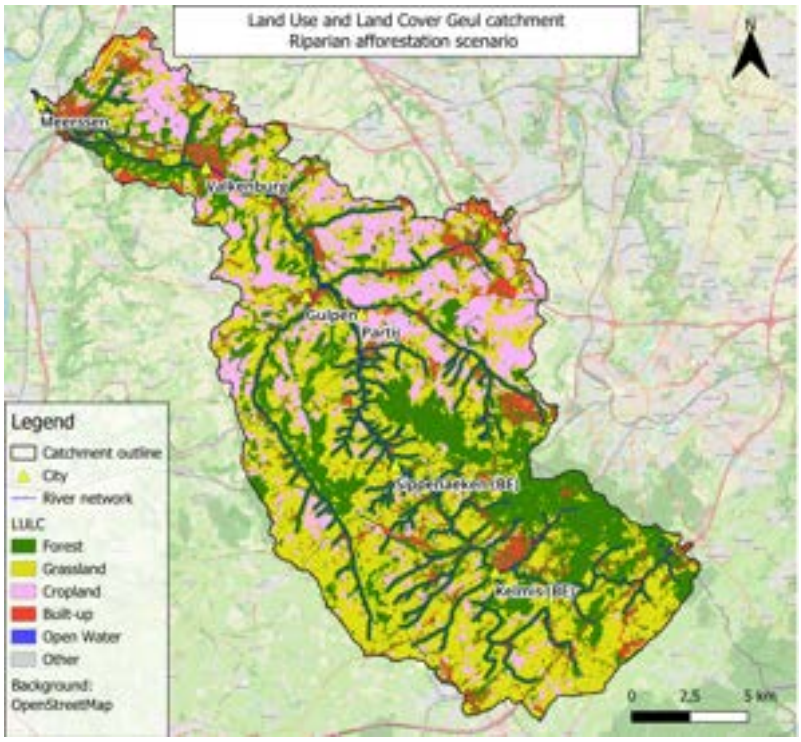

Figure 5: LULC riparian afforestation scenario

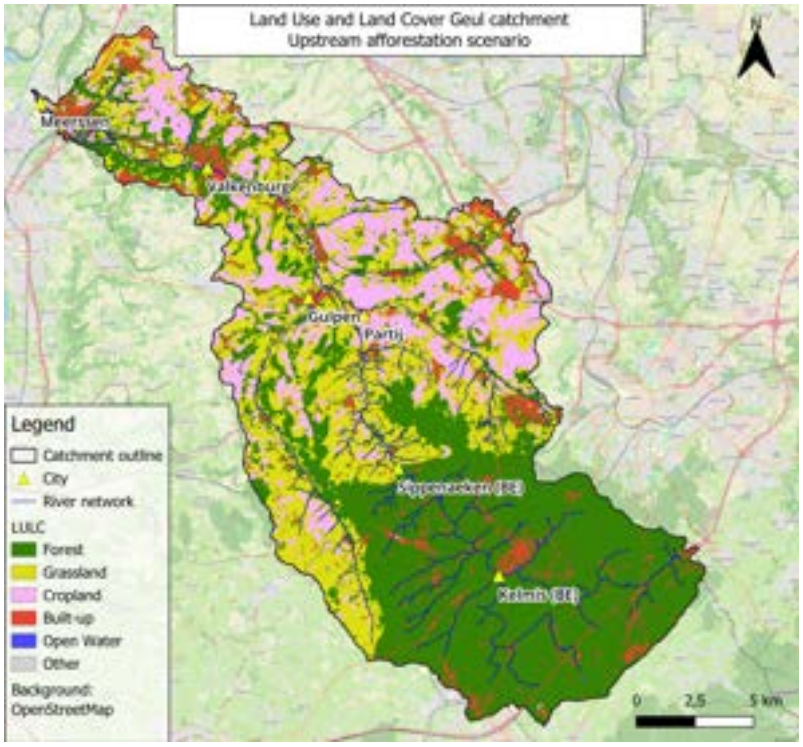

Figure 6: LULC upstream afforestation scenario

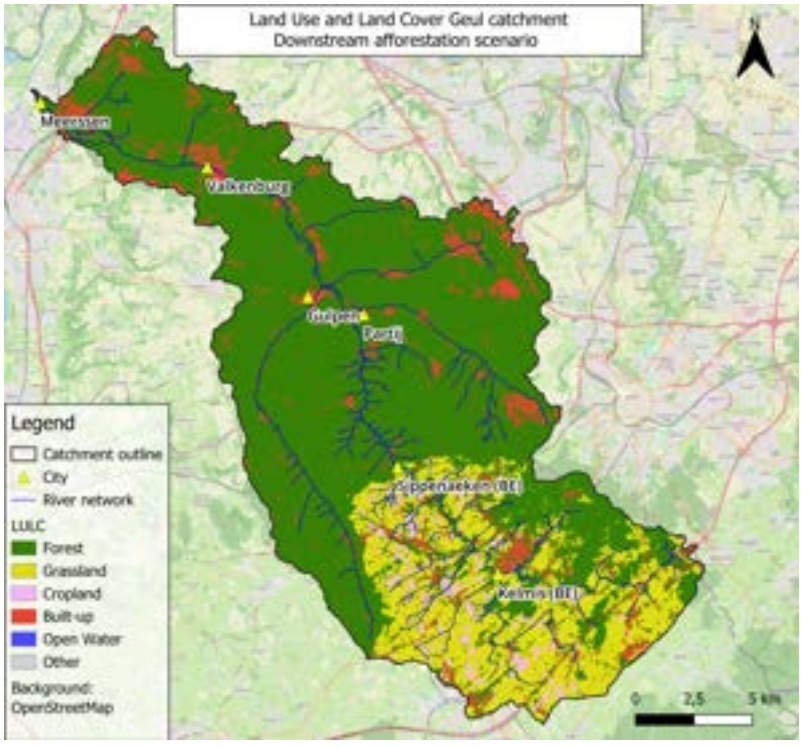

Figure 7: LULC downstream afforestation scenario

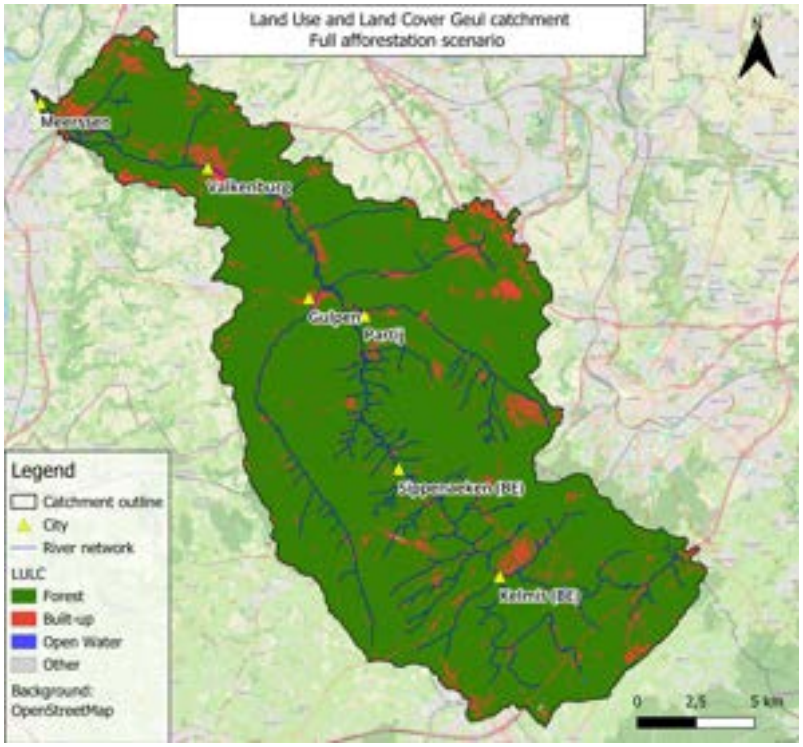

Figure 8: LULC full afforestation scenario

I LULC Hedgerows

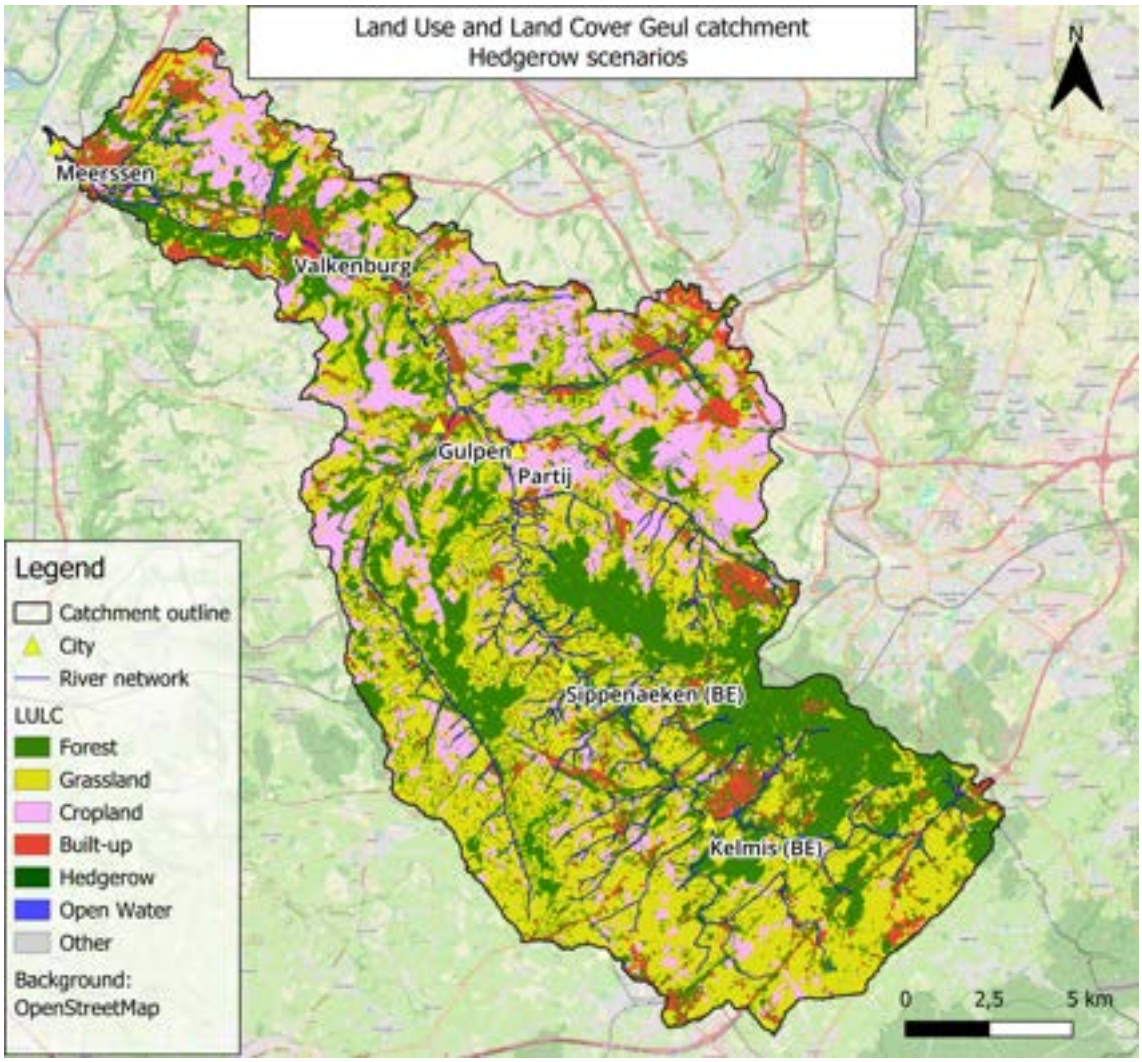

Figure 9: LULC hedgerow scenarios

J Hedgerow parameterizations

Table 6: Different hedgerow parameterizations used in the scenarios

LULC	RR [cm]	Manning's n [-]	rel. BD [-]	Smax [mm]	OMC [%]
Shrub hedgerow	1	0.12	0.95	2.56	4.5
Grass hedgerow	2	0.6	0.95	2.56	4.5

K Calibration Soil layer 1 & 2

The figures below display the final saturated hydraulic conductivities for soil layers 1 and 2 in the reference scenario, along with the soil depth of the second layer.

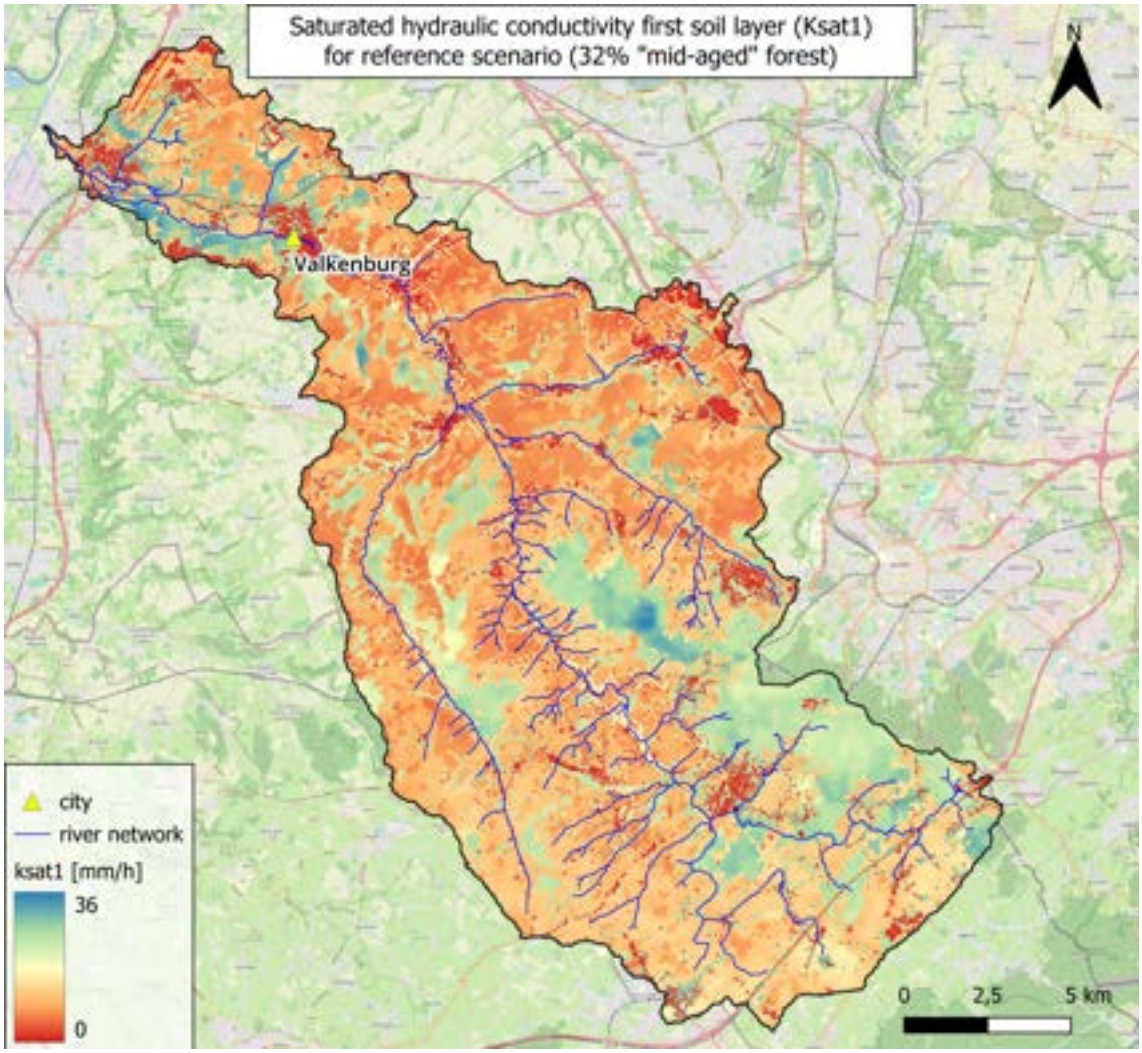

Figure 10: Ksat layer 1

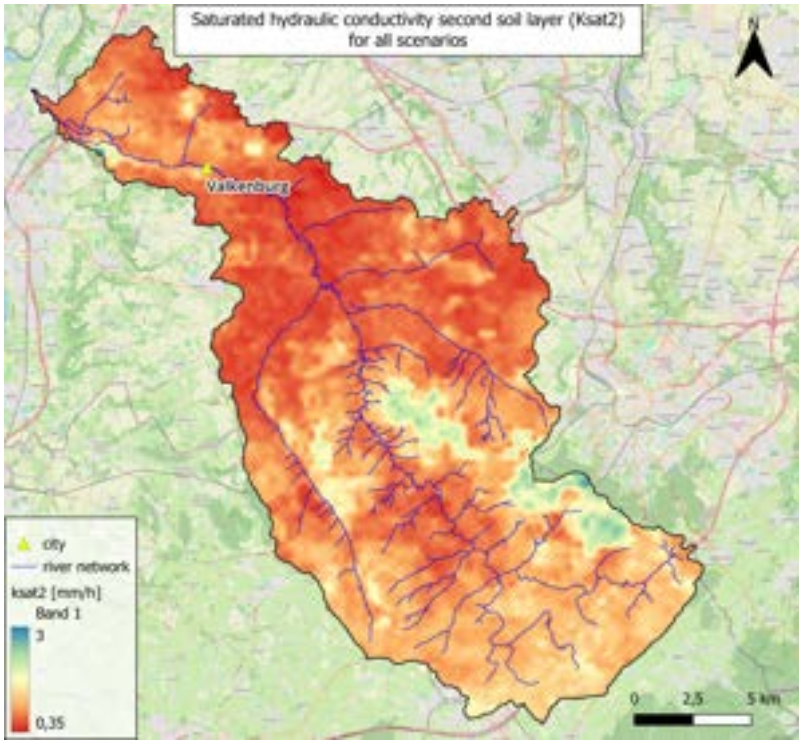

Figure 11: Ksat layer 2

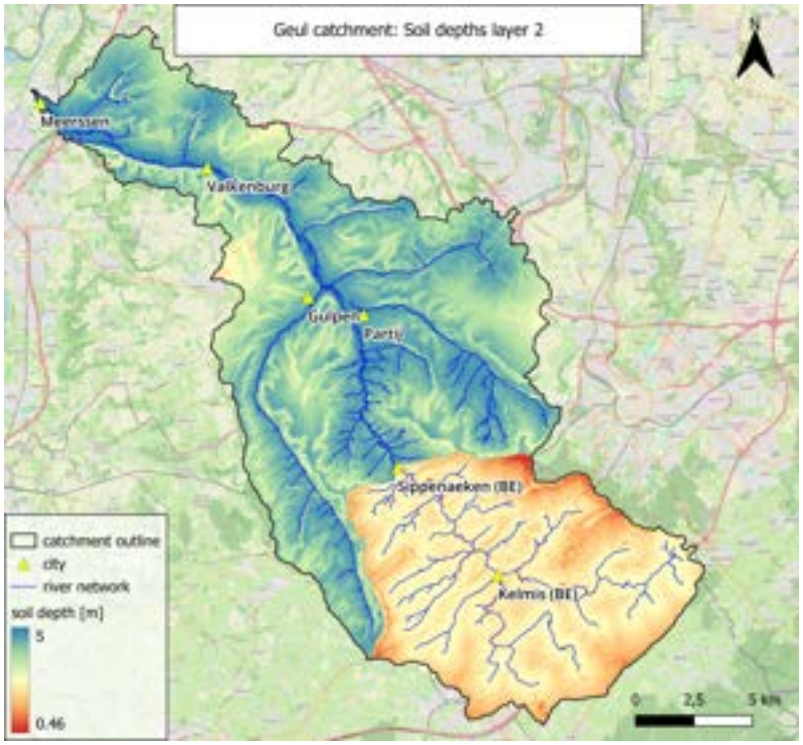

Figure 12: Soil layer 2 depths

L Calibration Steps

Table 7 shows the different steps during the calibration process and which parameters have been changed to obtain the optimal calibration for this study. Important calibration factors were the depth of the first soil layer, which is influenced by the above LULC, initial moisture content, and multiplication factors for the saturated conductivity of the first and second soil layer.

Table 7: Table with Calibration steps

calibration steps	**depth layer 1 (cm)**	**depth layer 2 (cm)**	**initial soil moisture content**	**cali- factor ksat layer 1**	**cali- factor ksat layer 2**	**Effect**
calibration step 1	50	max. 300	moisture content at field capacity	1	1	initial run without any calibration modifications
calibration step 2	50	max. 300	moisture content exactly between field capacity and full saturation	1	1	flashier response, more runoff due to increased saturation of soil
calibration step 3	30	max. 300	moisture content exactly between field capacity and full saturation	1	1	decrease of soil layer depth leads to less storage in soil and more runoff
calibration step 4	30	max. 300	moisture content exactly between field capacity and full saturation	0.7	1	reduction of ksat layer 1 results in flashier response and more runoff
Final Calibration	30	max. 300	moisture content exactly between field capacity and full saturation	0.7	0.3	decrease of ksat layer 2 results in flashier response and increases initial flood peaks

Figures 13, 14, 15 and 16 show observed and simulated channel water levels in Kelmis and Sippenaeken and observed and simulated discharges in Kelmis and Sippenaeken for different calibration steps, respectively. It is visible that the most substantial change in water levels and discharges occurred after adjusting the initial soil moisture conditions. Without the initial soil moisture content increase, the discharge and wl hydrographs show almost no response to the incoming heavy rainfall, suggesting that the soil would have taken up most of the incoming rain. This also indicates that the flooding during the event was caused by saturation excess overland flow, which has also been reported by other studies (Klein, 2022; Kuiper, 2023). Moreover, a further significant improvement can be observed

after the 3rd calibration step, when adjusting the soil depth of the first soil layer, as it ultimately decreases the volume of precipitation that can be stored in the soil. Reducing the saturated hydraulic conductivity of the first layers causes regional infiltration excess overland flow, in areas where incoming rainfall exceeds the infiltration capacity of the soil, this is visible in the increase of the maximum discharge peak and peak water level for both Kelmis and Sippenaeken. Lowering the saturated hydraulic conductivity of the second soil layer causes the velocity of percolating water to exceed the infiltration capacity of the second soil layer during rainfall peaks and after the first soil layer is saturated, which further increases the runoff, especially for the first small peak in the morning of the 14th of July and the first large peak around 18:00 at the 14th of July. Ksat is lowered for both soil layers by multiplying spatial ksat values with the calibration factor presented in table 7.

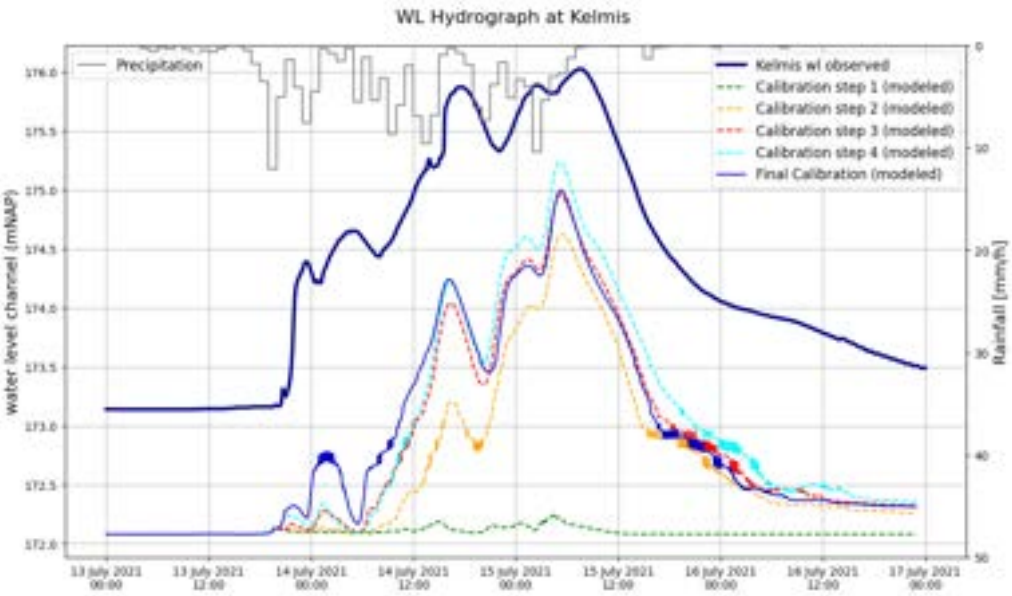

Figure 13: Observed and simulated channel water levels at Kelmis for different calibration steps

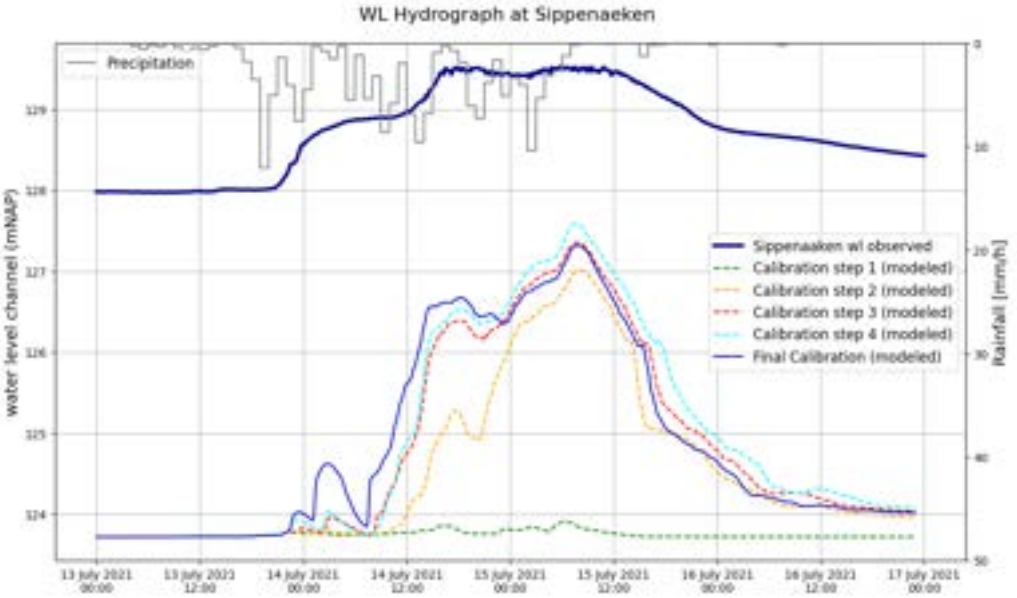

Figure 14: Observed and simulated channel water levels at Sippenaeken for different calibration steps

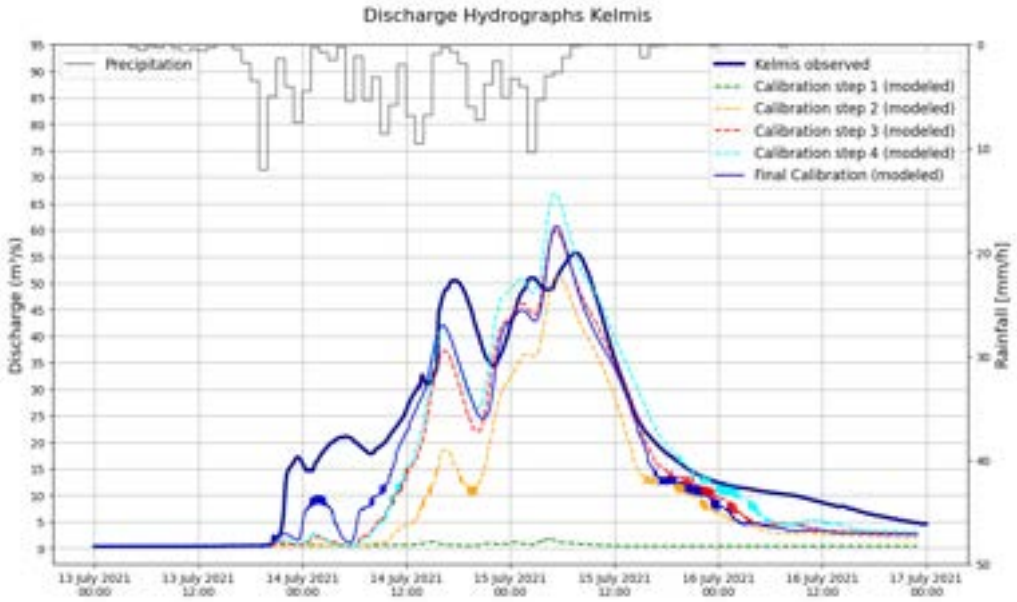

Figure 15: Observed and simulated channel discharge at Kelmis for different calibration steps

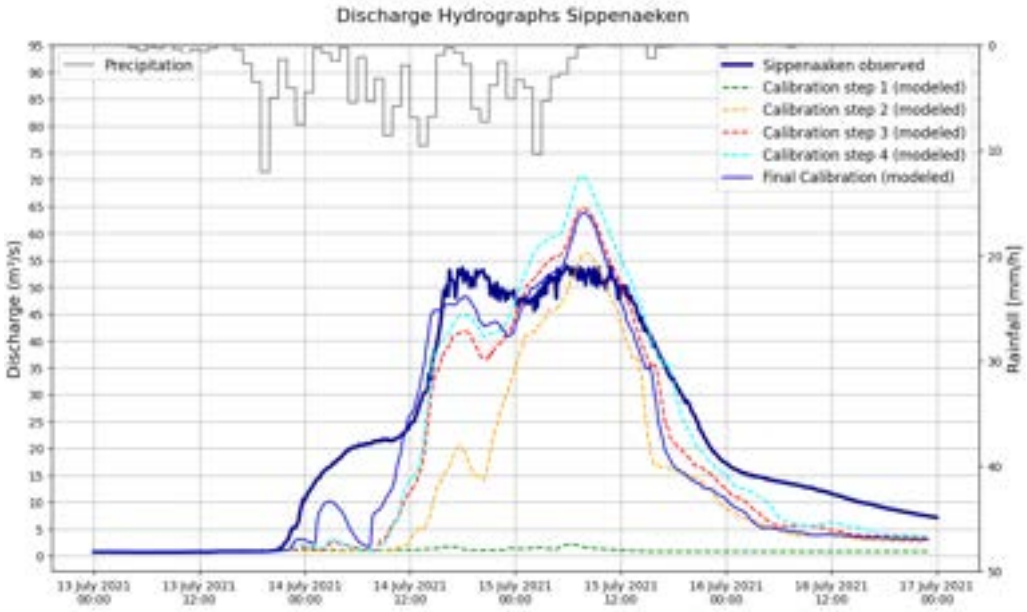

Figure 16: Observed and simulated channel discharge at Sippenaeken for different calibration steps

M Flood extents temporal dynamic afforestation scenarios

The below figures show the flood extents for "young", "mid-aged" and "old" afforestation scenarios.

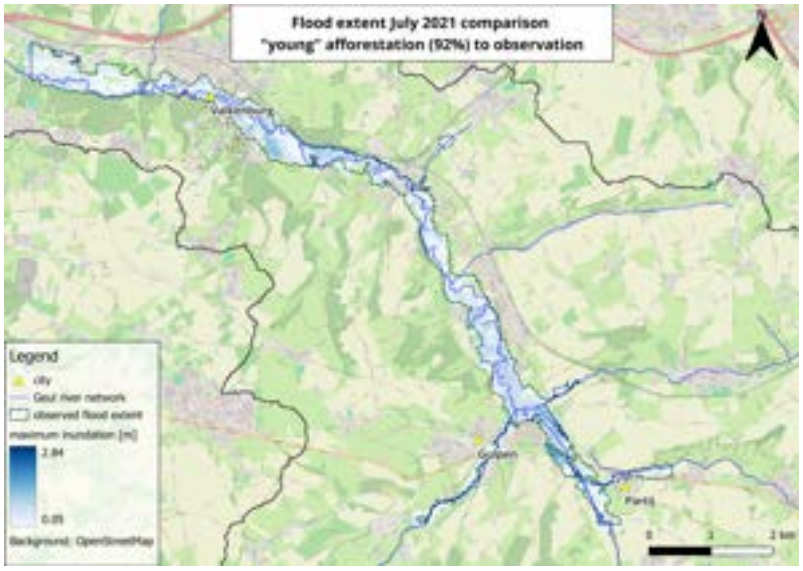

Figure 17: observed and simulated flood extent in zoomed-in area for "young" forest parameterization

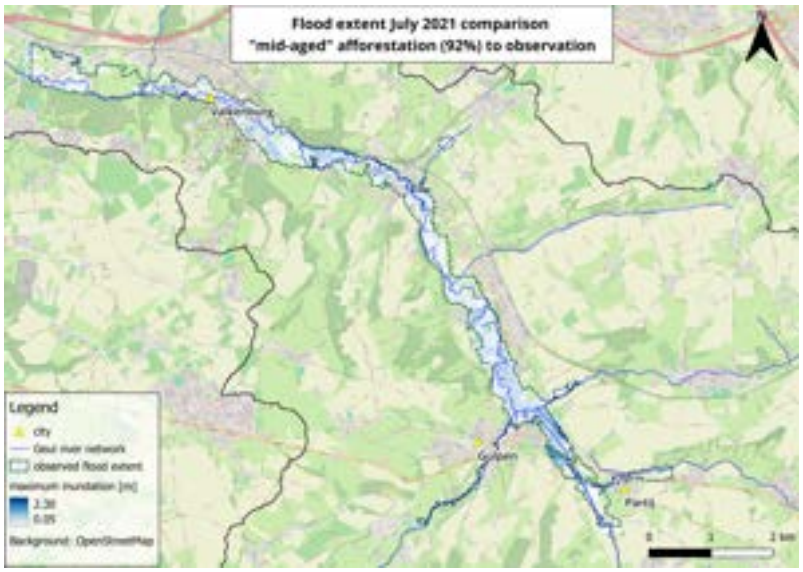

Figure 18: Observed and simulated flood extent in zoomed-in area for "mid-aged" forest parameterization

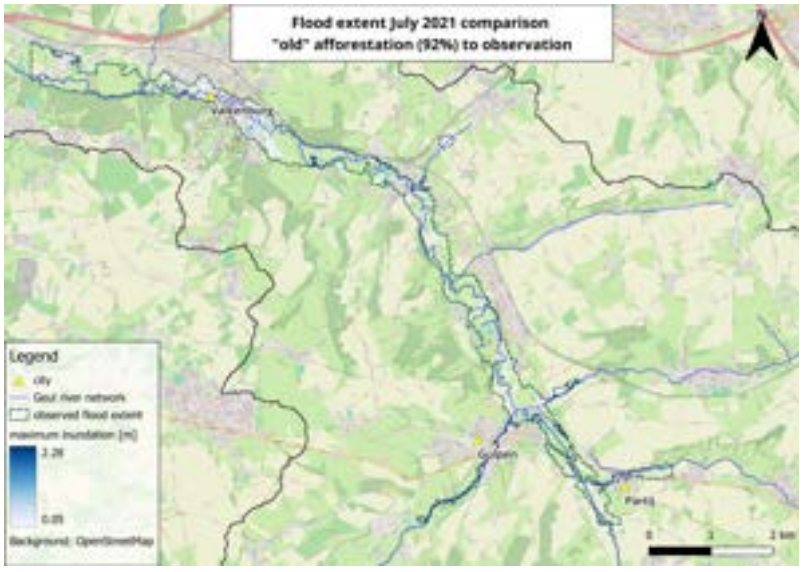

Figure 19: Observed and simulated flood extent in zoomed-in area for "old" forest parameterization

N Discharge Hydrographs Kelmis for temporal dynamic afforestation scenarios

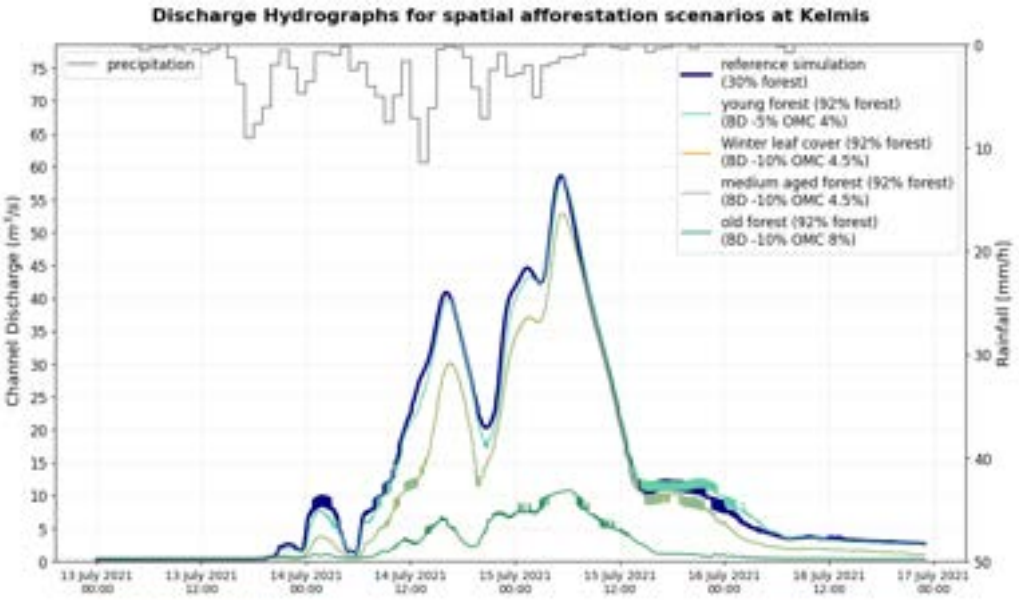

Figure 20: Observed and simulated channel discharge at Kelmis for different forest parameterizations

O Infiltration ratios

Hereafter are spatial varying infiltration ratios for different forest maturity scenarios presented. The figures 21, 22, 23 represent infiltration rates for young mid and old forest parameterizations, respectively. It can be observed that most of the incoming precipitation infiltrates for the young forest parameterization, especially in the downstream part of the catchment and central part. For the mid-aged forest parameterization, infiltration increases throughout the catchment, but it is clearly visible that in areas where the highest cumulative rainfall sums occur, in the southeast of Valkenburg and southeast of Kelmis in the upstream catchment (figure 2.3), the infiltration ratio is the lowest, suggesting that runoff is generated especially in those areas. In figure 23, it can be observed that most areas of the catchment take up all the incoming precipitation for the old forest scenario. Nevertheless, less infiltration occurs in the southeast of Valkenburg, which might be attributed to lower saturated hydraulic conductivity and higher clay content in the soil. In summary, those figures demonstrate that the increase in organic matter and lowering of bulk density related to different forest age parameterizations increase the overall uptake of incoming precipitation by the soil.

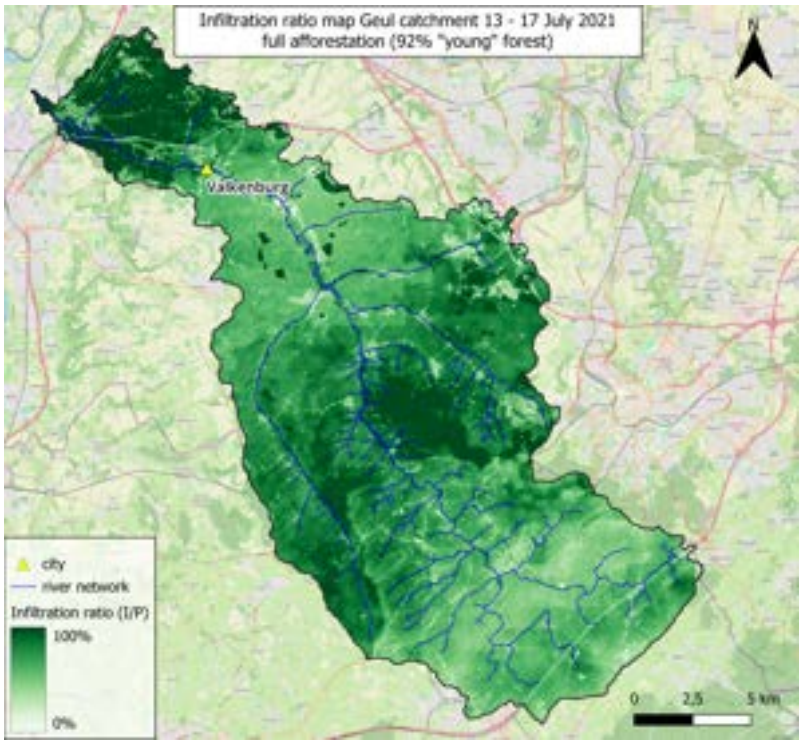

Figure 21: Infiltration ratios "young" forest parameterizations

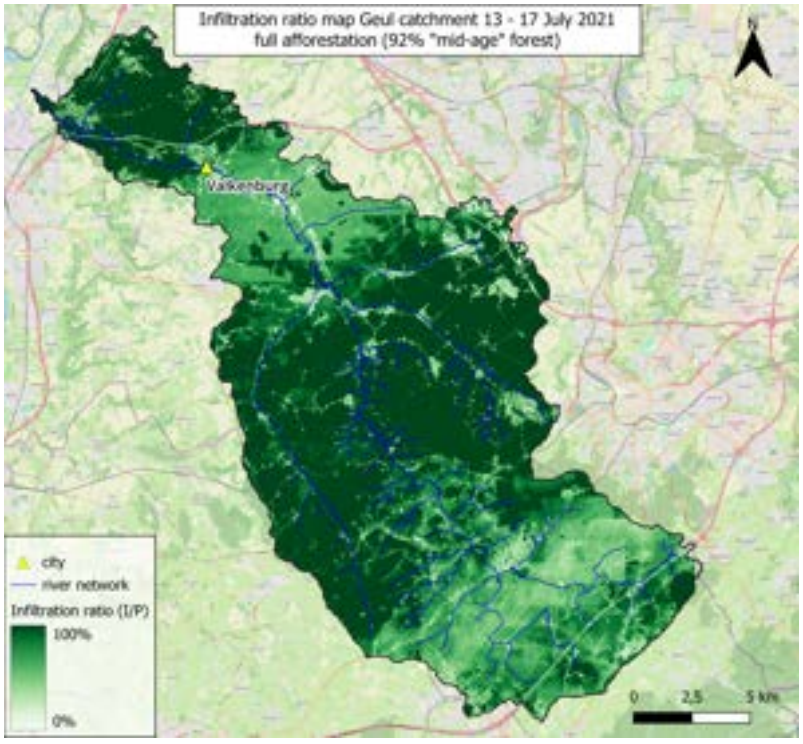

Figure 22: Infiltration ratios "mid-aged" forest parameterizations

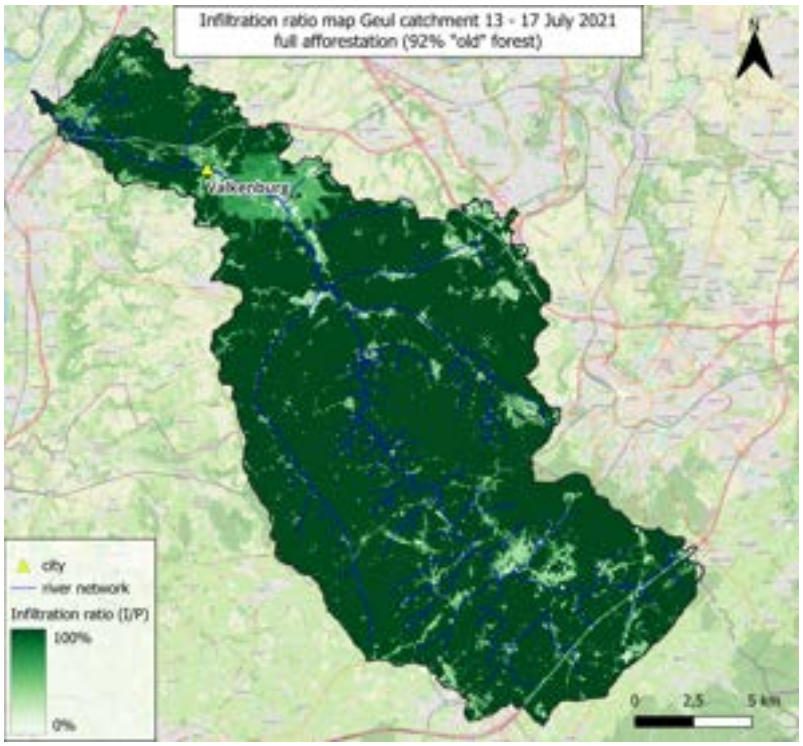

Figure 23: Infiltration ratios "old" forest parameterizations

P Flood extent 50% reduced rainfall

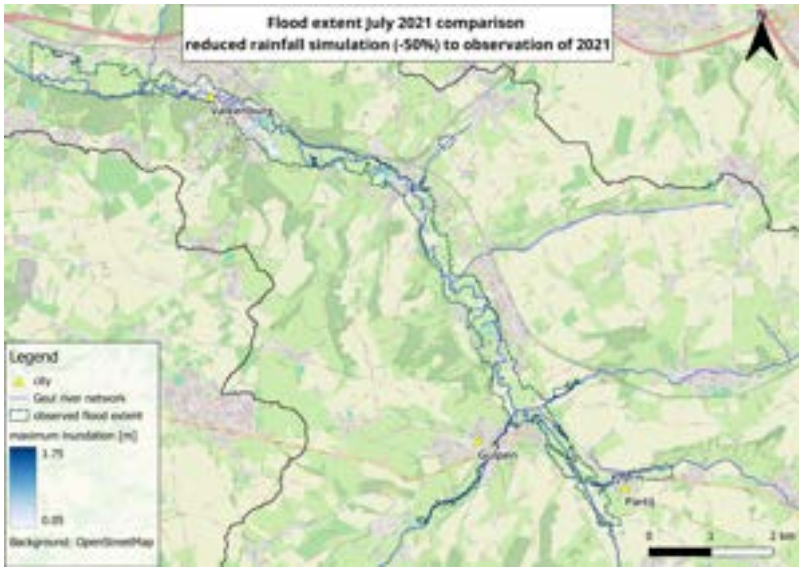

Figure 24: Zoomed-in flood extent for 50% reduction of event rainfall

Q Hedgerow hydrogrpahs

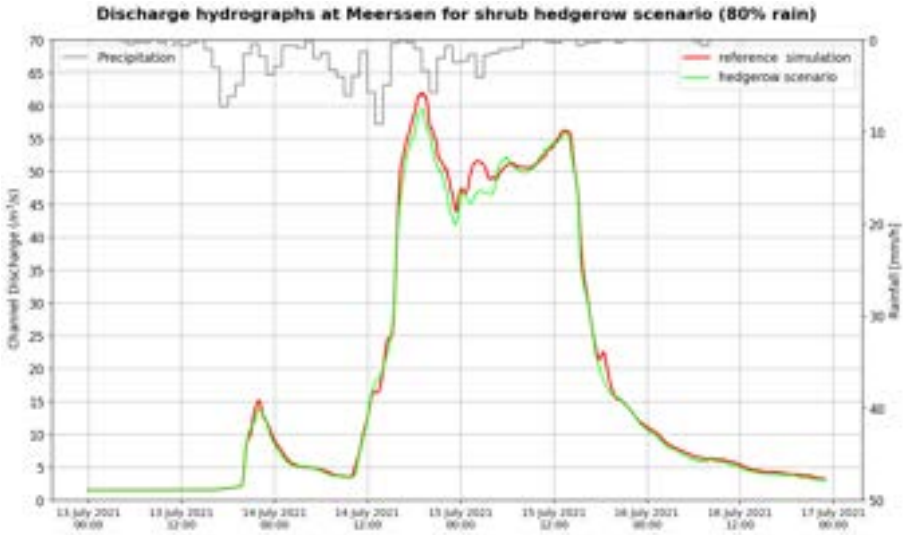

Figure 25: Discharge hydrograph shrub hedgerows for 80% of event rainfall

R Sensitivity analysis on discharge for different timesteps

The below figure 26 shows the simulated discharges for the reference simulation for different timesteps. The timestep used for calibration and assessing the scenarios was 60 seconds. Additionally, discharge was modeled for time steps of 30 seconds, 60 seconds, and 1 hour (3600 seconds).

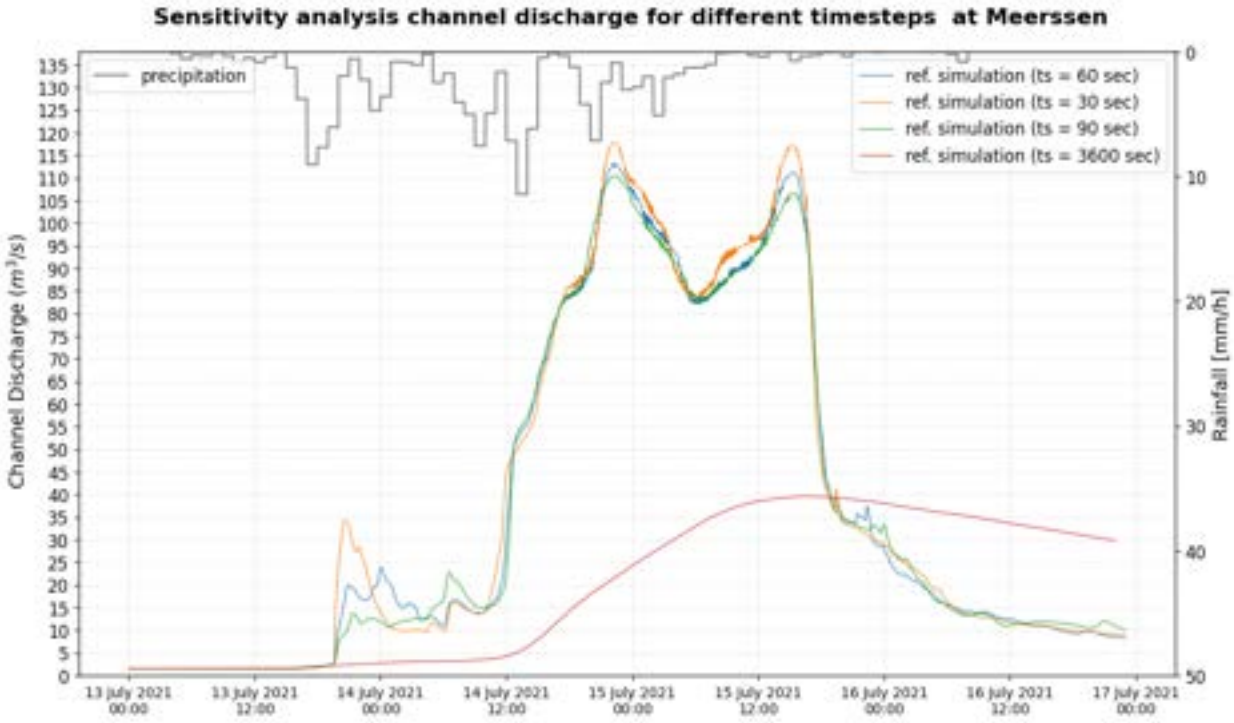

Figure 26: Sensitivity of channel discharge at Meerssen for different timesteps

It can be observed that a 30-second timestep shows the highest peak flows, followed by the simulated discharges using a 60-second timestep and, thereafter, simulated discharges with a 90-second timestep. The peak discharges vary by approximately 5 m^3/s between those simulations. The first smaller peak around the 14th of July at 00:00 shows the flashiest response for the simulation using a 30-second timestep. In large contrast, the simulation using hourly timestep shows a peak discharge of 40 m^3/s, whereas the simulation using 30 seconds timestep has a peak discharge of 118 m^3/s. Also, the first smaller peak around the 14th of July at 00:00 and the first larger peak on the 15th of July around 00:00 are not captured for the simulation with hourly timestep. This shows how sensitive the model is to changes in timesteps.